Homologous Evolution in the Post-Collapse Expansion of Globular Clusters

Rosemary K. Apple

Doctor of Philosophy
University of Edinburgh
2009

Abstract

We examine the evolution of globular star clusters, modelled as spherically symmetric stellar systems, using various techniques. Such clusters possess a central region of approximately uniform density which is referred to as the core. We concentrate our analysis on the evolution of the cluster after the core has undergone core collapse; a process where its radius decreases and its density increases. After this collapse, the system as a whole can expand in a self-similar fashion (homologous post-collapse evolution) which has long been thought to be due to gravitational interactions between different populations of single stars and binary stars in the core. We confirm this assumption by constructing a simple analytical model which combines much of the theoretical knowledge of previous research in the field. This model consists of two stellar populations, each defined by the mass of the individual stars, and a separate core. Our simple model is itself constructed from two simpler models – a two-component model without a core and a single mass model with a core – and takes into account the main gravitational interactions thought to drive the post-collapse evolution.

To ensure that no important mechanisms have been neglected in our simple model, we will compare it with an N-body simulation. We compute our N-body models with `NBODY6` (using a GPU version for large N). When we compare the N-body model with the simple model, we find qualitative agreement between them for most cases. Even though some mechanisms (e.g. escape of stars) are neglected in our simple model, we find that both models show homologous post-collapse evolution.

We also review the homologous post-collapse Fokker-Planck model in the case of equal stellar masses derived by Hénon (1961) with the intention of extending this for the two-component case. We present our numerical solutions for Hénon's model and find that our numerical solutions are in satisfactory agreement with the results shown in this paper. When we extend this work for a general two-component model (i.e. with no restriction on the number of heavier stars), we find that a homologous solution cannot be found with this approach. By contrast, we suggest that it would be possible to find a homologous two-component solution by extending the one-component solution published later by Hénon (1965), which differs from the earlier model by neglecting the external tidal field of the parent galaxy. Much of the work shown in this thesis would be relevant for such future study.

Declaration

I declare that this thesis was composed by myself and that the work contained therein is my own, except where explicitly stated otherwise in the text.

(Rosemary Apple)

Acknowledgements

It is a pleasure to thank those who made this thesis possible. First and foremost, I would like to thank my supervisor, Douglas Heggie who took the time to guide me through my studies during our weekly meetings and beyond. His meticulous reading and suggestions for my thesis were incredibly helpful and eased my mind during a time of great stress. In addition, I would like to thank my second supervisor, Maximilian Ruffert for all the conversations and encouragement over the years.

Thanks also to the members of the Mathematical Astronomy group: Otonyo Mangete and David Urminsky who took me under their wing when I was new and became much more than colleagues; they became my dearest friends. Thanks to my best friend and future maid of honor, Kate Gordon for our many conversations and her cynical humor that always brings a smile to my face.

I have been fortunate to have made many good friends during my PhD, Enrique Covarrubias, Pamela Docherty, Antonella D'Avanzo, Elena Méndez Escobar, Sunil Gadhia, Richard Hepworth, Achim Nonnenmacher, Emad Noorizadeh, Patricia Ritter, Daniele Sepe and Andrew Stothers to name a few. I am very grateful for the friendship, the laughter and the tea!

I am deeply indebted to my parents, James and Denise Apple whose love and encouragement enabled me to achieve more than I could have possibly imagined. Thank you for believing in me and teaching me that success means never giving up.

Finally, I owe my deepest gratitude to my fiancé and fellow mathematical astronomer, Richard Archibald who has done so much it is difficult to know where to begin. He proofread this thesis for me, brought dinner to my office and spent many late nights in the department so I never had to feel alone. Moreover, he has been my rock throughout my PhD. He made me laugh when I was down, he always listened when I had a problem and he believed in me even when I doubted myself. I'm very grateful to have met someone who completes me in every possible way and loves me unconditionally.

I dedicate this thesis to my parents and to my fiancé, Richard Archibald for their endless love and encouragement.

Contents

List of Figures

1 Introduction

1.1 An overview of globular clusters

Globular clusters are stellar systems containing between 10^4 and 10^7 stars. An example of a globular cluster can be seen in Fig 1.1. This is an image of globular cluster M80 taken by the Hubble Space Telescope. These stellar systems are tightly bound, giving them the spherical shape which gives rise to their name; globular is derived from the Latin word 'globulus' which means small sphere. Globular clusters are satellite systems that orbit around the galactic center of a parent galaxy. There are approximately 150 known globular clusters in our galaxy alone and many have been found in other galaxies (Binney and Tremaine 2008, Benacquista 2006). The average age of globular clusters is 12.9 ± 2.9Gyr (Carretta et al., 2000) and median radius is 10pc (Padmanabhan, 2001). Globular clusters have been of particular interest to astronomers because they are simpler than larger stellar systems, like galaxies, but contain much of the same dynamics with relatively small timescales. In short, globular clusters are the 'stellar laboratories' of the universe.

Figure 1.1: An image of M80 taken by the Hubble Space Telescope (`http://hubblesite.org`).

1.1.1 Virial theorem

A self-gravitating spherical system in equilibrium must satisfy the *virial theorem*,

$$2E_{\mathrm{Kin}} + E_{\mathrm{Pot}} = 0, \tag{1.1}$$

where T is the kinetic energy and V is the potential energy (Ostlie and Carroll, 1996). The virial theorem is frequently used in the study of globular clusters. When a system satisfies (1.1) then the system is said to be in *virial equilibrium*. When a system deviates from virial equilibrium the system adjusts in such a way as to return to virial equilibrium. We refer to this process as *revirialization*.

1.1.2 Characteristic radii

The important quantities of a globular cluster in the study of the dynamics are the mass and certain characteristic radii. A characteristic radius commonly used in theoretical work is the *half-mass radius* r_{h} which is the radius of a sphere containing half the mass of the cluster. The stars in globular clusters are not uniformly distributed; they have a

dense population in the center referred to as the core. Thus the *theoretical core radius* r_c is also an important characteristic radius of the globular cluster. The core radius is more difficult to define than the half-mass radius. We can see from the density profile at various points in time, shown in Fig 1.2, that the core radius is the radius which contains the nearly flat central region of the density profile. The theoretical core radius is written as

$$r_c = \sqrt{\frac{9\sigma^2}{4\pi G\rho_0}}, \tag{1.2}$$

where σ^2 is the one-dimensional velocity dispersion, ρ_0 is the central density and G is the gravitational constant (Binney and Tremaine, 2008).

The characteristic radii used in theoretical work are difficult to observe because we cannot observe a globular cluster as a three-dimensional system. Due to their distance we observe globular clusters as a two-dimensional projection of the three-dimensional system. Also, finding radii which are related to the total mass or mass density of a region in the system is tedious to obtain observationally as it would involve finding the individual masses of many stars in that region. Thus, observers use the characteristic radii such as the *half-light radius* and the *observational core radius*, instead. The half-light radius is the radius which emits half the light in the cluster. The observational core radius is defined as the radius at which the surface brightness is half the central surface brightness (King, 1962). The work presented in later chapters is theoretical and as such we use the half-mass radius and the theoretical core-radius as our characteristic radii.

1.2 Timescales

When studying the evolution of globular clusters, the evolutionary timescales of the main dynamical mechanisms are also important. The dynamical timescales are the *crossing time*, *relaxation time* and the *evaporation time*. The crossing time $t_{\rm cross}$ is the typical time necessary for a star to travel across a distance r. Generally, r is taken to be r_h unless otherwise specified. Therefore,

$$t_{\rm cross} \approx r/v, \tag{1.3}$$

where v is a typical velocity for a star in the cluster.

The relaxation time t_r is the time it takes for gravitational interactions to change the velocity of a star in such a way that the change in velocity will be on the order of its initial velocity. The relaxation time for the cluster as a whole (if in virial equilibrium) is given by the relation:

$$t_r \approx \frac{0.1N}{\ln N} t_{\rm cross}, \tag{1.4}$$

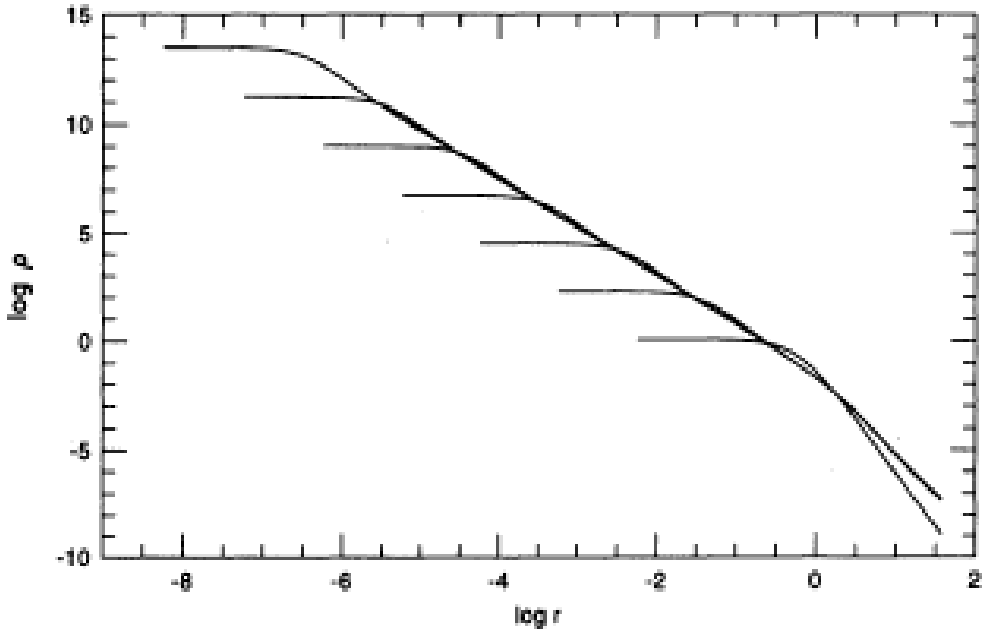

Figure 1.2: We show an image of the density profile of a Fokker-Planck model (see Sect. 1.6.4) calculated every 20 *Poisson steps*, where a Poisson step is chosen in such a way that the fractional increase of the central density is 2.5% for each step (Takahashi, 1995). The radius which contains the nearly flat central region of the density profile represents the core radius. As you can see from this figure the core radius becomes smaller and the density of the core increases as the system approaches core collapse.

where N is the number of stars in the cluster (Binney and Tremaine, 2008). The relaxation time depends on the position in the cluster. The commonly used relaxation times are the *half-mass relaxation time* $t_{\rm rh}$ and the *core relaxation time* $t_{\rm rc}$. The core relaxation time is the relaxation time at the center and the half-mass relaxation time is the relaxation time for average conditions within r_h. In the present work we use the half-mass relaxation time defined by Spitzer and Hart (1971b)

$$t_{\rm rh}(0) = \frac{0.06 M^{1/2} r_h^{3/2}(0)}{\langle m \rangle \, G^{1/2} \log\left(0.4N\right)}, \tag{1.5}$$

where M is the total mass, N is the total number of stars and $\langle m \rangle = M/N$.

Another mechanism that affects the evolution of globular clusters is mass loss. Two dynamical processes that cause mass loss in a globular cluster are *ejection* and *evaporation*. The process known as evaporation occurs when a series of weak gravitational interactions gradually gives a star enough energy to escape the system. The evaporation time $t_{\rm evap}$ is the time it would take for a cluster to lose all of its stars in the system through evaporation. The evaporation time is approximated by

estimating the fraction of stars in the cluster which are lost over the relaxation time. This was estimated by Spitzer and Thuan (1972a) to be

$$t_{\rm evap} = 300 t_{\rm rh}, \tag{1.6}$$

where the globular cluster is isolated (i.e. the tidal forces of the parent galaxy are neglected) and the stars have equal masses (also referred to as a *single-mass system*).

A less used timescale is known as the *ejection time*. The process known as ejection occurs when a single close encounter with another star or binary system gives a star enough energy to exceed the escape velocity of the globular cluster, ejecting the star from the system. Although ejection time is not a commonly used dynamical timescale, it is important to compare the timescale for evaporation and ejection. Binney and Tremaine (2008) show the ejection time $t_{\rm eject}$ to be

$$t_{\rm eject} = 1.1 \times 10^3 \ln\left(0.4N\right) t_{\rm rh}. \tag{1.7}$$

From (1.6) and (1.7) we can see that ejection occurs on a much longer timescale than evaporation. In fact, if we compare all these timescales to each other, we find

$$t_{\rm cross} \ll t_{\rm r} \ll t_{\rm evap} \ll t_{\rm eject}. \tag{1.8}$$

1.3 Mass segregation and equipartition

In most stages of globular cluster evolution, two-body relaxation is the primary mechanism which drives evolution. In a multi-mass system, when a heavier star encounters a lighter star then this usually results in kinetic energy transferring from the heavier star to the lighter star. This causes the heavier star to sink down the potential well and the lighter star to climb up the potential well. Over many encounters we find that the heavier stars tend to dominate the center of the cluster while the lighter stars tend to dominate the outer region of the cluster. This process is known as *mass segregation* and can be seen in Fig. 1.3. In this figure we follow the mean stellar mass at various Lagrangian radii over time. The n% Lagrangian radius is the radius which contains n% of the total mass, so the 1% Lagrangian radius contains 1% of the total mass and is much smaller than the 50% Lagrangian radius, which corresponds to the half-mass radius. As we can see from Fig. 1.3, after a period of time elapses the mean stellar mass of the smaller radii are significantly more than the larger radii. This is due to mass segregation.

The cluster should continue to segregate in this manner until it achieves *equipartition* of the masses. If we divide the stars into n groups characterized by the stellar mass, then equipartition occurs when

$$m_1 \left\langle v_1^2 \right\rangle = m_2 \left\langle v_2^2 \right\rangle = ... = m_n \left\langle v_n^2 \right\rangle, \tag{1.9}$$

where m_i is the stellar mass of the i^{th} group and $\langle v_i^2 \rangle$ is the mean square velocity of the i^{th} group.

The condition for equipartition was studied in the two-component case (i.e. a system with two mass groups with individual stellar mass m_1 and m_2, where $m_2 > m_1$) by Spitzer (1969) where it was concluded that equipartition was not always possible. When the total mass ratio M_2/M_1 ($M_i = m_i N_i$, where N_i is the total number of stars in group i) of the groups fulfilled the criterion

$$\frac{M_2}{M_1} \geq \beta_{\text{Spitzer}} \left(\frac{m_2}{m_1} \right)^{-3/2}, \tag{1.10}$$

where β_{Spitzer} is a constant, which Spitzer found to be 0.16, then it is impossible to achieve equipartition.

Equipartition in two-component and other multi-mass models was studied and found to be in qualitative agreement with Spitzer (1969). For example, Lightman and Fall (1978) created a simple model of a two-component cluster and found a criterion involving the total mass ratio and the individual mass ratio. Also, Inagaki and Wiyanto (1984) found that when they used a two-component Plummer model (see Sect. 1.6.2) for the initial conditions of their Fokker-Planck model (see Sect. 1.6.4), then the criterion described in Spitzer (1969) held.

A survey of many two-component N-body simulations in Khalisi et al. (2007), shows that the collapse of the core (which will be discussed further in Sect. 1.4) is slowed by temporary equipartition in the case where $\frac{M_2}{M_1} < \beta_{\text{Spitzer}} \left(\frac{m_2}{m_1} \right)^{-3/2}$.

1.4 Gravothermal catastrophe

Originally, it was thought that a globular cluster would follow the *evaporative model* meaning that the cluster would slowly lose stars over time through evaporation until it completely dissolved (Spitzer 1940, Chandrasekhar 1942). This was until a phenomenon was found in the study of globular cluster evolution called *gravothermal catastrophe*. Gravothermal catastrophe occurs when the central density of a globular cluster becomes infinite in a finite time and is caused by a mechanism referred to as *gravothermal instability* (Cohn, 1980). We see in Fig. 1.2, the evolution of the density profile for a Fokker-Planck model with gravothermal instability. As we can see, the core radius decreases while the density of the core increases indefinitely. This process is also known as *core collapse* because of the the shrinking of the core radius. This phenomenon was originally discovered by Hénon (1961) and has been repeatedly shown with many types of modeling techniques (Larson 1970, Spitzer and Thuan 1972b, Aarseth et al. 1974, to name a few).

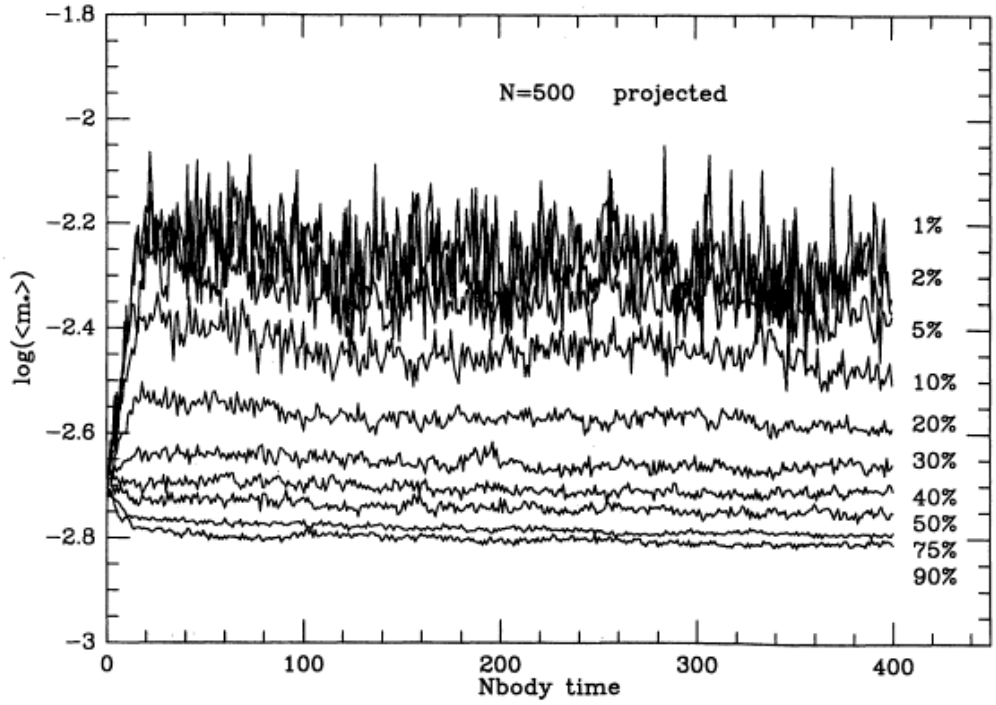

Figure 1.3: The evolution of the mean individual stellar mass within various Lagrangian radii in a multi-mass N-body simulation (See Sect. 1.6.3) is shown in Giersz and Heggie (1996). The 1% Lagrangian radius is the radius which contains 1% of the total mass of the system. The 50% Lagrangian radius correspond to the half-mass radius. We see that after a period of time the smaller Lagrangian radii have a notably larger mean stellar mass than the larger Lagrangian radii. This is due to mass segregation.

Several observational surveys of globular cluster surface brightness profiles have been done to assess the number of globular clusters in our galaxy that have undergone core collapse (Djorgovski and King 1986, Chernoff and Djorgovski 1989, Trager et al. 1995). This estimate is made by dividing the globular clusters into two types. These types are the clusters that fit the King model (King models will be discussed further in Sect. 1.6) which have a flat surface brightness profile in their core and the clusters which do not fit the King model, but have a power law surface brightness profile in the core. From these surveys it was found with reasonable agreement that approximately 20% of the globular clusters have the latter surface-brightness profile and are thought to have undergone core collapse.

To understand gravothermal instability, we employ a commonly used method in studying globular clusters; we compare a globular cluster to a self-gravitating thermodynamical system. When a thermodynamical system which is not self-gravitating is surrounded by an adiabatic wall, we would expect that after a certain

period of time has elapsed, the system would be in a state of thermal equilibrium. However, as originally shown by Antonov (1962) and Lynden-Bell and Wood (1968), this is not necessarily the case for self-gravitating systems. When we have a self-gravitating system enclosed in an adiabatic wall, the system evolves as follows: if the core has a higher temperature (temperature in this context means the mean kinetic energy per star) than the outer region then the heat flows outwards; thus heating the outer region. The core loses heat initially and contracts. This contraction causes the particles in the core to convert potential energy into kinetic energy, which heats the core as well. Therefore, the core has a negative specific heat (Hachisu and Sugimoto, 1978). Whether this means that the system is tending towards or away from thermal equilibrium depends on certain conditions. If these conditions are met then the temperature difference between the core and the outer region increases; the system tends away from thermal equilibrium (Meylan and Heggie, 1997) and gravothermal catastrophe is inevitable unless a sufficient 'energy source' can be created in the core of the cluster.

1.4.1 Homologous evolution

When a globular cluster has homologous, or self-similar, evolution the system may expand or contract in a similar manner but the general structure of the system remains the same. A mathematical description of self-similar evolution was given in Lynden-Bell and Eggleton (1980) with the density and radii

$$\rho(r,t) = \rho_c(t)\alpha_\rho(r_c(t)/r). \tag{1.11}$$

It is important to note that at any point in time the evolution of ρ at a distance r from the center evolves similarly to $\rho_c(t)$ and the value of $\rho(r,t)$ can be found using the scaling factor $\alpha_\rho(r_c(t)/r)$. An example of such a relation between ρ and r can be seen in pre-collapse Fokker-Planck model shown in Fig 1.2. We extend this to other important quantities in the cluster

$$\begin{aligned} \left\langle v^2(r,t)\right\rangle &= \left\langle v_c^2(t)\right\rangle \left\langle v_*^2(r_*)\right\rangle, \\ M(r,t) &= M_c(t)M_*(r_*). \end{aligned} \tag{1.12}$$

where, $\left\langle v_*^2(r_*)\right\rangle$ and $M_*(r_*)$ are the scaling factors for $\left\langle v^2(r,t)\right\rangle$ and M, respectively at each radius r, given r_c. A system with homologous evolution can also be seen in the post collapse phase in Fig 1.4, where the Lagrangian radii evolve at the same rate on a logarithmic plot.

It had been suggested previously that globular clusters in the late stages of core collapse evolved self-similarly (Lynden-Bell, 1975), but it was Lynden-Bell and

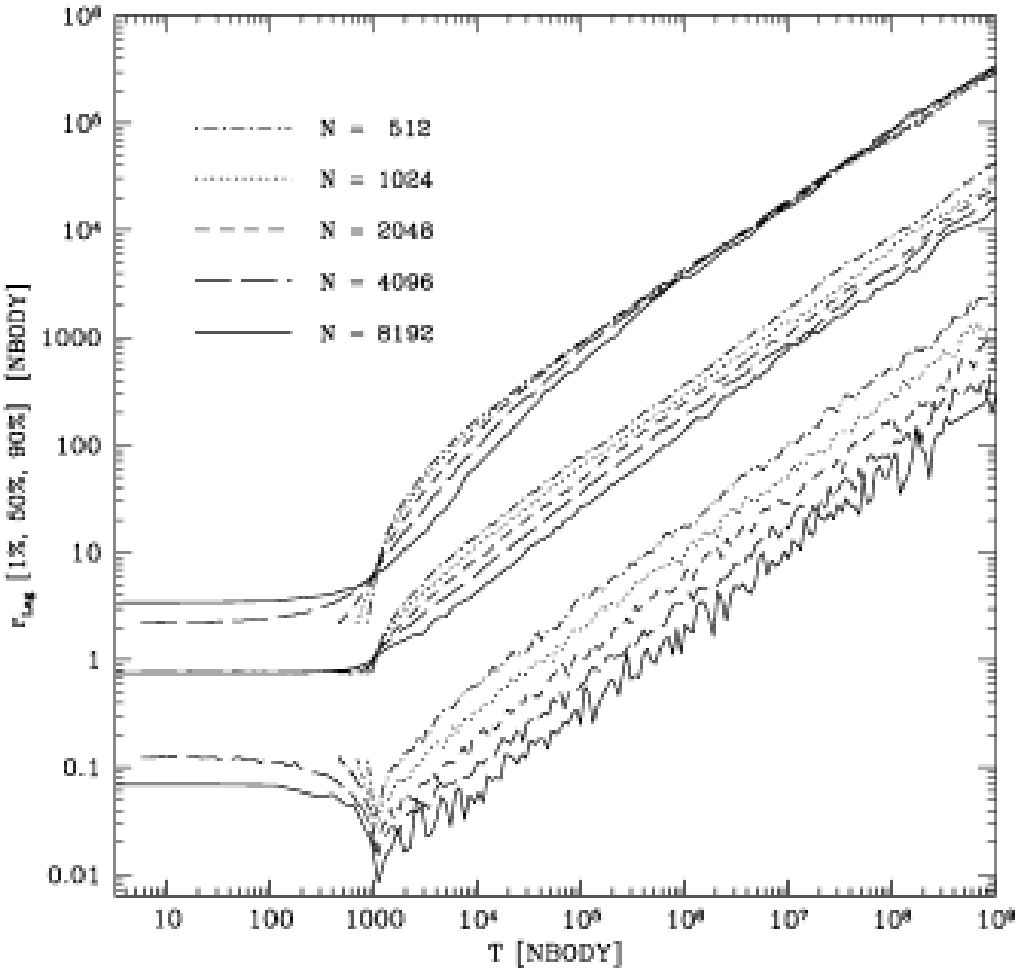

Figure 1.4: The evolution of the 1%, 50% and 90% Lagrangian radii (i.e. the radii which contain 1%, 50% and 90% of the total mass, respectively) over time for several N-body simulations. Times are shifted such that the clusters collapse at the same time. As we can see post-collapse evolution is self-similar because the radii in this log-log plot evolve at the same rate after core collapse (Baumgardt et al., 2002).

Eggleton (1980) that first showed this through a self-similar gas model (see Sect. 1.6.5). This was shortly followed with a Fokker-Planck model which exhibited self-similarity in the center (Cohn, 1980). A full self-similar Fokker-Planck model was later developed by Heggie and Stevenson (1988).

Since then, many people have studied homologous evolution in globular clusters. It has also been shown to occur in post collapse expansion (Inagaki and Lynden-Bell 1983, Giersz and Heggie 1996) in addition to the late stages of core collapse.

1.5 Binary heating and post-collapse expansion

It is clear from the work discussed in the previous section that a significant number of globular clusters have undergone core collapse. Therefore, there must be a mechanism to enable clusters to survive the infinite density at the end of core collapse. This mechanism would need to heat the core of the cluster to reverse the run-away effect of the gravothermal catastrophe. Binary stars can provide heat to the core through a process known as *binary heating*. Binary heating has long been considered as the mechanism which allows a system to survive core collapse (Binney and Tremaine, 2008).

A *binary star*, or binary stellar system, is a system of two stars orbiting around their center of mass. The mass of star 1 in the system is m_1 and the mass of star 2 in the system is m_2. The relative motion in a binary system is elliptic and the largest radius in this ellipse is referred to as the semi-major axis a of the system.

From the study of three-body interactions, Heggie (1975a) has shown that when a single star interacts with a binary stellar system the outcome of the interaction depends on the binding energy of the binary system. The binding energy $E_{\rm bind}$ is the energy required to pull the stars apart to infinity. This is equivalent in magnitude to the internal energy of the binary system which can be described as

$$E_{\rm bind} = -E_{\rm int} = G\frac{m_1 m_2}{2a}, \tag{1.13}$$

where $E_{\rm int}$ is the internal energy of the system, a is the semi-major axis and m_i is the individual stellar mass of star i.

The behavior of binary systems can be explained more easily by categorizing binary stars into *soft binary systems* and *hard binary systems*. Soft binary systems fulfill the condition

$$\beta_{\rm sh} E_{\rm bind} < 1, \tag{1.14}$$

and hard binary systems fulfill the condition

$$\beta_{\rm sh} E_{\rm bind} > 1, \tag{1.15}$$

where $\frac{3}{2}\beta_{\rm sh}^{-1}$ is the local mean kinetic energy of the single stars. For simplicity, we will focus on the behavior of very soft binary systems and very hard binary systems. We will neglect binary systems with binding energy $E_{\rm bind} \approx 1/\beta_{\rm sh}$.

We will discuss the general behavior of binary stars when interacting with single stars. The theory is referred to as *Heggie's Law* and was discovered independently by Hills (1975). It was later confirmed through a comprehensive numerical study of scattering shown in Hut and Bahcall (1983) and Hut (1983).

1.5.1 Soft binary stars

On average, three-body interactions with a soft binary and a single star transfer energy from the single star to the binary. In a globular cluster, the soft binary would have several encounters with single stars which would in turn result in an increase of the internal energy of the binary system. The internal energy of the binary system gradually increases and eventually $E_{\text{int}} \geq 0$ and the stars are no longer gravitationally bound to each other. The time required for this process to take place is much shorter than the relaxation time. Due to the short lifetime of soft binary stars and their small binding energy, they do not have a significant impact on the evolution of globular clusters (Heggie 1975b, Mikkola 1983a, Mikkola 1983b).

1.5.2 Hard binary stars

The interactions of single stars with hard binary stars is not as easily described as the interactions of single stars with soft binary stars. When a single star interacts with a hard binary system, a gravitationally bound three-body system can temporarily be formed and *exchanges* may occur. An exchange takes place when the single star and one of the stars in the binary system form a binary system of their own, ejecting the third star from the original binary. This process of exchange can happen many times before one of the stars escapes.

Although three-body interactions involving hard binary stars are more complicated than those involving soft binary stars, we know the qualitative results of such an interaction from previous work (Heggie 1975a, Hut and Bahcall 1983). Generally, an interaction of this kind results in the transfer of binding energy from a binary system to the single star and the center of mass of the binary system in the form of kinetic energy. Thus, the internal energy of the binary system decreases and the binding energy increases (1.13) creating a harder binary system. Considering the results on hard binary systems and soft binary systems we arrive at Heggie's Law: hard binary stars get harder and soft binary stars get softer.

There is extensive observational evidence for binary stars in globular clusters. A good overview can be found in Hut et al. (1992).

1.5.3 Post-collapse expansion

We have discussed the behavior of single star interactions with binary stars in Sect. 1.5.1 and Sect. 1.5.2. We now discuss the relevance that these interactions have on globular cluster evolution. Interactions with soft binary systems will usually result in a decrease in kinetic energy of the single star and the center of mass of the binary star. The long-term effects of interactions with soft binary stars are minimal because these systems

dissolve in a short timescale (much less than the relaxation time) and their energy is much less than that of the stars. Interactions with hard binary stars usually result in an increase in kinetic energy of center of mass of the binary star and the kinetic energy of the single star. Also, hard binary stars usually increase binding energy as a result of interactions with a single star and then are more difficult to break up. Overall, interactions between single stars and binary stars over time results in an increase in temperature of the system.

In some respects, a binary star behaves similarly to a star with mass $m = m_1 + m_2$ and as we know from Sect. 1.3 stars with heavier mass sink towards the center of the cluster. The binary stars sink towards the center of the system due to mass segregation and when the core collapses the center of the cluster becomes increasingly more dense. Thus, the interactions between single stars and binary stars increase and this becomes a heat source for the center of the region. This mechanism is referred to as binary heating.

If there is enough binary heating, this heat source can prevent gravothermal catastrophe or halt it when the density becomes large enough. The central region expands, which results in an expansion of the entire cluster. The works of Hénon (1961, 1965), were the first to use a Fokker-Planck model of globular clusters with a self-similar solution. Self-similarity was originally used as an assumption to make the solution tractable. It is fortunate that the assumption of self-similarity leads to a solution of great significance in applications. We review the work of Hénon (1961) in Chapter 3 and generalize this work for a two-component model in Chapter 4. In Inagaki and Lynden-Bell (1983), they find a homologous post-collapse expansion similar to the self-similar contraction found in the late stages of core collapse (Lynden-Bell and Eggleton, 1980). Self-similar post collapse expansion can be seen in the results of the N-body simulations from Baumgardt et al. (2002), shown in Fig. 1.4. After core collapse (which has been scaled to occur at $T \approx 1000$ for all simulations) the log-log plot of the Lagrangian radii expand at the same rate.

Although, binary heating is the primary energy source considered for post-collapse expansion (as it is the only mechanism which works in a pure N-body problem), there is some debate as to how the binary population was formed in the first place. A binary system is formed either by a close interaction between three stars or the binary system is formed simultaneously with the formation of the stars. Binary stars that are formed from birth are referred to as *primordial binary stars*. Since binary star formation through three-body interactions is difficult, it may be that many binary stars are primordial. There is also some debate as to whether the core expands indefinitely or if the evolution takes place in a series of expansions and contractions known as *gravothermal oscillations* (Hut et al., 1992).

1.6 Models for globular clusters

There are various techniques used in modeling globular clusters. Each model is founded on different principles and assumptions. We will discuss the more commonly used models, the theory behind the model and any advantages or disadvantages for each particular model.

1.6.1 Simple models

Simple models, often referred to as toy models, take well-known theory along with certain assumptions to create a simplified model of the system. Simple models vary widely depending on the particular interest of the person creating the model.

The advantage to simple evolving models is the ability to isolate various mechanisms so that one can determine which mechanisms are important in the study of certain effects; which may not be clear in a more realistic model. This is particularly true with 'kitchen sink' models which try to include as many mechanisms into the model as possible to realistically model globular clusters. Some examples of work done through evolving simple models is the theoretical work of Spitzer (1969) and Lightman and Fall (1978). The simple model presented in Chapter 2 is based upon the work shown in these papers.

1.6.2 Static models

A static model makes the assumption that the system is in quasi-static equilibrium and therefore can be described by a model which does not evolve. A classic example of a static model is the *isothermal sphere*. In the isothermal sphere the positions of stars are represented by a continuous *distribution function*.

The distribution function f is defined such that $f(\overrightarrow{x}, \overrightarrow{v}, t)\mathrm{d}^3\overrightarrow{x}\mathrm{d}^3\overrightarrow{v}$ is the probability at time t that a randomly chosen star is found in a box $\mathrm{d}^3\overrightarrow{x}\mathrm{d}^3\overrightarrow{v}$ around the coordinate $(\overrightarrow{x}, \overrightarrow{v})$ in *phase space*. Any stellar orbit follows a path in the six-dimensional space referred to as phase space, where the coordinates are the three-dimensional position vector and velocity vector. We can also write the distribution function as a function of E, where E is the total energy per unit mass at the coordinate $(\overrightarrow{x}, \overrightarrow{v})$.

In an isothermal sphere, the distribution function f is described by the equation

$$f = Ae^{-BE} \tag{1.16}$$

where A and B are constants. In this model the velocity distribution is *Maxwellian* with a one-dimensional velocity dispersion $\sigma^2 = 1/B$ (Heggie and Hut, 2003).

The isothermal sphere model is not a particularly realistic model of globular clusters, as it has a density $\rho(r) \propto r^{-2}$ for larger r, which implies that the system has infinite mass. However the isothermal sphere has been of great importance for the thermodynamic understanding of globular clusters (Antonov 1962, Lynden-Bell and Wood 1968) .

The static models that have had the most significant observational relevance are the King models. These models are based upon the work of King (1966). The distribution function is similar to that of the isothermal sphere except that the King model includes a maximum energy E_0 which is the escape energy of the system. This can be described by the piece-wise function

$$f(x) = \begin{cases} A\left(e^{-BE} - e^{-BE_0}\right) & : E < E_0 \\ 0 & : E > E_0 \end{cases} \tag{1.17}$$

The King model has been very successful in comparison with observations of globular clusters.

The final commonly used static model that we will discuss is Plummer's model. This model was created by Plummer (1911) in an attempt to fit the observations of clusters. The physical properties density ρ, total mass M and gravitational potential U within the radius r are

$$\begin{aligned} \rho(r) &= \frac{3M}{4\pi R^3} \times \frac{1}{(1 + r^2/R^2)^{5/2}}, \\ M(r) &= M \times \frac{r^3/R^3}{(1 + r^2/R^2)^{3/2}}, \\ U(r) &= -\frac{GM}{R} \times \frac{1}{(1 + r^2/R^2)^{1/2}} = -2\left\langle v^2(r)\right\rangle, \end{aligned} \tag{1.18}$$

where R is a scaling factor related to the half-mass radius.

Plummer's model is based on an $n = 5$ *polytrope*. A polytrope is a solution to the Lane-Emden equation

$$\frac{1}{\xi^2}\frac{d}{d\xi}\left(\xi^2 \frac{d\mu_T}{d\xi}\right) = -\mu_T^n, \tag{1.19}$$

where ξ is a radial coordinate obtained by scaling with the central density ρ_0 and pressure P_0 through the expression

$$\xi = r\sqrt{\frac{4\pi G\rho_0^2}{(n+1)P_0}} \tag{1.20}$$

and μ_T is related to the density ρ and the central density ρ_0 through the expression

$$\rho = \rho_0 \mu_T^n. \tag{1.21}$$

A polytrope is known for its relationship between P and ρ which is of the form $P \propto \rho^{1+1/n}$ (Heggie and Hut 2003, Padmanabhan 2000).

The advantage to using a Plummer's model is that it is a reasonably realistic static model but can also be described in terms of very simple functions. For this reason it is commonly used to derive the initial conditions of N-body models.

1.6.3 N-body models

Simulating the evolution of globular clusters through N-body modeling involves finding the change in position of the i^{th} star by calculating the gravitational force from every other star in the system. This can be described by the equation of motion

$$\overrightarrow{\ddot{r}}_i = \overrightarrow{a}_i = -\sum_{j \neq i} \frac{Gm_j\,(\overrightarrow{r}_i - \overrightarrow{r}_j)}{|\overrightarrow{r}_j - \overrightarrow{r}_i|^3}, \tag{1.22}$$

where $\overrightarrow{r}_i$ is the position vector, $\overrightarrow{a}_i$ is the acceleration vector and m_i is the individual stellar mass. This is often written as the system of equations

$$\begin{aligned} \overrightarrow{\dot{r}}_i &= \overrightarrow{v}_i \\ \overrightarrow{\dot{v}}_i &= -\sum_{j \neq i} \frac{Gm_j\,(\overrightarrow{r}_i - \overrightarrow{r}_j)}{|\overrightarrow{r}_j - \overrightarrow{r}_i|^3}, \end{aligned} \tag{1.23}$$

where $\overrightarrow{v}_i$ is the velocity vector (Aarseth, 2003). The first N-body calculation of this kind was shown in von Hoerner (1960) for $N = 16$. The advantage to N-body simulation, especially direct N-body simulation, is no assumptions are made, other than those required for the initial conditions.

The disadvantage of N-body calculations is the computation time required for large N. A straightforward N-body integration would require computational time of order N^2 for each t_{cross}. However, there has been significant improvement in the computation time through implementing a *tree code*. A tree code is a method of subdividing the stars in the cluster so that when calculating (1.23) for star i, n stars that are distant from star i can be approximated with one massive star instead of calculating these n stars individually. When a tree code is implemented, the computation time is of order $N \log N$ for each t_{cross} (Barnes and Hut, 1986). Even with this improvement, running N-body calculations for realistic values of N is extremely time consuming.

This problem of computation time for N-body models has also been addressed through a series of hardware devices known as the GRAPE[1] (Gravity Pipe) which are designed to speed up the N-body calculation. GRAPEs have the function $1/r^2$ built into their hardware. This speeds up the force calculation in an N-body system, which

[1] www.astrogrape.org

is the most time consuming calculation for N-body simulations. The most recent of the GRAPE series is the GRAPE-DR. This promises to be very successful in increasing the speed of computing N-body calculations.

The disadvantage is that GRAPEs are expensive and they will likely become increasingly more expensive unless they can be marketed to other areas of research as well. The latest high-end GPUs (graphics processing units) have become incredibly fast and are reasonable cheap as there is a large demand for these advanced GPUs in the retail market. The speed, accessibility and relatively low cost of these GPUs has generated interest in utilizing them for N-body simulation (Schive et al., 2008). The downside to programming on a GPU is that they are generally only single precision. Double precision is possible to achieve in software, but this slows down the speed of the calculation. There are some double precision GPUs which have recently become available, but they are much more expensive than the single precision GPUs. Nevertheless, GPUs have for the present replaced GRAPEs as the method of choice for N-body simulations of star clusters.

1.6.4 Fokker-Planck models

The *Fokker-Planck equation* is frequently used to describe the evolution of the distribution function of a globular cluster with time. In its simplest form, the Fokker-Planck equation for a globular cluster can be written generally as

$$\left(\frac{\partial f}{\partial t}\right)_{\rm enc} = -\sum_{i=1}^{3}\frac{\partial}{\partial v_i}\left(fD[v_i]\right) + \frac{1}{2}\sum_{i,j=1}^{3}\frac{\partial}{\partial v_i \partial v_j}\left(fD[v_i v_j]\right), \tag{1.24}$$

where

$$\begin{aligned} D[v_i] &= \int \Psi(v,\Delta v)\Delta v_i {\rm d}\Delta v, \\ D[v_i v_j] &= \int \Psi(v,\Delta v)\Delta v_i \Delta v_j {\rm d}\Delta v, \end{aligned} \tag{1.25}$$

are known as the diffusion coefficients. In (1.25), $\Psi(v,\Delta v)d\Delta v$ is the probability that during a unit time interval a star with velocity v will change by Δv within the range $d\Delta v$. In addition, Poisson's equation

$$\bigtriangledown^2 U = 4\pi G m \int f {\rm d}^3 v, \tag{1.26}$$

must hold.

This was first used by Chandrasekhar (1943a, 1943b) to describe two-body relaxation of globular clusters. Since the evolution of a globular cluster takes place on the relaxation timescale, which we have shown in Sect. 1.2 to be much longer than

the crossing time, we can average over the orbital motion. The orbit-averaged Fokker-Planck equation was first shown in Kuzmin (1957). It was later used by Hénon (1961, 1965).

For a long time, Fokker-Planck models were limited to one dimensional models (i.e. it is assumed that the distribution function depends on the velocity only through its magnitude). This is largely due to the success of a finite-difference scheme which was developed by Chang and Cooper (1970). This scheme was implemented for the purpose of calculating Fokker-Planck models of stellar systems by Cohn (1979, 1980) and later used by Inagaki and Wiyanto (1984) and Chernoff and Weinberg (1990).

Unfortunately, no one has been able to extend a finite-difference scheme like the one shown in Chang and Cooper (1970) for multiple dimensions. If we are limited to one dimensional Fokker-Planck models then we cannot have a distribution function that is dependent on other useful variables like the angular momentum J. Therefore, these one-dimensional Fokker-Planck equations must have an isotropic velocity distribution. In a one-dimensional Fokker-Planck model we can create a multi-mass system by using multiple distribution functions. Each distribution functions f_m represents one group of stars with the same mass. If we do this we cannot get a continuous mass distribution, but we can certainly have multiple star populations with varying stellar mass.

Amongst some of the major advances in Fokker-Planck models are the extensions to make an anisotropic Fokker-Planck model and a rotating Fokker-Planck model. Originally, the Fokker-Planck models were mainly for isotropic systems. Spherical symmetry was assumed, thus f can be independent from J. Takahashi (1993a) created a scheme for calculating multi-dimensional models and has effectively used this scheme to calculate two-dimensional Fokker-Planck models which depend on E and J (Takahashi 1995, Takahashi 1996). The work shown in Einsel and Spurzem (1999) utilizes the two-dimensional Fokker-Planck model and finds f as a function of E and the angular momentum in the z-direction J_z in order to make a rotating system.

1.6.4.1 Monte-Carlo method

Although this does not have significant importance to the work described in this thesis, it is important to note that a commonly used method for approximating the solution of the Fokker-Planck equations is through a Monte-Carlo method. Generally stated, the method involves subdividing the globular cluster into shells, where the stars in the shell have the same mass m, radial velocity v_r and tangential velocity v_t and the effects on the stars through gravitational encounters are emulated through randomly generated perturbations.

There are two main branches of Monte-Carlo Schemes for modeling globular

clusters: the Princeton models and Hénon's models. The Princeton models are based on the work described in Spitzer and Hart (1971a) and Spitzer and Hart (1971b) and follow the stars around in their orbits, allowing them to model processes that occur on crossing timescales and relaxation timescales. Hénon's models are based on the work described in Hénon (1971b, 1971a) and assumes dynamical equilibrium. Hénon's work is the basis of the Monte Carlo methods which are in current use, including those of Giersz (1998) and Fregeau et al. (2003) .

1.6.5 Gas models

A commonly used model, which will not be discussed in depth here, but is certainly worth mentioning is the gas model. This approach was introduced in Larson (1970). It uses the similarities between a gas consisting of many atoms and a stellar system consisting of many stars to develop a fluid-dynamical approach for modeling globular clusters.

1.7 Present work

The work described in this thesis will focus on homologous evolution in the post-collapse phase of globular cluster evolution with particular emphasis on two-component systems. The outline of the thesis is as follows:

Chapter 2: We will build a simple two-component model with a core, considering only two-body relaxation and a binary heating term (which can be removed) to consider the effects of binary heating on globular cluster evolution. We will do this by first considering two simpler models; a two-component model without a core and a single mass model with a core. To create our simple model we merge these two simpler models together and some constants need to be considered while doing this. We then compare the simple model to N-body calculations which use a GPU for large values of N.

Chapter 3: We will review the theoretical work of Hénon (1961) to derive a single mass Fokker-Planck model in the post-collapse phase of evolution. We will then discuss the numerical scheme we used to approximate the solution of the distribution function of the Fokker-Planck model and compare our results to the results presented in Hénon (1961).

Chapter 4: We will derive a two-component Fokker-Planck model in the post-collapse phase of evolution in a similar manner to deriving the single mass model. This model will have two distribution functions; f_1, the distribution of stars with an individual stellar mass m_1 and f_2, the distribution of stars with individual stellar mass

$m_2 > m_1$. Unlike the work in Hénon (1961) which assumes that the number of stars with mass m_2 are small, we will have no restrictions on this population. We will find that the Fokker-Planck equation cannot be solved numerically using this approach.

Chapter 5: We will summarize the work shown in this thesis and discuss possible future work.

2

Simple Two-component Models of Stellar Systems

In this chapter, we build a simple two component model with a core. We do this by constructing two simpler models – a two-component model without a core and a single mass model with a core – and merging these to models to form our final model. With the final model we show that 2-body relaxation and binary heating is enough to explain homologous post-collapse expansion.

2.1 Simple two-component model

In this section, we will consider a stellar system of two populations; a population of stars with an individual stellar mass m_1 and a population of stars with an individual stellar mass m_2, where $m_2 > m_1$. A system with two stellar populations is also referred to as a two-component system. We will construct two such cases of this two-component model. In the first case, we only consider two-body relaxation to construct the dynamical system. In the second case, we consider binary heating in addition to two-body relaxation.

2.1.1 Model Ia: Two-component model neglecting binary heating

In the construction of a simple two-component model, we make many assumptions that are similar to those of Lightman and Fall (1978). We assume that the cluster is spherically symmetric and that the stellar system can be subdivided into a region dominated by stars of mass m_2 (we will refer to these as the heavy stars) and a region dominated by stars of mass m_1 (we will refer to these as the light stars). The light stars are uniformly distributed within the system and have a half-mass radius of r_1 (see Sect. 1.1.2 for the definition of the half-mass radius). The heavy stars are uniformly distributed throughout a sphere with the half-mass radius r_2, where $r_2 \leq r_1$. The total mass and the number of stars for population i are denoted as M_i and N_i, respectively.

We begin with a two-component globular cluster in virial equilibrium. If the system is in virial equilibrium, we can use an approximation of the mean square velocity of population i, $\langle v_i^2 \rangle$, found in Spitzer (1969) to obtain the total kinetic energy T_i of each population

$$\begin{aligned} T_1 &= \frac{1}{2}\left(\frac{GM_1^2}{r_1} + \frac{GM_1M_2}{r_1}\right), \\ T_2 &= \frac{1}{2}\left(\frac{GM_2^2}{r_2} + \frac{GM_1M_2r_2^2}{r_1^3}\right), \end{aligned} \tag{2.1}$$

where G is the gravitational constant. Since the system is in virial equilibrium, the condition

$$2T + U = 0, \tag{2.2}$$

where U is the potential energy, must hold. It is important to note that some of the constants in (2.1a) and (2.1b) have been set to unity for simplicity and will be addressed in Section 2.3.3. However, we have left the constant of one half in these equations to ensure that the system can be in virial equilibrium even when M_1 or M_2 is null.

To construct this model, we consider the exchange of energy between the two-components through gravitational interactions and the changes in our system to reestablish virial equilibrium. Since escape takes place on a timescale much slower than relaxation (as discussed in Sect. 1.2), escape does not have a significant effect on the evolution of the system and can therefore be neglected for simplicity.

At present, we only consider the change in energy of each population through gravitational interactions. When encounters between light stars and heavy stars occur, kinetic energy is transferred between each mass group. This is expressed in Spitzer (1969) as

$$\dot{T}_{\mathrm{enc},1} = -\dot{T}_{\mathrm{enc},2} = N_2\left(\frac{T_2}{N_2} - \frac{T_1}{N_1}\right)/t_{\mathrm{eq}}(2,1), \tag{2.3}$$

where

$$t_{\rm eq}(2,1) = \frac{\left[\langle v_1^2\rangle + \langle v_2^2\rangle\right]^{3/2}}{8\sqrt{6\pi}\rho_{01}G^2 m_2 \ln N_1}. \tag{2.4}$$

We use ρ_{01} to denote the central density of the light stars, as done in Spitzer (1969).

Firstly, we allow the kinetic energy to transfer for a small time interval, Δt, without allowing the system to revirialize. The kinetic energy of population i, the total energy of population i and the total energy of the system after the time interval Δt has elapsed, are referred to as T_i', W_i' and W', respectively. Note that when the interval Δt has elapsed the system is no longer in virial equilibrium. The kinetic energy of each component can be described by

$$\begin{aligned} T_1' &= T_1 + \dot{T}_{\rm enc,1}\Delta t, \\ T_2' &= T_2 - \dot{T}_{\rm enc,1}\Delta t. \end{aligned} \tag{2.5}$$

Although the kinetic energy of the populations has changed, the half-mass radii have not changed. The system will adjust further until it returns to virial equilibrium. During this process of revirialization, the kinetic energies and the half-mass radii both adjust such that (2.2) holds. We denote quantities at the end of this revirialization phase with double primes.

To consider the changes in the kinetic energies and the half-mass radii that occur during revirialization, we first examine the total energy of light stars. Since heavy stars exist in a denser region in the center of the system (see Sect. 1.3 for explanation), we can approximate the heavy stars as a stationary point mass. In this scenario, the potential due to the heavy stars is static. Thus, the total energy of the light stars is nearly constant during revirialization. In other words,

$$W_1'' = W_1'. \tag{2.6}$$

The total energy of the light stars before revirialization can be written as

$$W_1' = T_1' - \frac{GM_1^2}{r_1} - \frac{GM_1M_2}{r_1} \tag{2.7}$$

and the total energy of the light stars after revirialization can be written as

$$W_1'' = T_1'' - \frac{GM_1^2}{r_1''} - \frac{GM_1M_2}{r_1''}, \tag{2.8}$$

where W_i'', T_i'', r_i'' and W'' are the total energy of population i, the kinetic energy of population i, the half-mass radius of population i and the total energy of the system after the system has revirialized, respectively.

We find the equations for T_1'' and T_2'' by substituting r_1 and r_2 in equations (2.1a) and (2.1b) with r_1'' and r_2'', respectively. Given (2.6), we use (2.7) and (2.8) for W_1' and W_1'', respectively, to approximate the change in kinetic energy during this process

$$T_1'' - T_1' = -\left(\frac{GM_1^2}{r_1^2} + \frac{GM_1M_2}{r_1^2}\right)(r_1'' - r_1). \tag{2.9}$$

From the equation above and (2.5a), we find the total change in kinetic energy of the light stars

$$T_1'' - T_1 = -\left(\frac{GM_1^2}{r_1^2} + \frac{GM_1M_2}{r_1^2}\right)(r_1'' - r_1) + \dot{T}_{\text{enc},1}\Delta t. \tag{2.10}$$

Similarly, we use the equation for total energy

$$W = T_1 + T_2 - \frac{GM_1^2}{r_1} - \frac{GM_2^2}{r_2} - \frac{GM_1M_2}{r_1}, \tag{2.11}$$

and the conservation of total energy of the system

$$W'' = W, \tag{2.12}$$

where W'' is found by substituting T_1'', T_2'', r_1'' and r_2'' for T_1, T_2, r_1 and r_2, respectively in (2.11), to approximate the change in kinetic energy of the heavy stars

$$T_2'' - T_2 = -\frac{GM_2^2}{r_2^2}(r_2'' - r_2) - \dot{T}_{\text{enc},1}\Delta t. \tag{2.13}$$

We use the expression for T_1 from equation (2.1a) and the equivalent for T_1'' to find

$$T_1'' - T_1 = \frac{1}{2}\frac{GM_1^2}{r_1''} + \frac{1}{2}\frac{GM_1M_2}{r_1''} - \left(\frac{1}{2}\frac{GM_1^2}{r_1} + \frac{1}{2}\frac{GM_1M_2}{r_1}\right), \tag{2.14}$$

We compare the Taylor series expansion for the above equation with the equation for $T_1'' - T_1$ found in (2.10) to obtain the approximate equation

$$\dot{T}_{\text{enc},1} = \frac{1}{2}\left(\frac{GM_1^2}{r_1^2} + \frac{GM_1M_2}{r_1^2}\right)\frac{r_1'' - r_1}{\Delta t}. \tag{2.15}$$

Due to our assumption that Δt is small, this is simplified to

$$\dot{T}_{\text{enc},1} = \frac{1}{2}\left(\frac{GM_1^2}{r_1^2} + \frac{GM_1M_2}{r_1^2}\right)\dot{r_1}. \tag{2.16}$$

We then substitute $\dot{T}_{\text{enc},1}$ in the above equation with (2.3), using (2.1a) and (2.1b) for T_1 and T_2, respectively. Solving for $\dot{r}_1$, we arrive at the first of two differential equations which describe our dynamical system

$$\dot{r_1} = \frac{M_2^2r_1^3 + M_1M_2r_2^3 - (M_1 + M_2)N_2m_1r_1^2r_2}{r_1r_2M_1(M_1 + M_2)t_{\text{eq}}(2,1)}. \tag{2.17}$$

In (2.13), we use (2.1b) with the values r_1 and r_2 for T_2 and the values r_1'' and r_2'' for T_2'', to obtain a relation between $\dot{r}_1$, $\dot{r}_2$ and $\dot{T}_{\text{enc},1}$. We eliminate $\dot{T}_{\text{enc},1}$, with (2.3) and (2.16) to obtain a second differential equation

$$\dot{r_2} = \frac{M_1 r_2^2 (3M_2 r_2^2 - M_1 r_1^2 - M_2 r_1^2)}{M_2 r_1 (M_2 r_1^3 + 2M_1 r_2^3)} \dot{r_1}. \tag{2.18}$$

Equations (2.17) and (2.18) are the fundamental equations for this two-component system.

2.1.2 Equipartition and equilibrium

In the two-component model shown in Spitzer (1969) equipartition was not possible when the ratio M_2/M_1 was sufficiently large. In this section, we will examine the criterion for equipartition for this model (model Ia) and compare this to the model in Spitzer (1969). We will also examine the condition for thermal equilibrium (which we will refer to as equilibrium) and the stability of the equilibrium.

Equipartition occurs when the temperature of the light stars is the same as the temperature of the heavy stars, where we use the term *temperature* to describe the mean kinetic energy per star. The definition of equipartition can be written as

$$T_1/N_1 = T_2/N_2 \tag{2.19}$$

(note this is the same as (1.9) for $n = 2$). From the expressions of kinetic energy of the light stars T_1 and the kinetic energy of the heavy stars T_2, found in (2.1a) and (2.1b), we find that (2.19) holds true when

$$\theta\left(\tilde{r}, \tilde{M}, \tilde{m}\right) := \tilde{M}\tilde{m} + \tilde{m}\left(\tilde{r}\right)^3 - \left(1 + \tilde{M}\right)\tilde{r} = 0, \tag{2.20}$$

where $\tilde{r}$, $\tilde{M}$, $\tilde{m}$ represent r_2/r_1, M_2/M_1 and m_2/m_1, respectively.

We say that our system is in a state of equilibrium when $\dot{r}_2 = \dot{r}_1 = 0$. To examine the requirements of equilibrium in our system we begin by rewriting (2.17) and (2.18) in terms of the functions η, ζ, θ and t_{eq},

$$\begin{aligned} \dot{r}_1 &= \eta(r_1, r_2) \frac{\theta(\frac{r_2}{r_1})}{t_{\text{eq}}(r_1, r_2)}, \\ \dot{r}_2 &= \zeta(r_1, r_2)\eta(r_1, r_2) \frac{\theta(\frac{r_2}{r_1})}{t_{\text{eq}}(r_1, r_2)}, \end{aligned} \tag{2.21}$$

where

$$\begin{aligned} \eta(r_1, r_2) &:= [r_1^4 r_2 M_1^2 M_2 (M_1 + M_2)]^{-1}, \\ \zeta(r_1, r_2) &:= \frac{M_1 r_2^2 (3M_2 r_2^2 - M_1 r_1^2 - M_2 r_1^2)}{M_2 r_1 (M_2 r_1^3 + 2M_1 r_2^3)}. \end{aligned} \tag{2.22}$$

It can be seen from (2.21a) and (2.21b) that our system can only be in a state of equilibrium if $f = 0$ or $\theta = 0$. From the definition of η, shown in (2.22a), we can see that η must always be greater than zero. Therefore, our system is in a state of equilibrium when

$$\theta\left(\tilde{r}, \tilde{M}, \tilde{m}\right) = 0. \tag{2.23}$$

From (2.20) and (2.23), we see the condition for equilibrium in this system is the same as the condition for equipartition. Therefore, when the system achieves equilibrium, then it is also is in equipartition. Thus, to find the criterion for equipartition, we must also understand the conditions for equilibrium and the stability of the equilibrium.

We proceed to examine the conditions for equilibrium. Given $\tilde{m}$, we find $\tilde{M}(\tilde{r})$ such that $\theta = 0$

$$\tilde{M}_{\theta=0}(\tilde{r}) \;=\; \frac{\tilde{m}\tilde{r}^3 - \tilde{r}}{\tilde{r} - \tilde{m}}. \tag{2.24}$$

In Fig. 2.1, the solid curve represents (2.24) when $\tilde{m} = 2$, $\tilde{M} \geq 0$ and $\tilde{r} \geq 0$. In this figure, we can see that there exists an $\tilde{r}_{\tilde{M}_{\max}} \geq 0$ such that $\tilde{M}_{\theta=0}(\tilde{r}_{\tilde{M}_{\max}})$ is the maximum value, $\tilde{M}_{\max}$, of the curve. If $\tilde{M} > \tilde{M}_{\max}$, the system cannot be in equilibrium and it follows that the system cannot achieve equipartition. These findings are similar to Spitzer (1969), where it is also shown that, given $\tilde{m}$, if $\tilde{M}$ is sufficiently large equipartition is no longer possible (see Sect 1.3).

We determine the stability of the system from the eigenvalues of the Jacobian matrix. We use (2.21a) and (2.21b) to find the characteristic equation of the Jacobian

$$\left|\breve{J} - \lambda\right|_{\theta=0} = \begin{vmatrix} \frac{-r_2}{r_1^2}\frac{\eta}{t_{\rm eq}}\theta'(\frac{r_2}{r_1}) - \lambda & \frac{1}{r_1}\frac{\eta}{t_{\rm eq}}\theta'(\frac{r_2}{r_1}) \\ \frac{-r_2}{r_1^2}\frac{\eta\zeta}{t_{\rm eq}}\theta'(\frac{r_2}{r_1}) & \frac{1}{r_1}\frac{\eta\zeta}{t_{\rm eq}}\theta'(\frac{r_2}{r_1}) - \lambda \end{vmatrix},$$

with eigenvalues

$$\begin{aligned} \lambda_1 &= 0, \\ \lambda_2 &= \frac{\eta}{r_1 t_{\rm eq}}\left(\zeta - \frac{r_2}{r_1}\right)\theta'. \end{aligned} \tag{2.25}$$

In this system, equilibrium occurs when $\theta(\tilde{r}) = 0$. Assuming that r_i, m_i and M_i are positive and $\tilde{r} \leq 1$ we find that $f > 0$, $(\zeta - \frac{r_2}{r_1}) < 0$ (see Appendix A) and $\frac{1}{r_1 t_{\rm eq}} > 0$. Therefore the stability of the system will be determined by the sign of θ', where the prime represents the derivative with respect to $\tilde{r}$. For $\theta' > 0$ the equilibrium is stable and for $\theta' < 0$ the equilibrium is unstable. If we find the derivative of condition (2.23) while assuming $\tilde{M} = \tilde{M}(\tilde{r})$ we obtain

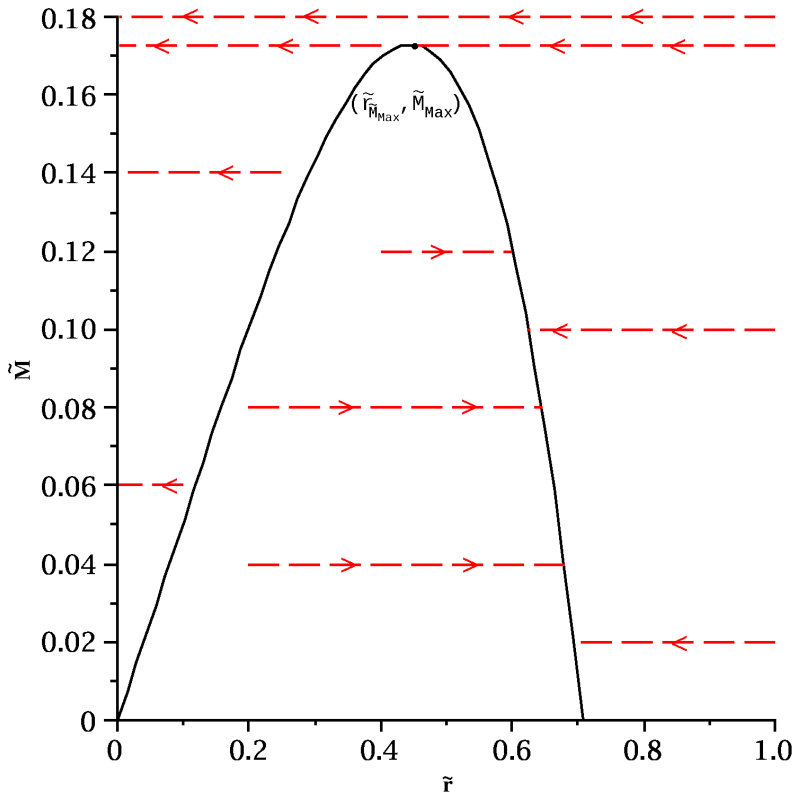

Figure 2.1: We show the equilibrium of the system and the stability of that equilibrium for $\tilde{m} = 2$. Given $\tilde{M}$, we begin with a given value $\tilde{r}(0)$ and $\tilde{r}$ evolves in the direction of the arrows. The solid curve is the predicted equilibria shown in (2.24). If $\tilde{r}$ reaches a point on the solid curve then it is in a state of equilibrium and $\tilde{r}$ remains constant. Depending on the value of $\tilde{M}$, the system has 0, 1 or 2 points of equilibrium. These points are the value of $\tilde{r}$ that corresponds to the solid curve. In the case where there are two equilibria, the equilibrium with the larger value is stable and the equilibrium with the smaller value is unstable. (2.24).

$$\theta'(\tilde{r}, \tilde{M}_{\theta=0}(\tilde{r})) + \frac{\partial\theta}{\partial\tilde{M}_{\theta=0}}\tilde{M}'_{\theta=0} = 0. \tag{2.26}$$

This can be simplified to

$$\theta'(\tilde{r}, \tilde{M}_{\theta=0}(\tilde{r})) = (\tilde{r} - \tilde{m})\tilde{M}'_{\theta=0}, \tag{2.27}$$

$$\tilde{M}'_{\theta=0} = \frac{2\tilde{r}^3 - 3\tilde{m}\tilde{r} + 1}{m(\tilde{r} - \tilde{m})^2}. \tag{2.28}$$

Considering that $\tilde{r} \leq 1$ and $\tilde{m} > 1$, then $(\tilde{r} - \tilde{m}) < 0$. As can be seen in Fig. 2.1, $\tilde{M}'_{\theta=0} > 0$ for $\tilde{r} < \tilde{r}_{\tilde{M}_{\max}}$ and $\tilde{M}'_{\theta=0} < 0$ for $\tilde{r} > \tilde{r}_{\tilde{M}_{\max}}$. Therefore, when $\tilde{r} < \tilde{r}_{\tilde{M}_{\max}}$, $\theta' < 0$ and the system is unstable. For $\tilde{r} > \tilde{r}_{\tilde{M}_{\max}}$, $\theta' > 0$ and the system is stable.

In Sect. 2.1.4, we use the computer mathematics package Maple[1] to examine the curve of equipartition and the stability found above. From our predictions, we anticipate the equilibria with $\tilde{r} < \tilde{r}_{\tilde{M}_{\max}}$ to be unstable and the equilibria with $\tilde{r} > \tilde{r}_{\tilde{M}_{\max}}$ to be stable. We also expect that the system should not be able to achieve equilibrium when $\tilde{M} > \tilde{M}_{\max}$. In Fig. 2.1, we assume that $\tilde{m} = 2$. Given a value for $\tilde{M}$ and an initial condition for $\tilde{r}$, the dashed lines represent the evolution of $\tilde{r}$ over time. The black curve is the predicted curve of equilibria given in (2.24). When $\tilde{M}$ is greater than the predicted $\tilde{M}_{\max}$, equipartition is not achievable and $\tilde{r}$ approaches zero. When $\tilde{M} < \tilde{M}_{\max}$, the initial value of $\tilde{r}$ determines whether the solution approaches or recedes from equilibrium. For $\tilde{r}_0$ greater than the predicted unstable equilibrium, $\tilde{r}$ tends towards the stable equilibrium. Otherwise, the system recedes from equilibrium. From Fig. 2.1, we can see that the stability of the equilibria agree with our predictions.

2.1.3 Model Ib: Two-component model where binary heating is considered

We will consider the changes to our model due to the introduction of binary stars. We will only consider the contribution of hard binary stars because the impact of soft binary stars on the system as a whole is negligible by comparison. Hard binary stars affect our system through a process known as binary heating. When a single star has a close encounter with a hard binary system, the usual outcome is that the binary stars becomes harder and, by energy conservation, the kinetic energy of the single star and the kinetic energy of the center of mass of the binary increase (see Sect 1.5 for a more detailed explanation). Binary stars, which are not primordial, are formed by an interaction between three stars. The likelihood of such an interaction depends strongly on the density of stars for the region in which the interaction would occur. For this reason, it is assumed that binary stars are predominately formed in the center of the cluster, which is dominated by heavy stars.

The kinetic energy per unit mass ϵ increases at a rate of

$$\epsilon \approx 85 \frac{G^5 m^5 n^2}{\sigma_c^7} \tag{2.29}$$

due to binary heating (Heggie and Hut, 2003), where σ_c is the one-dimensional velocity dispersion in the center of the cluster, n is the stellar number density in the core and m is the mean stellar mass in the core. Although (2.29) is a rate, we use the notation ϵ in accordance with the literature. We assume the region of heavy stars to have a uniform density in the construction of this model. Therefore, the region of heavy stars is also

[1] http://www.maplesoft.com/

the core of the system. We substitute $\langle v_2^2 \rangle$, n_2 and m_2 for σ_c^2, n and m, respectively.

A simple model can be constructed which is similar to the model in Section 2.1.1. The additional kinetic energy of heavy stars implies that T_2' defined in (2.5b) must now have an additional term. Thus,

$$T_2' = T_2 - \dot{T}_{\mathrm{enc},1}\Delta t + \epsilon M_2 \Delta t. \tag{2.30}$$

The binary stars do not directly change T_1, so (2.17) remains the same. It is important to note that $\dot{r_1}$ will be affected indirectly by binary heating; r_2 is directly affected by binary heating and has a direct influence on $\dot{r_1}$. The equations of the dynamical system can be described by the following equations

$$\begin{aligned} \dot{r_1} &= \frac{\eta}{t_{\mathrm{eq}}}\theta, \\ \dot{r_2} &= \frac{\eta\zeta}{t_{\mathrm{eq}}}\theta + \dot{T}_{\mathrm{b}}, \end{aligned} \tag{2.31}$$

where $\dot{T}_{\mathrm{b}}$ is referred to as the binary heating term for this system and is given by

$$\dot{T}_{\mathrm{b}} = 9.688 \frac{G^{1/2} N_2^2 m_2^5 r_1^{27/2}}{r_2^{1/2}(M_2 r_1^3 + M_1 r_2^3)^{7/2}(M_2 r_1^3 + 2M_1 r_2^3)}. \tag{2.32}$$

For equilibrium to be possible, both $\dot{r_1}$ and $\dot{r_2}$ must vanish. As we have shown earlier, $\dot{r_1} = 0$ when $\theta = 0$. When $\theta = 0$, $\dot{r_2}$ cannot be zero as the latter term in (2.31) is always positive. Unlike the model without binary heating, this system cannot be in equilibrium.

2.1.4 Comparing model Ia and model Ib

2.1.4.1 Phase portraits

To examine the impact that the binary heating term has on model I, we will compare the behavior of our system without this term and examine the changes when the binary heating term is added. We will do this with phase portraits and with plots of $r_1(t)$ and $r_2(t)$. We will use Maple for this analysis.

We create phase portraits for both models in three different cases. Fig. 2.2 shows the phase portrait of models Ia and Ib in the subcritical case ($\tilde{M} < \tilde{M}_{\max}$) , critical case ($\tilde{M} = \tilde{M}_{\max}$) and the supercritical case ($\tilde{M} > \tilde{M}_{\max}$), where $\tilde{M}_{\max}$ is the maximum value of $\tilde{M}$ at which equilibrium is achievable in the model which excludes the influence of binary stars.

In Fig. 2.2a, the arrows represent the direction of the gradient at that point. Two lines of equilibria are shown in this figure; one is stable, the other is unstable. When

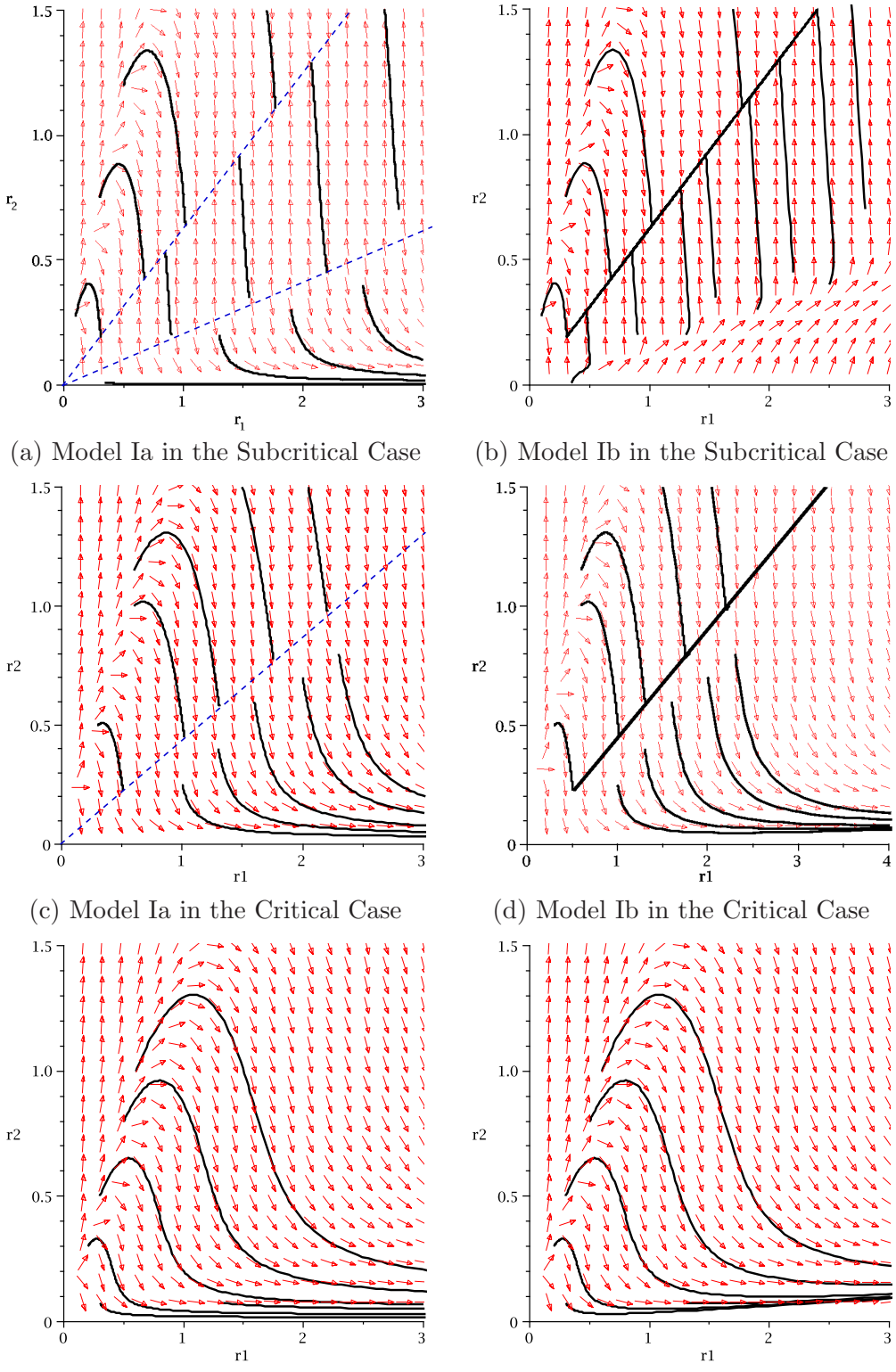

(a) Model Ia in the Subcritical Case (b) Model Ib in the Subcritical Case

(c) Model Ia in the Critical Case (d) Model Ib in the Critical Case

(e) Model Ia in the Supercritical Case (f) Model Ib in the Supercritical Case

Figure 2.2: Phase portraits for model Ia and model Ib. We compare model Ia and model Ib in 3 cases: the subcritical case ($\tilde{M} < \tilde{M}_{\max}$), the critical case ($\tilde{M} = \tilde{M}_{\max}$) and the supercritical case ($\tilde{M} > \tilde{M}_{\max}$). For all of these cases $N_1 = 200$ and $N_2 = 10, 17.2849, 30$ for the subcritical, critical and supercritical case, respectively.

the initial point (r_1, r_2) lies below the line of unstable equilibria, r_2 approaches zero as r_1 approaches infinity. Thus, the system cannot reach equilibrium and the core collapses. If the initial values are above the lines of unstable equilibria , but below the stable equilibria line, r_2 expands while r_1 contracts slightly until the system achieves equilibrium. Otherwise, the system will tend towards equilibrium, although in some cases where $r_2(0) > r_1(0)$ there is a period where r_2 expands before contracting towards equilibrium. Even though $r_2 > r_1$ is a very unlikely initial condition, we include this in Fig. 2.2 as it may serve some academic interest.

In Fig. 2.2b, the subcritical case for the model with binary stars is shown. The system no longer achieves equilibrium. There is a quasi-equilibrium where the line of stable equilibria existed and a remnant of what was the line of unstable equilibria in Fig. 2.2a. When r_1 and r_2 reach the line of quasi-equilibrium, the system expands slowly, along that line. For the initial conditions that resulted in a collapsing system in our original model, r_2 expands until the system reaches quasi-equilibrium.

The second case we will consider is the critical case. This occurs when $\tilde{M} = \tilde{M}_{\max}$. Fig. 2.2c shows the phase portrait for the model without the binary heating term. In the critical case, there is only one line of equilibria. When the initial values of r_2 and r_1 are above the equilibria line, the system reaches equilibrium. Otherwise, r_2 approaches zero while r_1 expands to infinity. Fig. 2.2d shows the model which includes binary heating. When the initial conditions are above the quasi-equilibrium line, r_2 and r_1 tend towards the line until the system is in a quasi-equilibrium state and the system then slowly expands along the line of quasi-equilibria. When the initial conditions are below the line of quasi-equilibrium, r_1 expands indefinitely while r_2 contracts to a minimum then slowly expands.

The last case we will examine is when the system is supercritical. This implies that $\tilde{M} > \tilde{M}_{\max}$. In Fig. 2.2e, we show the phase portrait of the model which excludes binary stars. In this model, the system is unstable for all $r_1(0)$ and $r_2(0)$. No matter what initial conditions we choose, r_1 will expand indefinitely and r_2 will collapse to zero. When binary stars are introduced to the system, as seen in Fig. 2.2f, r_2 collapses to a minimum value and expands with r_1 thereafter.

2.1.4.2 Comparing $r_1(t)$ and $r_2(t)$ in model Ia and model Ib

We investigate the impact that binary heating has on our model through examining the evolution of r_1 and r_2 in the case without binary heating (model Ia) and the case with binary heating (model Ib). We will do this for the supercritical case and the subcritical case. We omit the critical case as it behaves similarly to the subcritical case when $\tilde{r}(0) > \tilde{r}_{\tilde{M}_{\max}}$ and similarly to the supercritical case when $\tilde{r}(0) < \tilde{r}_{\tilde{M}_{\max}}$.

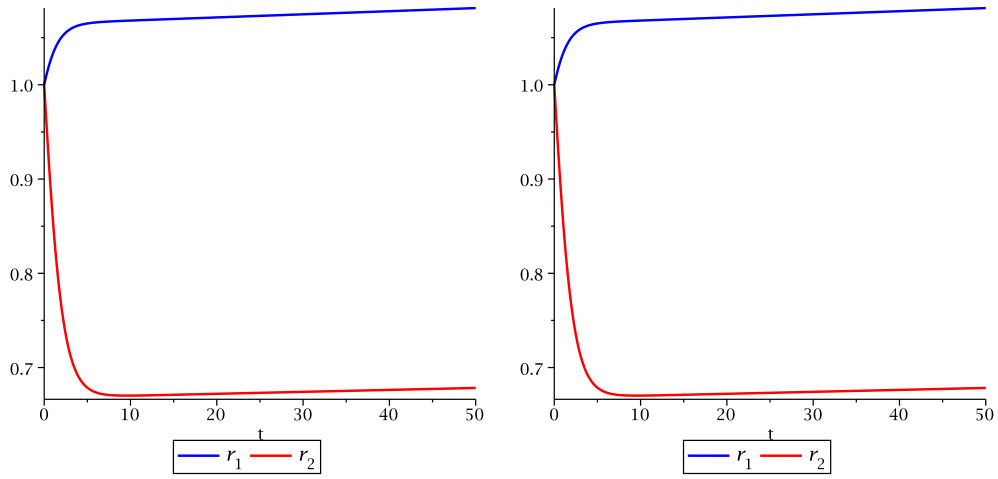

Figure 2.3: We plot $r_2(t/t_{rh}(0))$ (represented by the red line) and $r_1(t)$ (represented by the blue line) for the subcritical case where $\tilde{m} = 2$ and $\tilde{M} = 0.10$. We do this for model Ia (left) and model Ib (right).

The units of time are scaled for the initial half-mass relaxation time $t_{\rm rh}(0)$. To derive this, we use the expression for $t_{\rm rh}$ found in Spitzer and Hart (1971b) (see Sect. 1.2 for equation) with the initial value $r_{\rm h}(0)$.

In Fig. 2.3, we plot model Ia (left) and model Ib (right) in the subcritical case where $N_1 = 200$, $N_2 = 10$, $\tilde{M} = 0.10$ and $\tilde{m} = 2$. The initial value of $\tilde{r}$ is 1 and as you can see in Fig. 2.1, this is greater than the value which would lead to a stable equilibrium. In the left of Fig. 2.3, where there is no binary heating, the mass segregation takes place until equipartition is achieved. The system also reaches equilibrium at the same time and there is no further evolution of r_2 and r_1. When binary heating is considered (right of Fig. 2.3), there is also mass segregation until equipartition is achieved. Even though the system has reached a state of equipartition, equilibrium in the strictest sense is not possible. However, the system expands self-similarly in a quasi-equilibrium state.

In Fig. 2.4, we have model Ia (left) and model Ib (right) in the supercritical case where $N_1 = 200$, $N_2 = 30$, $\tilde{M} = 0.18$ and $\tilde{m} = 2$. We begin with $\tilde{r} = 1$ in both cases. In the left of Fig. 2.4 we have the supercritical system without binary heating. In this case we have indefinite mass segregation without ever reaching a state of equipartition. When we include binary heating (right of Fig. 2.4), r_1 expands indefinitely while r_2 contracts to a minimum value and then expands for the rest of the run. There is still some mass segregation after r_2 begins to expand, however the additional mass segregation is insignificant. In both the supercritical and subcritical case, the inclusion

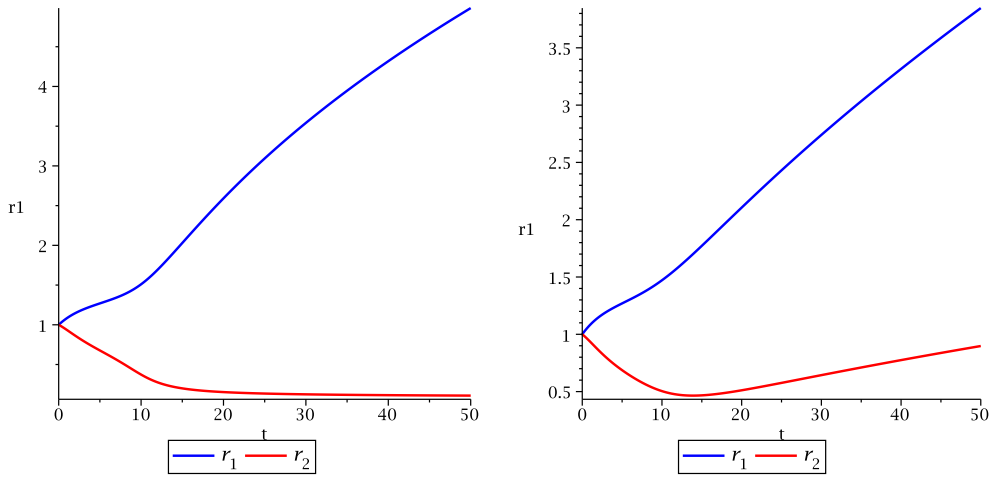

Figure 2.4: We plot $r_2(t/t_{rh}(0))$ (represented by the red line) and $r_1(t)$ (represented by the blue line) for the supercritical case where $\tilde{m} = 2$ and $\tilde{M} = 0.18$. We do this for model Ia (left) and model Ib (right).

of the binary heating term prevents the contraction of r_2. In the subcritical case, equipartition is achieved and there are no further signs of mass segregation even with the inclusion of binary heating. Whereas, in the supercritical case, equipartition is not achieved and there is mass segregation for the entire run, although in the case where we include a binary heating term the mass segregation is negligible once r_2 begins to expand.

We have shown in this simple two-component model the effects of binary heating. However, to obtain these results, we assumed that the core could be identified with the region of heavy stars. In actuality, there should be a denser core region within the region of heavy stars. To create a simple model that serves as a valid comparison to observed stellar systems, we will need to treat the core region as a separate entity. We will begin by examining a single mass model which is characterized by the half-mass radius of the cluster and the core radius.

2.2 Single mass model

In models Ia and Ib, we assumed that the heavy stars are uniformly distributed within a sphere. In actuality, a denser core region dominated by heavy stars should exist within the region of heavy stars. Since binary heating depends strongly on the distribution of heavy stars, the binary heating term in model Ib is inaccurate. In the present section,

we create a single mass model with a denser core region to later combine with our two-component model to create a two-component model with a denser core region within the region of heavy stars (Sect. 2.3).

In this section we will examine the behavior of a single mass model without binary heating and compare it to a single mass model with binary heating. We expect the behavior of the system which excludes binary heating to be approximately the same as the system which includes binary heating during the early stages of core collapse, because the binary heating term should not be significant until r_c is small. From N-body simulations of isolated single mass clusters we know that before the onset of core-collapse, the half-mass radius $r_{\rm h}$ should remain nearly constant (Baumgardt et al., 2002). We also know from the work on gravothermal instability (see Sect. 1.4) that after some time has elapsed the core radius $r_{\rm c}$ will contract. The difference between the two models should be shown in the late stages of core collapse when the core radius is small enough for the binary heating term to have a significant impact on the evolution of they system. In the case with no binary heating, we expect $r_{\rm c}$ to collapse completely and $r_{\rm h}$ to remain roughly constant. In the case where binary heating is included, we anticipate the core to collapse until it is small enough for binary heating to dominate the evolution of the star cluster and we shall see that $r_{\rm c}$ and $r_{\rm h}$ evolve self-similarly for the rest of the simulation.

2.2.1 Model IIa: Single mass model without binary heating

In the case with no binary heating, we consider a system with individual stellar mass m and total number of stars N. We consider the energy of the system

$$W = -\frac{1}{2}\frac{GM^2}{r_{\rm h}}. \tag{2.33}$$

When escape is ignored, any increase in W can only be caused by binary heating. Since we are considering a system without binary heating, we can conclude that

$$\dot{W} = 0. \tag{2.34}$$

It follows that

$$\dot{r}_{\rm h} = 0. \tag{2.35}$$

To find the equation for $\dot{r_{\rm c}}$, we consider the approximation given by Lynden-Bell and Eggleton (1980)

$$\dot{r}_{\rm c} = -k\frac{r_{\rm c}}{t_{\rm rc}}, \tag{2.36}$$

where the relaxation time of the core $t_{\rm rc}$ is

$$t_{\rm rc} = \left\langle v_{\rm c}^2 \right\rangle^{3/2} \left(8\pi G^2 m \rho_c \log N_{\rm c}\right)^{-1}, \tag{2.37}$$

k is constant and N_c is the number of stars in the core. To find an expression for $t_{\rm rc}$ in terms of r_c and r_h we will use the approximations shown in (2.47). This will be discussed further in Sect. 2.2.2.

To find the value for k, we consider the timescale for core collapse. From previous work, we know that core collapse takes place around $15t_{\rm rh}(0)$, where $t_{\rm rh}(0)$ is the initial half-mass relaxation time (Lynden-Bell and Eggleton 1980, Louis 1990, Quinlan 1996). Given N, we use Matlab[2] to find the value of k such that the time of core collapse, $t_{\rm cc}$, is approximately $15t_{\rm rh}(0)$. We repeated this process with many different values of N. From this we found the value for k to be about 0.01 for all values of N. This leads us to the following equations for our dynamical system, in the case where binary heating is ignored

$$\begin{aligned} \dot{r}_{\rm h} &= 0, \\ \dot{r}_{\rm c} &= -0.01\frac{r_{\rm c}}{t_{\rm rc}}. \end{aligned} \tag{2.38}$$

2.2.2 Model IIb: Single mass model with binary heating

When considering the case where binary heating is included, we take a similar approach to that in Sect 2.1.3. The energy, W, is the same as in (2.33), but now that the binary heating term is non-zero, $\dot{W}$ becomes

$$\dot{W} = \dot{T}_{\rm b}, \tag{2.39}$$

We define $\dot{T}_{\rm b}$ to be

$$\dot{T}_{\rm b} = M_{\rm c}\epsilon. \tag{2.40}$$

The subscript c is to denote the quantity in the core and ϵ was defined previously in (2.29). For future computations of this model, it will be useful to express $\dot{T}_{\rm b}$ as a function of r_c and r_h. From (2.29) we can rewrite ϵ as

$$\epsilon \approx 85\frac{G^5 m^3 \rho_c^2}{\sigma_c^7} \tag{2.41}$$

with the one-dimensional velocity dispersion

$$\sigma_c = \frac{1}{3}\left\langle v_c^2 \right\rangle, \tag{2.42}$$

since we have assumed that velocity dispersion is isotropic.

From (2.40), (2.41) and (2.42) we can see that approximations of $\rho_{\rm c}$, $\left\langle v_{\rm c}^2 \right\rangle$ and $M_{\rm c}$ in terms of r_c and r_h will be needed to find $\dot{T}_{\rm b}\left(r_{\rm c}, r_{\rm h}\right)$. The term $\dot{T}_{\rm b}$ will not be significant

[2] http://www.mathworks.com/products/matlab/

until the late stages of core collapse, therefore we will use the self-similar solution (see Sect 1.4.1) from Lynden-Bell and Eggleton (1980) to make these approximations. The density in the halo of the cluster can be found with the self-similar equation

$$\rho(r,t) = \tilde{A}\rho_c(t)\,(r/r_c(t))^{-\alpha}\,, \tag{2.43}$$

where r_c is the core radius, ρ_c is the density in the core, A is a constant and α is a constant which we will discuss further on. At $r = r_c$ the halo must turn smoothly over to the core, so (2.43) must still be a valid approximation for $r = r_c$. This means that

$$\rho(r_c,t) \approx A\rho_c(t), \tag{2.44}$$

which implies that $A \approx 1$.

We rearrange the self-similar solution for ρ, shown in (2.43), for $r = r_h$ to find the relation

$$\frac{\rho_{\rm c}}{\rho_{\rm h}} = \left(\frac{r_{\rm c}}{r_{\rm h}}\right)^{-\alpha}, \tag{2.45}$$

where r_h is the half-mass radius and ρ_h is the average density within the half-mass radius. We can also use the approximations

$$\begin{aligned} M &\propto \rho r^3, \\ \left\langle v^2 \right\rangle &\propto \frac{M}{r} \propto \rho r^2, \end{aligned} \tag{2.46}$$

to find the relations

$$\begin{aligned} \frac{\left\langle v_{\rm c}^2 \right\rangle}{\left\langle v_{\rm h}^2 \right\rangle} &= \left(\frac{r_{\rm c}}{r_{\rm h}}\right)^{2-\alpha}, \\ \frac{M_{\rm c}}{M_{\rm h}} &= \left(\frac{r_{\rm c}}{r_{\rm h}}\right)^{3-\alpha}, \\ \frac{N_{\rm c}}{N_{\rm h}} &= \left(\frac{r_{\rm c}}{r_{\rm h}}\right)^{3-\alpha}. \end{aligned} \tag{2.47}$$

Note that the division of the quantities at the core and the half-mass radius make the constants of proportionality in (2.46a) and (2.46b) insignificant. Using the approximations (2.45), (2.47a) and (2.47b), we can simplify the binary heating term as a function of $r_{\rm c}$ and $r_{\rm h}$

$$\dot{T}_{\rm b} = 28.3189 G^{\frac{3}{2}} N^{-\frac{1}{2}} m^{\frac{5}{2}} r_{\rm c}^{-4+\frac{\alpha}{2}} r_{\rm h}^{\frac{3}{2}-\frac{\alpha}{2}}, \tag{2.48}$$

where α is the constant found in Lynden-Bell and Eggleton (1980). There are varying values of α in the literature. Lynden-Bell and Eggleton (1980) found the value to be 2.21, where others have found $\alpha = 2.23$ (Cohn 1980, Heggie and Stevenson 1988, Takahashi 1993b, 1995). There have been some other values found, but most would

agree that $2 < \alpha < 2.5$ (Makino 1996, Baumgardt et al. 2003, Louis 1990). We have tried varying α within the range of values found in the literature and found no meaningful difference in our system, so we choose $\alpha \approx 2.21$, as found in Lynden-Bell and Eggleton (1980).

Now that we have our approximation for $\dot{T}_{\rm b}$, we will derive the first equation of our model by substituting the derivative of (2.33) into (2.39). We can find the the first equation of our single mass system with binary heating to be

$$\dot{r_{\rm h}} = \frac{r_{\rm h}\dot{T}_{\rm b}}{W}. \tag{2.49}$$

To construct the equation for $\dot{r}_{\rm c}$, we must understand the connection between the behavior of the system as a whole and the behavior of the core. We consider the explanation given by Hénon (1975). At any point in time the structure of the system corresponds to a temperature difference between the inner and outer regions and therefore dictates a definite outward flow of energy. Thus, the rate of this flow of energy is controlled by the system as a whole. If $r_{\rm c}$ was small enough that binary heating created more energy than is required, then the excess heat would remain in the core. This would cause the core to expand and this expansion would result in less binary heating. However, if the core was large enough that the required flow of energy is not met, then the core would contract and binary heating would increase. This feedback mechanism causes binary heating to supply the energy flux required by the system. In other words, the binary heating must adjust towards the energy flux of the system.

We can define the energy flux of the system to be the energy flux at half-mass radius, $\dot{W}_{\rm h}$. This can be approximated by

$$\dot{W}_{\rm h} \propto \frac{W_{\rm h}}{t_{\rm rh}}. \tag{2.50}$$

We require our system to have $\dot{r}_{\rm c} \propto r_{\rm c}/t_{\rm rc}$ when there is no binary heating, but with binary heating the system should mimic the behavior of the core as explained in Hénon (1975). Thus, we can describe $\dot{r}_c$ as

$$\dot{r}_{\rm c} = \frac{\left(\dot{T}_{\rm b} - \frac{|W_h|}{t_{\rm rh}}\right)\frac{r_{\rm c}}{t_{\rm rc}}}{\frac{|W_h|}{t_{\rm rh}}}. \tag{2.51}$$

As you can see from (2.51), when $\dot{T}_{\rm b} < \frac{|W_h|}{t_{\rm rh}}$, r_c decreases which would increase binary heating. When $\dot{T}_{\rm b} > \frac{|W_h|}{t_{\rm rh}}$, r_c increases which leads to a decrease in binary heating. This can be simplified to

$$\dot{r}_{\rm c} = \frac{r_{\rm c}}{t_{\rm rc}}\left(-0.01 + \frac{\dot{T}_{\rm b}t_{\rm rh}}{T_{\rm h}}\right) \tag{2.52}$$

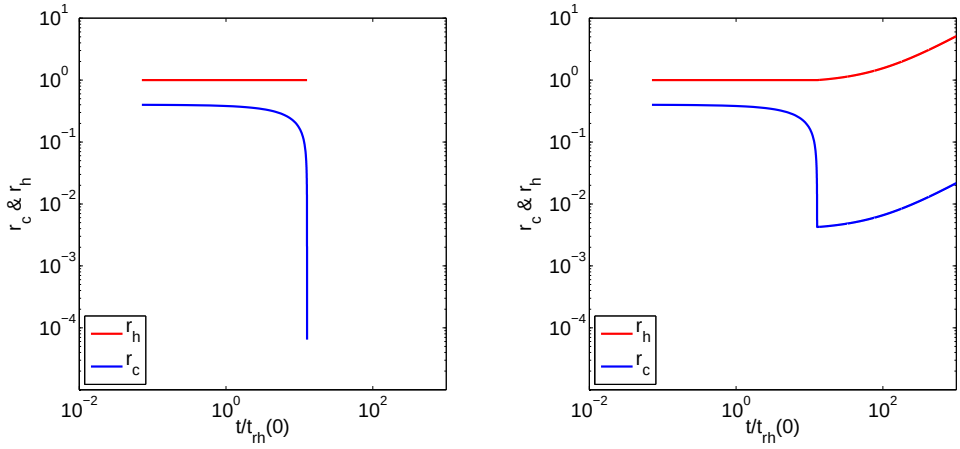

Figure 2.5: Here we show the single mass model for a system of 4,096 stars. The total mass of the system is unity. The plot on the left shows $r_h(t)$ (red)and $r_c(t)$ (blue) in the case which excludes binary heating (i.e. $\dot{T}_\mathrm{b} = 0$) and the plot on the right shows the case which includes binary heating.

where $|W_h| \propto T_h$ according to the virial theorem. As done in (2.38b), we have the constant 0.01 to the first term of (2.52), so in the case of no binary heating the core collapse time would be around $15t_{rh}(0)$.

It is apparent from these equations that the system can not achieve equilibrium in either of the two cases considered. In the system without binary heating, r_c is non-zero, therefore the right side of (2.38b) must always be non-zero. In the system with binary heating, r_h and $\dot{T}_\mathrm{b}$ are also non-zero, therefore the right side of (2.49) is also non-zero.

As predicted for the case without binary heating, in the left plot of Fig. 2.5 we see r_h remain constant while the core collapses towards zero. In our model the core does not collapse fully because of our approximation of N_c as shown in (2.47c). It is not physically possible for N_c to be less than one, but our approximation allows this to occur. To prevent this inconsistency, we stop the simulation when $N_\mathrm{c} \leq 1$.

When binary heating is introduced into the system, the behavior is about the same as the non-binary case until the core radius becomes small, as shown in the right of Fig. 2.5. Afterwords, the binary heating term dominates the evolution of the cluster causing it to expand. The core radius and the half-mass radius expand until the end of the run. In the post-collapse phase of evolution r_h is expanding at the same rate as r_c, therefore the post-collapse evolution is self-similar with no further signs of mass segregation

The results from the single mass model are consistent with our predictions. In the case with no binary heating, the core radius collapses to a small value which is

nevertheless greater than zero due to the approximation of N_c. Fortunately, this is not a problem in the case where binary heating is included; the core radius is always large enough for $N_c > 1$. The evolution of our single mass model when binary heating is considered is in qualitative agreement with the expected behavior of single mass models. The system behaves as it does in the case without binary stars until r_c becomes sufficiently small for the binary heating term to be significant to the cluster evolution. The binary heating eventually gives the system enough energy to halt core collapse and to set the system in a self-similar post-collapse evolution.

2.3 Combining model I and model II

2.3.1 Model IIIa: Combined model without binary heating

From sections (2.1) and (2.2), we have two models with different attributes. The first model is a two-component model which assumes that the region of heavy stars has a uniform distribution. The second model is a single-mass model with a separate denser region for the core. The aim is to combine these models together to obtain a two-component model with a separate core radius in addition to the half-mass radius of each population. The necessity for a separate core radius is simple; binary heating is concentrated in the core, so an unrealistic approximation of the core radius leads to an unrealistic binary heating term.

In this section, we consider our single mass model described in Sect. 2.2 and let the individual stellar masses be m_2. Now we embed this system in a uniformly distributed sphere of stars with the stellar mass m_3, where $m_2 > m_3$. To follow convention, we will refer to the half-mass radius of the light stars, the half-mass radius of the heavy stars and the core radius as r_3, r_2 and r_1, respectively.

Firstly, we will consider the case without binary heating. To obtain our equations for $\dot{r}_3$ and $\dot{r}_2$, we follow the same method used in deriving (2.21a) and (2.21b)

$$\begin{aligned} \dot{r}_3 &= \frac{\eta\theta}{C_1 t_{\rm eq}}, \\ \dot{r}_2 &= \zeta\frac{\eta\theta}{C_1 t_{\rm eq}} \end{aligned} \tag{2.53}$$

where

$$\begin{aligned} \eta(r_3, r_2) &= [r_3^4 r_2 M_3^2 M_2(M_3+M_2)]^{-1}, \\ \zeta(r_3, r_2) &= \frac{M_3 r_2^2(3M_2 r_2^2 - M_3 r_3^2 - M_2 r_3^2)}{M_2 r_3(M_2 r_3^3 + 2M_3 r_2^3)}, \\ \theta\left(\frac{r_2}{r_3}\right) &= \frac{M_2}{M_3}\frac{m_2}{m_3} + \frac{m_2}{m_3}\left(\frac{r_2}{r_3}\right)^3 - \left(1+\frac{M_2}{M_3}\right)\frac{r_2}{r_3}. \end{aligned}$$

As explained in Sect. 2.1, some constants have been ignored hitherto. These constants may not have changed the general features of these models but, when these models are combined and, especially, when it comes to quantitative comparison with simulations, these constants become important. We will deal with this by adding the constant C_1.

When examining the evolution of the core radius, we must take into account additional considerations. In some ways, the core should evolve independently as it does in the single mass model when binary heating is ignored. On the other hand, the core radius develops within the region of heavy stars and the evolution of these two regions is intertwined. For example, if the entire region of heavy stars contracts because of mass segregation, we would expect the core radius to follow the same contraction. Supposing we had a system as in the previous example where the evolution of r_1 followed the evolution of r_2 homologously, then we would have the condition

$$\dot{\left(\frac{r_1}{r_2}\right)} = 0, \tag{2.54}$$

where $\dot{\left(\frac{r_1}{r_2}\right)}$ denotes the derivative of the ratio r_1/r_2 with respect to time. On the other hand, if r_1 was not directly affected by r_2, we would obtain an equation similar to (2.38b). Therefore in our new model, we also incorporate the notion that r_1 should evolve on its own timescale. This can be achieved by replacing (2.54) with

$$\dot{\left(\frac{r_1}{r_2}\right)} = -0.01\frac{r_1/r_2}{t_{\rm rc}}. \tag{2.55}$$

We also know that

$$\dot{\left(\frac{r_1}{r_2}\right)} = \frac{\dot{r}_1}{r_2} - \frac{r_1}{r_2^2}\dot{r}_2 \tag{2.56}$$

From (2.55) and (2.56) we can derive $\dot{r}_1$

$$\dot{r}_1 = -0.01\frac{r_1}{t_{\rm rc}} + \frac{r_1}{r_2}\dot{r}_2. \tag{2.57}$$

Thus, (2.53a), (2.53b) and (2.57) describe our dynamical system.

2.3.2 Model IIIb: Combined model with binary heating

To add binary heating to this system we simply add the additional term that is found in (2.49) and (2.52), which is not in (2.38a) and (2.38b). These are the terms which are caused by binary heating. We substitute r_1 and r_2 for $r_{\rm c}$ and $r_{\rm h}$, respectively. From this we obtain the equations for our system with binary heating

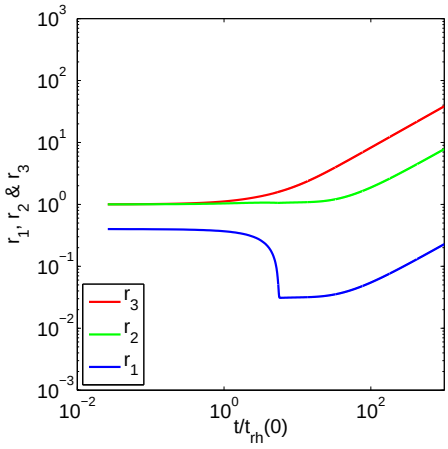

Figure 2.6: This is an example of our model using the values for C_1 and C_2 found in (2.61a) and (2.61b), respectively. We follow $r_3(t)$ (red), $r_2(t)$ (green) and $r_1(t)$ (blue) for $N = 8,192$, $N_2 = 2,048$ and $\tilde{m} = 4$.

$$\begin{aligned}
\dot{r}_3 &= \frac{\eta\theta}{C_1 t_{\rm eq}}, \\
\dot{r}_2 &= \zeta\frac{\eta\theta}{C_1 t_{\rm eq}} + C_2\frac{r_2\dot{T}_{\rm b}}{T_2}, \\
\dot{r}_1 &= \frac{r_1}{t_{\rm rc}}\left(-0.01 + C_2\frac{\dot{T}_{\rm b}t_{\rm rh}}{T_2}\right) + \frac{r_1}{r_2}\dot{r}_2
\end{aligned} \tag{2.58}$$

The explanation for an additional constant C_2 is similar to that for C_1, originally shown in (2.53). Until now, we have been largely concerned with the qualitative results of our models. To compare this model quantitatively with N-body simulation we need to consider constants for binary heating which were not previously needed. To take this into account we adjust the heating terms in our equations by a factor of C_2.

2.3.3 Deriving constants

As explained previously, when deriving the equations for the dynamical system in Sect. 2.1 some constants were ignored. To remedy this, we need a constant, C_1 for the equations from the original two-component system. Also, the binary heating term in Sect. 2.2 is neglecting a constant, C_2. Ignoring these constants may not have made a qualitative change in the results shown so far, but for direct comparison to N-body models these constants will become significant.

We will compare the final analytical model with binary heating (model IIIb) to N-body model to verify its validity. In order to do this we must first derive C_1 and

C_2. To derive C_1 and C_2 empirically, we first look at the conditions for the self-similar post-collapse evolution

$$\begin{aligned} \dot{\left(\frac{r_3}{r_2}\right)} &= 0, \\ \dot{\left(\frac{r_2}{r_1}\right)} &= 0. \end{aligned} \tag{2.59}$$

We expand (2.59a) and (2.59b). Then we substitute (2.58a), (2.58b) and (2.58c) to arrive at the general solution for the constants

$$\begin{aligned} C_1 &= 100\frac{\eta t_{\rm r2}}{t_{\rm eq} r_3}\left(1-\zeta\frac{r_3}{r_2}\right), \\ C_2 &= 0.01\frac{T_2}{\dot{T}_{\rm b} t_{\rm r2}}. \end{aligned} \tag{2.60}$$

We use `NBODY6` (Aarseth, 2000) with an initial Plummer model (for a description of the Plummer model see Sect. 1.6) for two components to find the average post-collapse values of r_2/r_1 and r_3/r_2 at many times in the post-collapse evolution. From r_2/r_1 and r_3/r_2, we derive C_1 and C_2. The results from this are shown in Table 2.1. From the range of values of N in Table 2.1, it is clear that there is an N dependence for the individual values of C_1 and C_2 (shown in the two latter columns in the table) that is not captured by the model. For this reason, we do not anticipate that our model would agree, even to the order of magnitude, with N-body simulation where N is greatly different to the values shown in Table 2.1.

We average the values in Table 2.1 to obtain

$$\begin{aligned} C_1 &= 2.51, \\ C_2 &= 1.30. \end{aligned} \tag{2.61}$$

We test these constants with an example which was not used to derive them (i.e. none of the cases found in Table 2.1). If these constants are acceptable then we expect this example to yield reasonable results. In Fig. 2.6, we examine a case not used in the derivation of C_1 and C_2. In this figure, the system exhibits all of the general features that an N-body simulation would contain. The core collapses to some minimum value at around $6t_{\rm rh}(0)$. While the core is collapsing, there is some sign of mass segregation; $(\log(r_3) - \log(r_2))$ increases. After the core reaches its minimum value, r_1 and r_2 immediately show a similar expansion and, after a certain period of time, the whole system expands self-similarly and there is no further mass segregation. Even though this example was not used in the derivation of our constants, the system seems to behave as one would expect.

N	N_2	$\frac{m_2}{m_3}$	C_1	C_2
1024	64	4	1.50	1.13
1024	64	8	2.10	0.84
1024	128	2	1.53	0.81
1024	128	4	2.14	0.87
1024	128	8	3.41	0.35
1024	256	2	2.67	1.79
1024	256	4	2.83	0.57
1024	256	8	4.35	0.51
2048	128	4	1.20	2.17
2048	128	8	2.32	1.43
2048	256	2	1.23	2.13
2048	256	4	1.88	1.38
2048	256	8	2.89	0.66
2048	512	2	2.77	1.23
2048	512	4	3.52	0.83
2048	512	8	4.42	0.42
4096	256	4	1.07	4.58
4096	256	8	1.68	1.48
4096	512	2	1.22	1.89
4096	512	4	1.88	1.59
4096	512	8	2.90	0.67
4096	1024	2	2.62	1.41
4096	1024	4	3.60	1.46
4096	1024	8	4.54	0.92

Table 2.1: Estimating the values of C_1 and C_2 by finding the ratios r_2/r_1 and r_3/r_2 after core collapse and substituting them into (2.60a) and (2.60b). The values of C_1 and C_2 found in (2.61a) and (2.61b) are the average of the individual values found in this table.

To further test the accuracy of our model, we will compare this model to N-body simulations. Due to fundamental differences in our model and an N-body simulation, we cannot expect our model to behave exactly as the simulation. However, we can expect our model to contain similar features to the simulations and the evolution will agree to order of magnitude.

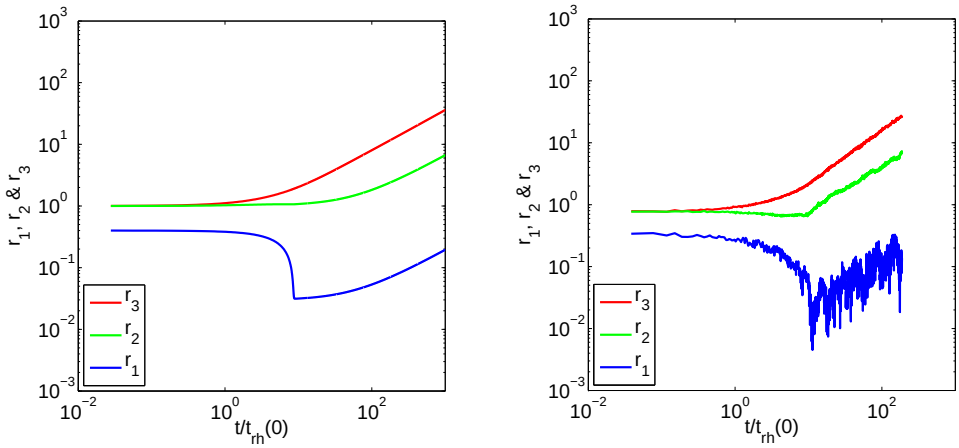

Figure 2.7: We compare $r_3(t)$ (red), $r_2(t)$ (green) and $r_1(t)$ (blue) for the analytical model IIIb (left) with the N-body simulation (right) in the case where $N = 4,096$, $N_2 = 2,048$ and $\tilde{m} = 4$.

2.4 Comparison with N-body simulations

In this section, we will examine the results of N-body simulations with the results of our analytical model (model IIIb). As before we use Aarseth's `NBODY6`, with an initial two-component Plummer model and examined the evolution of the half-mass radius of the light stars, r_3, the half-mass radius of the heavy stars, r_2 and the core radius r_1. Again, time t is scaled in units of the initial half-mass relaxation time $t_{\rm rh}(0)$

We do not expect our model to replicate the N-body model precisely. Besides variations in constants C_1 and C_2, there are several fundamental differences which would prevent this from happening. One fundamental difference is that our model does not take escape into account whereas the N-body model loses stars to escape throughout the simulation. We do however, expect our model to contain similar features to the simulation and evolve on a timescale that is the correct order of magnitude.

In Fig. 2.7, we have an example of our model where $N = 4,096$, on the left, and an N-body simulation with the same initial conditions on the right. Both of these models contain similar features. Both of these models show signs of mass segregation (i.e. $(\log(r_3) - \log(r_2))$ increases) before core collapse . Also, the core collapses to a minimum value and, after a certain period of time, the system undergoes a self-similar expansion with little evidence of further mass segregation for both of these models.

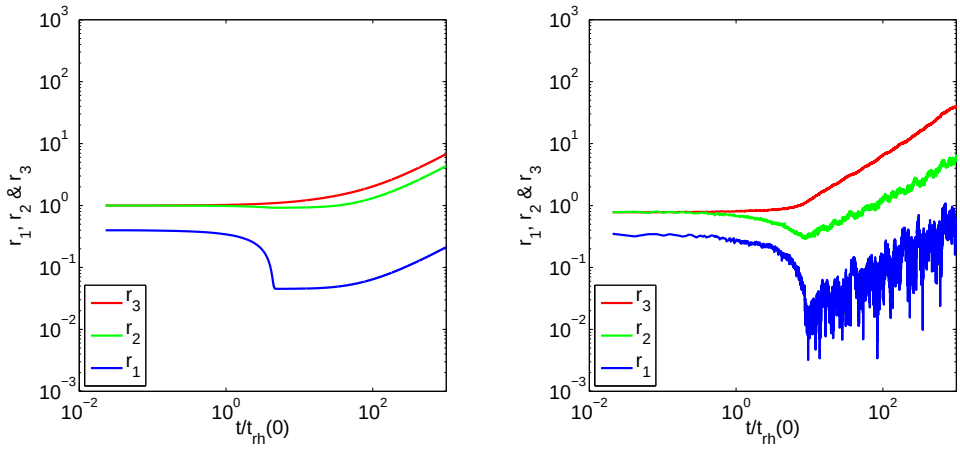

Figure 2.8: We compare $r_3(t)$ (red), $r_2(t)$ (green) and $r_1(t)$ (blue) for the analytical model IIIb (left) with the N-body simulation computed on a GPU (right) in the case where $N = 8,192$, $N_2 = 1,024$ and $\tilde{m} = 2$.

There are some differences between our model, on the left of Fig. 2.7, and the N-body model, on the right of Fig. 2.7. Core collapse occurs later and the minimum value of the core is smaller in the N-body model, than in our model. The expansion of the core immediately after core collapse is notably steeper in the N-body model and the final value of r_3, r_2 and r_1 are higher in the N-body model than in our model.

We now compare our final model for an example with $N = 8,192$. To accommodate the larger value of N, we use a GPU for the N-body simulation. We found that the GPU reached over 47 GFlops during the gravity calculations and took just over 24 hours to complete the run. We compared this to the results calculated on a 32-bit CPU, which took 2 weeks to complete, and found very little difference in our results. We show, in Fig. 2.9, the results of our N-body simulation as calculated on the CPU (left) and as calculated on the GPU (right), where $N = 8,192$, $N_2 = 1,024$ and $m_2/m_3 = 2$. We use `NBODY6` for both of these models. For the case with the GPU we use the additional

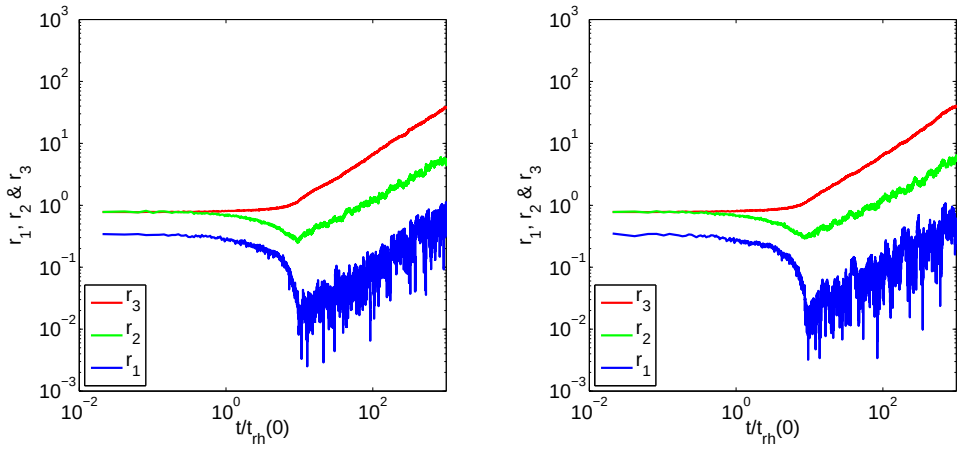

Figure 2.9: Comparing an N-body simulation computed with a CPU (left) to an N-body simulation calculated with a GPU (right). For details see text.

code written by Sverre Aaresth and Kiego Nitadori to run `NBODY6` on a GPU[3]. We find that the use of the GPU makes little difference to r_1, r_2 and r_3 in this example.

In Fig. 2.8, we have the results of the analytical model (left) and the results of the N-body simulation using a GPU. In this example we have $N = 8192$, $N_2 = 1024$ and $m_3/m_2 = 2$. The analytical model and the N-body results have very similar dynamical features. The analytical model undergoes core collapse and has a self-similar expansion, thereafter with little, if any, further mass segregation. The N-body simulation also undergoes core collapse and the post-collapse evolution does show signs of mass segregation, although this is very slow and there is no significant difference in mass segregation until $1000t_{\rm rh}(0)$. Also, the ratio of the half-mass radius of the two components is rather different in these two models. This confirms that the simple model may differ significantly from real systems, at a quantitative level.

In Fig. 2.10, we plot the analytical results and the N-body results for $N = 16,384$, $N_2 = 4,096$ and $m_2/m_3 = 8$. Again, we use the GPU to perform the N-body simulation. The results in this example are similar to the previous examples. Both models experience core collapse on a similar timescale, but the N-body simulation experiences faster expansion of the core directly after core collapse. There is little sign of ongoing mass segregation in the post-collapse regime.

[3]http://www.ast.cam.ac.uk/ sverre/web/pages/nbody.htm

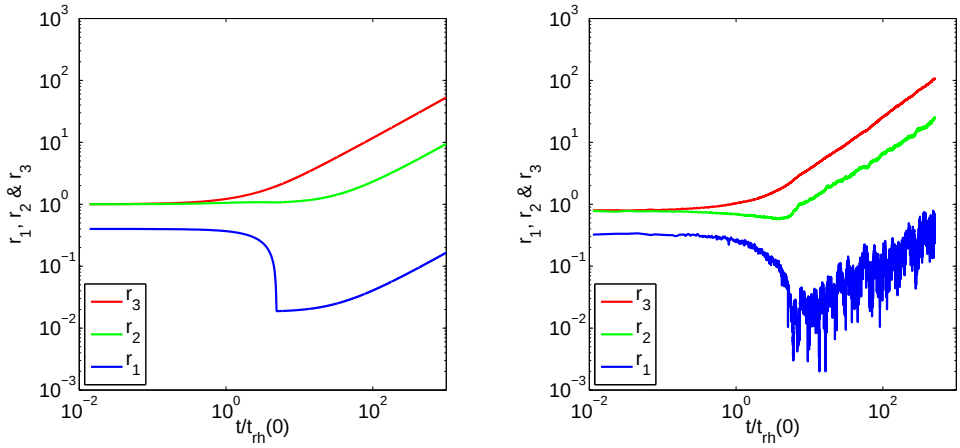

Figure 2.10: We compare $r_3(t)$ (red), $r_2(t)$ (green) and $r_1(t)$ (blue) for the analytical model IIIb (left) with the N-body simulation computed on a GPU (right) in the case where $N = 16,384$, $N_2 = 4,096$ and $\tilde{m} = 8$.

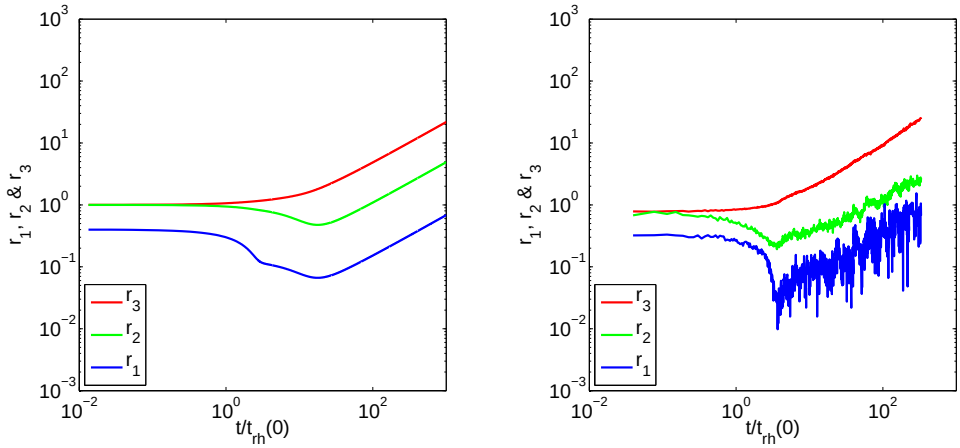

Figure 2.11: We compare $r_3(t)$ (red), $r_2(t)$ (green) and $r_1(t)$ (blue) for the analytical model IIIb (left) with the N-body simulation (right) in the case where $N = 4,096$, $N_2 = 256$ and $\tilde{m} = 4$.

The derivation of our constants in Sect. 2.3.3 assumes that the post collapse evolution is self-similar. However, this is not always the case. An example of this is $N = 4,096$, $N_2 = 256$ and $\tilde{m} = 4$. It can be seen in Table 2.1 that this case yields the value $C_2 = 4.58$ which is the highest for C_2 in the table. We can see from the N-body simulation of this case, shown on the right of Fig. 2.11, that the post-collapse evolution does show a notable degree of ongoing mass segregation (i.e. $\log(r_2) - \log(r_1)$ increases slightly with time after core collapse). Although mass segregation is still not significant, it is much more so than the other N-body simulations. When applying the constants C_1 and C_2 to this case, our analytical model, shown on the left of Fig. 2.11, does not behave as one would expect. The model appears to undergo core collapse prematurely, then continues to collapse due to mass segregation. The core then reaches a minimum value and expands self-similarly for the rest of the simulation. It is fair to say that our model is not qualitatively satisfactory for this particular N-body case, even though it has been effective in other cases.

We have shown some examples of the simple two-component model in comparison with the two-component N-body simulations. The analytical model does not give the same result as the N-body model but, as stated previously, we would not expect them to yield the same results, quantitatively. We do, however, show that our simple model contains many of the dynamical features of the N-body simulations and is qualitatively similar to the N-body models in most cases. Our model did not seem to model the case shown in Fig 2.11a, well. The timescales for core collapse and mass segregation do not coincide in the same manner as it has in previous cases. Its important to note that the N-body model for this case (shown in Fig 2.11b) has more post-collapse mass segregation than the other cases. A possible way to improve this could be to include an additional constant, which was ignored in (2.50). Although it is not clear whether adding such a constant would improve our model. The ongoing effects of mass segregation in Fig 2.11b may be due to the small number of heavy stars in the system, but further study would need to be done to say for sure. Despite this limitation, we have shown that the processes considered in the development of this simple two-component model are enough to have a self-similar post collapse evolution.

2.5 Discussion

We have developed a simple two-component model which takes account of three processes of evolution; gravitational interactions, mass segregation and binary heating. We created our analytical model by considering two simpler models, a two-component model without a separate core radius and a single mass model with a separate core radius, and combined them to obtain a model that consists of two populations with a

separate core radius.

It has been shown, through numerous examples, that mass segregation in the final model does not continue in the post-collapse phase even though the system has not reached equipartition. The processes considered in the derivation of our two-component model are enough to replicate this phenomenon. Gravitational interactions could not cause this self-similar behavior, as gravitational interactions would only lead to mass segregation, therefore the binary heating term (which does not include primordial binary stars) must be preventing further developments in mass segregation after core collapse. In addition, it is important to note is that the departure from equipartition is necessary to transfer energy from the core to the halo.

Comparing our analytical model to the N-body results, some common patterns arise. Although the value of N is relatively small, the large number of N-body simulations are enough to show a consistent pattern. The minimum value of the core radius is larger in the analytical model and directly after core collapse, the rate at which the system expands in the analytical model is much slower than the N-body simulations (for an example of this, see Fig 2.8a and Fig 2.8b). We can see from (2.48) and (2.58) that the rate of the post-collapse expansion would increase if the minimum value of the core radius decreased. Therefore, the analytical model could approximate the N-body model better if we could adjust the model so the core collapses as much as in the N-body models. A possible explanation for this could be that after a certain degree of core collapse occurs the evolution of the core becomes dominated by gravothermal instability and evolves almost independently from the rest of the system (Lynden-Bell and Wood, 1968). A possible improvement on this simple model is to create the evolution of the core radius in such a way that when the central density exceeds a threshold then the core evolution is dominated by gravothermal instability. A possible candidate for this threshold would be related to ρ_0/ρ_h as discussed in Table 1 of Lynden-Bell and Wood (1968).

The N-body simulations do not exhibit a self-similar post collapse evolution for every case, though the deviations are modest. It is interesting to note, that the larger degrees of ongoing mass segregation after core collapse occurred in our models where N_2 was small relative to N (as shown in Fig. 2.11). One possible explanation for this could be that the effects of ejection on clusters with a small number of heavy stars may be more significant in clusters with a large number of heavy stars. Even though there may not be many heavy stars lost, the loss of heavy stars by escape is significant with respect to the total number of heavy stars. The region of heavy stars would then contract towards the core. Further investigation on the relative mass loss for each population due to escape is needed to confirm this.

3

Single Mass Fokker-Planck Model

3.1 Deriving the fundamental equations

We follow the work of Hénon (1961) for a Fokker-Planck model in the general case and then in the case where the stellar masses are equal. We follow Hénon's work with the intention of replicating and extending upon this work in Chapter 4.

The system is described by its distribution function, $f\left(\overrightarrow{r}, \overrightarrow{v}, m, t\right)$, where $\overrightarrow{r} = (x, y, z)$ is the position vector, $\overrightarrow{v} = (v_x, v_y, v_z)$ is the velocity vector, m is the stellar mass and t is time. We consider a spherically symmetric system which has a simplified distribution function

$$f(E, \overrightarrow{J}, m, t) = f\left(\overrightarrow{r}, \overrightarrow{v}, m, t\right), \tag{3.1}$$

where $\overrightarrow{J}$ is the angular momentum of a star and E is the total energy of a star per unit mass. For simplicity we only consider the isotropic case (i.e. isotropy of the velocity dispersion). If we assume that the system is isotropic at every point, the distribution function will not depend on angular momentum, leaving us with a distribution function of the form

$$f(E, m, t). \tag{3.2}$$

The total stellar energy per unit mass, E (which shall be referred to as the total

energy), is defined as

$$E = U + \frac{v^2}{2}, \tag{3.3}$$

where v is the magnitude of $\overrightarrow{v}$ and U is the potential energy per unit mass (this is the same as the gravitational potential discussed in Sect. 1.6.4).

3.1.1 General Fokker-Planck model

The mass density at a point in our distribution is

$$\rho = \int\int\int\int mf\left(\overrightarrow{r}, \overrightarrow{v}, m, t\right) \mathrm{d}v_x \mathrm{d}v_y \mathrm{d}v_z \mathrm{d}m. \tag{3.4}$$

If we take into account that the system is isotropic and use the definition of E found in (3.3), the equation for ρ becomes

$$\rho = 4\pi \int_0^\infty m \int_U^\infty (2E - 2U)^{1/2} f(E, m, t) \mathrm{d}E \mathrm{d}m. \tag{3.5}$$

In our system, Poisson's Equation must be satisfied. This can be written generally as

$$\bigtriangledown^2 U = 4\pi G\rho. \tag{3.6}$$

For our derivations, we will consider Poisson's Equation in polar coordinates

$$\frac{\partial^2 U}{\partial r^2} + \frac{2}{r}\frac{\partial U}{\partial r} = 4\pi G\rho, \tag{3.7}$$

where r is the distance to the center of the cluster and G is the gravitational constant.

U and ρ depend on r and t. In other words, if f is known, then we can obtain ρ and U. Thus, f can be considered as the essential description of our system.

We can also find the distribution function as a function of r and v by

$$f\left(E, m, t\right) = f\left(U(r,t) + \frac{v^2}{2}, m, t\right) = f_{(r,v)}\left(r, v, m, t\right). \tag{3.8}$$

The equation of evolution for a system with this distribution was originally shown in Rosenbluth and Judd (1957) for a general case, where spherical symmetry is not assumed. Hénon adjusted this equation for a spherically symmetric system. The equation of evolution that Hénon found is

$$\left(\frac{\partial f_{(r,v)}}{\partial t}\right)_{\text{coll}} = 16\pi^2 G^2 \log N \int_0^\infty m_* \frac{1}{v^2}\frac{\partial}{\partial v}\left[mf_{(r,v)} \int_0^v f_{(r,v_*)} v_*^2 \mathrm{d}v_* + \right.$$
$$\left. \frac{m_*}{3}\frac{\partial f_{(r,v)}}{\partial v}\left(\frac{1}{v}\int_0^v f_{(r,v_*)} v_*^4 \mathrm{d}v_* + v^2 \int_v^\infty f_{(r,v_*)} v_* \mathrm{d}v_*\right)\right] \mathrm{d}m_*, \tag{3.9}$$

where N is the number of stars in the cluster and the subscript $*$ is used to show which variables are being used for integration. Note that $f_{(r,v_*)} = f_{(r,v)}(r, v_*, m, t)$. In (3.9), $\left(\partial f_{(r,v)}/\partial t\right)_{\text{coll}}$ is the rate of change in the distribution function caused by collisions.

After a small amount of time has elapsed, the distribution function changes by gravitational encounters between stars, as described in (3.9). Then $U(r,t)$ adjusts in response to the changes in the distribution function and this causes further change in f. We can calculate the change in the distribution function from the change in potential, by taking the partial derivative of (3.8) with respect to time

$$\frac{\partial f_{(r,v)}}{\partial t} = \frac{\partial f}{\partial E}\left(\frac{\partial E}{\partial t}\right)_v + \frac{\partial f}{\partial m}\frac{\partial m}{\partial t} + \frac{\partial f}{\partial t}\frac{\partial t}{\partial t}. \tag{3.10}$$

By using (3.3) and taking into account that m is always constant, (3.10) becomes

$$\frac{\partial f_{(r,v)}}{\partial t} = \frac{\partial f}{\partial E}\frac{\partial U}{\partial t} + \frac{\partial f}{\partial t}. \tag{3.11}$$

It is important to note for further derivation that $\left(\partial f_{(r,v)}/\partial t\right)_{\text{coll}}$, given in (3.9), is equivalent to $\partial f_{(r,v)}/\partial t$, found in (3.11).

We define the total number of stars with an energy within the range $[E, E + \mathrm{d}E]$ and a mass within the range $[m, m + dm]$ to be $g(E, m, t)\mathrm{d}E\mathrm{d}m$, which is expressed as

$$g(E,m,t)\mathrm{d}E\mathrm{d}m = \int_0^{r_{\max}} 4\pi r^2 \mathrm{d}r \cdot 4\pi v^2 f_{(r,v)}\mathrm{d}v\mathrm{d}m, \tag{3.12}$$

where $r_{\max}$ is the maximum radius for a given energy E, which we define as

$$U(r_{\max}, t) = E. \tag{3.13}$$

By rearranging (3.3), we write v to be

$$v = \left(2E - 2U\right)^{1/2}. \tag{3.14}$$

Then, with a substitution of (3.13) for (3.14) in (3.12) we obtain

$$g = 16\pi^2 \int_0^{r_{\max}} f_{(r,v)} v r^2 \mathrm{d}r. \tag{3.15}$$

It follows that

$$\frac{\partial g}{\partial t} = 16\pi^2 \int_0^{r_{\max}} \left[v\frac{\partial f_{(r,v)}}{\partial t} + \frac{\partial\left(f_{(r,v)} \cdot v\right)}{\partial v}\left(\frac{\partial v}{\partial t}\right)_E \right] r^2 \mathrm{d}r. \tag{3.16}$$

Since (3.9) is equivalent to (3.11), we find

$$\int_0^{r_{\max}} v\left[\left(\frac{\partial f_{(r,v)}}{\partial t}\right)_{\text{coll}} - \frac{\partial f}{\partial E}\frac{\partial U}{\partial t} - \frac{\partial f}{\partial t}\right] r^2 \mathrm{d}r = 0. \tag{3.17}$$

When substituting f, f_* and v for $f_{(r,v)}$, $f_{(r,v_*)}$ and (3.14), respectively, we arrive at the general fundamental equation for the system

$$16\pi^2 G^2 \log N \int_0^{r_{\max}} \left[\int_0^\infty m_* \frac{\partial}{\partial E} \left[mf \int_U^E f_* \left(2E_* - 2U\right)^{1/2} \mathrm{d}E_* + \right.\right.$$
$$\left. \frac{m_*}{3} \frac{\partial f}{\partial E} \int_U^E f_* \left(2E_* - 2U\right)^{3/2} \mathrm{d}E_* + \frac{m_*}{3} \frac{\partial f}{\partial E} \left(2E - 2U\right)^{3/2} \int_E^\infty f_* \mathrm{d}E_* \right] \mathrm{d}m_*$$
$$\left. - \left(2E - 2U\right)^{1/2} \left(\frac{\partial f}{\partial E} \frac{\partial U}{\partial t} + \frac{\partial f}{\partial t} \right) \right] r^2 \mathrm{d}r = 0. \quad (3.18)$$

Taking into account $(2E - 2U) = 0$ when $r = r_{\max}$ through the definition found in (3.13), we can invert the operations $\int_0^{r_{\max}} \mathrm{d}r$ and $\partial/\partial E$

$$16\pi^2 G^2 \log N \int_0^\infty m_* \frac{\partial}{\partial E} \left[mf \int_{-\infty}^E f_* \left[\int_0^{r_{\max}} \left(2E_* - 2U\right)^{1/2} r^2 \mathrm{d}r \right] \mathrm{d}E_* + \right.$$
$$\frac{m_*}{3} \frac{\partial f}{\partial E} \int_{-\infty}^E f_* \left[\int_0^{r_{\max}} \left(2E_* - 2U\right)^{3/2} r^2 \mathrm{d}r \right] \mathrm{d}E_* +$$
$$\left. \frac{m_*}{3} \frac{\partial f}{\partial E} \left[\int_0^{r_{\max}} \left(2E - 2U\right)^{3/2} r^2 \mathrm{d}r \right] \int_E^\infty f_* \mathrm{d}E_* \right] \mathrm{d}m_*$$
$$- \int_0^{r_{\max}} \left(2E - 2U\right)^{1/2} \left(\frac{\partial f}{\partial E} \frac{\partial U}{\partial t} + \frac{\partial f}{\partial t} \right) r^2 \mathrm{d}r = 0. \quad (3.19)$$

In (3.19), we also assume that the minimum value of U is $-\infty$.

Using the substitutions

$$q(E,t) = \frac{1}{3} \int_0^{r_{\max}} \left(2E - 2U\right)^{3/2} r^2 \mathrm{d}r, \quad (3.20)$$
$$\frac{\partial q}{\partial E} = \int_0^{r_{\max}} \left(2E - 2U\right)^{1/2} r^2 \mathrm{d}r \quad (3.21)$$

and

$$\frac{\partial q}{\partial t} = - \int_0^{r_{\max}} \left(2E - 2U\right)^{1/2} \frac{\partial U}{\partial t} r^2 \mathrm{d}r, \quad (3.22)$$

we can simplify (3.18) to the following equation

$$16\pi^2 G^2 \log N \int_0^\infty m_* \frac{\partial}{\partial E} \left[mf \int_{-\infty}^E f_* q_*' \mathrm{d}E_* + m_* f' \left(\int_{-\infty}^E f_* q_* \mathrm{d}E_* + \right.\right.$$
$$\left. \left. q \int_E^\infty f_* \mathrm{d}E_* \right) \right] \mathrm{d}m_* + f' \frac{\partial q}{\partial t} - q' \frac{\partial f}{\partial t} = 0. \quad (3.23)$$

The prime, used in (3.23), denotes a partial derivative with respect to E. In Sect. 2.2 of Spitzer (1987), the general Fokker-Planck equation is also derived. The result of this derivation is found in (2-86) and is similar to (3.23), but in a different form.

The fundamental equations for a general system (i.e. a system where the stellar masses and the number of stellar mass groups are not restricted) are (3.5), (3.7), (3.20) and (3.23). Using these equations we can find ρ, U, f and q. We now consider the case in which the stellar masses are equal and will need to undergo some transformations to simplify our single mass system.

3.2 Single mass case

We continue to follow the work of Hénon (1961). We consider the case where the stellar masses are equal. With this assumption the distribution function can be written as

$$f(E, m, t) = \delta(m - m_1)F(E, t), \tag{3.24}$$

where m_1 is the individual mass of a star, δ is the Dirac δ-function and $F(E, t)$ is the distribution function for a single mass system.

In order to simplify our equations by removing the constants, we use the following transformations

$$\begin{aligned} \rho &= 4\pi m_1 D, \\ r &= \left(16\pi^2 G m_1\right)^{-1/2} R, \\ q &= \left(16\pi^2 G m_1\right)^{-3/2} Q, \\ dt &= \left(16\pi^2 G^2 m_1^2 \log N\right)^{-1} \mathrm{d}T. \end{aligned} \tag{3.25}$$

Using these transformations, our fundamental equations become

$$\begin{aligned} D &= \int_U^\infty (2E - 2U)^{1/2} F \mathrm{d}E, \\ \frac{\partial^2 U}{\partial R^2} &+ \frac{2}{R}\frac{\partial U}{\partial R} = D, \\ Q &= \frac{1}{3}\int_0^{R_{\max}} (2E - 2U)^{3/2} R^2 \mathrm{d}R, \\ 0 &= \frac{\partial}{\partial E}\left[F\int_{-\infty}^{E} F_* Q'_* \mathrm{d}E_* + F'\left(\int_{-\infty}^{E} F_* Q_* \mathrm{d}E_* + Q\int_E^\infty F_* \mathrm{d}E_*\right)\right] \\ &\quad + F'\frac{\partial Q}{\partial T} - Q'\frac{\partial F}{\partial T}. \end{aligned} \tag{3.26}$$

Now we will look at the integral of the distribution function. We define $F^{(-1)}$ as

$$F^{(-1)} = -\int_E^\infty F_* \mathrm{d}E_*. \tag{3.27}$$

For the purpose of simplifying our system we define a function $S(E)$ to be

$$S = F^{(-1)} \int_{-\infty}^E F_* Q'_* \mathrm{d}E_* - F \int_{-\infty}^E F_*^{(-1)} Q'_* \mathrm{d}E_*. \tag{3.28}$$

Then taking the derivative of S with respect to E, we obtain

$$S' = F \int_{-\infty}^E F_* Q'_* \mathrm{d}E_* - F' \int_{-\infty}^E F_*^{(-1)} Q'_* \mathrm{d}E_*. \tag{3.29}$$

If we use integration by parts and take into account that Q tends to zero as $E \to -\infty$, S' can be written as

$$S' = F \int_{-\infty}^E F_* Q'_* \mathrm{d}E_* + F' \left(\int_{-\infty}^E F_* Q_* \mathrm{d}E_* + Q \int_E^\infty F_* \mathrm{d}E_* \right). \tag{3.30}$$

Therefore, (3.26) can be simplified to

$$S'' + F' \frac{\partial Q}{\partial T} - Q' \frac{\partial F}{\partial T} = 0 \tag{3.31}$$

3.2.1 Removing the time dependency

We follow the work of Hénon (1961) and create a self-similar system of equations. The homologous evolution from Lynden-Bell and Eggleton (1980), described in Sect. 1.4.1, used ρ and r for the basis of their system. Instead of ρ and r, Hénon uses F and E. If the system evolves self-similarly, we can create canonical equations depending on F and E, whereby a simple transformation can return the system to the canonical equations.

We show an example of a transformation to a canonical form through a system which is independent of time. Consider the equation for an isothermal sphere

$$f(E) = Ae^{-BE}, \tag{3.32}$$

where A and B are constants. For any value of A and B, this system can always be transformed to its canonical equation

$$\tilde{f}(E) = e^{-\tilde{E}}, \tag{3.33}$$

through the transformation

$$\begin{aligned} \tilde{f} &= \frac{1}{A} f \\ \tilde{E} &= \frac{1}{B} E. \end{aligned} \tag{3.34}$$

In this simplified example we show how a time-independent transformation can bring the equation of an isothermal spherical system to its canonical equation.

In our system we are interested in an evolving model, which evolves in such a way that at any moment it can be brought back to its canonical form. Thus, we will use time-dependent variables, $\beta(t)$ and $\gamma(t)$, to transform our equations. The transformation is

$$\begin{aligned} E &= \beta(t)\,\mathbf{E}, \\ F &= \gamma(t)\,\mathbf{F}. \end{aligned} \tag{3.35}$$

Note that we use the bold text to show the variables which are transformed to the canonical form.

To find the canonical equations for our system we must first apply the transformations in (3.35), to obtain the transformations for the other essential variables,

$$\begin{aligned} U &= \beta\mathbf{U}, \\ D &= \beta^{3/2}\gamma\mathbf{D}, \\ R &= \beta^{-1/4}\gamma^{-1/2}\mathbf{R}, \\ Q &= \beta^{3/4}\gamma^{-3/2}\mathbf{Q}, \\ \mathrm{d}T &= \gamma^{-1}\mathrm{d}\mathbf{T}, \\ S &= \beta^{7/4}\gamma^{1/2}\mathbf{S}. \end{aligned} \tag{3.36}$$

We would like to use these transformations on our system of equations (3.26a - c) and (3.31). This can be done directly when applied to (3.26a - c) and the first term in (3.31). However, using these transformations on the latter two term in (3.31) requires a little more care.

The latter two terms of (3.31) can be written as the determinant of the Jacobian

$$\frac{\partial(F,Q)}{\partial(E,T)} = \begin{vmatrix} \frac{\partial F}{\partial E} & \frac{\partial F}{\partial T} \\ \frac{\partial Q}{\partial E} & \frac{\partial Q}{\partial T} \end{vmatrix} = \frac{\partial F}{\partial E}\frac{\partial Q}{\partial T} - \frac{\partial Q}{\partial E}\frac{\partial F}{\partial T} \tag{3.37}$$

Transforming this determinant involves the following process

$$\frac{\partial(F,Q)}{\partial(E,T)} = \frac{\partial(F,Q)}{\partial(\mathbf{E},\mathbf{T})}\frac{\partial(\mathbf{E},\mathbf{T})}{\partial(E,T)}. \tag{3.38}$$

Using (3.35a) and (3.36e), we can evaluate the Jacobian matrix

$$\frac{\partial(\mathbf{E},\mathbf{T})}{\partial(E,T)} = \begin{vmatrix} \frac{1}{\beta} & -\frac{1}{\beta^2}\frac{\mathrm{d}\beta}{\mathrm{d}T}E \\ 0 & \gamma \end{vmatrix}. \tag{3.39}$$

Thus,

$$\frac{\partial F}{\partial E}\frac{\partial Q}{\partial T} - \frac{\partial Q}{\partial E}\frac{\partial F}{\partial T} = \frac{\gamma}{\beta}\left[\frac{\partial F}{\partial \mathbf{E}}\frac{\partial Q}{\partial \mathbf{T}} - \frac{\partial Q}{\partial \mathbf{E}}\frac{\partial F}{\partial \mathbf{T}}\right]. \tag{3.40}$$

By utilizing the transformations in (3.36) this becomes

$$\frac{\partial F}{\partial E}\frac{\partial Q}{\partial T} - \frac{\partial Q}{\partial E}\frac{\partial F}{\partial T} = \beta^{-1/4}\gamma^{1/2}\left[\frac{\partial \mathbf{F}}{\partial \mathbf{E}}\frac{\partial \mathbf{Q}}{\partial \mathbf{T}} - \frac{\partial \mathbf{Q}}{\partial \mathbf{E}}\frac{\partial \mathbf{F}}{\partial \mathbf{T}} + \mathbf{Q}\frac{\partial \mathbf{F}}{\partial \mathbf{E}}\left(\frac{3}{4\beta}\frac{\partial \beta}{\partial \mathbf{T}} - \frac{3}{2\gamma}\frac{\partial \gamma}{\partial \mathbf{T}}\right) - \mathbf{F}\frac{\partial \mathbf{Q}}{\partial \mathbf{E}}\frac{1}{\gamma}\frac{\partial \gamma}{\partial \mathbf{T}}\right]. \tag{3.41}$$

The fundamental equations can be written in its canonical form

$$\begin{aligned}
\mathbf{D} &= \int_{\mathbf{U}}^{\infty} (2\mathbf{E} - 2\mathbf{U})^{1/2}\,\mathbf{F}\mathrm{d}\mathbf{E}, \\
\frac{\partial^2 \mathbf{U}}{\partial \mathbf{R}^2} &+ \frac{2}{\mathbf{R}}\frac{\partial \mathbf{U}}{\partial \mathbf{R}} = \mathbf{D}, \\
\mathbf{Q} &= \frac{1}{3}\int_0^{\mathbf{R}_{\max}} (2\mathbf{E} - 2\mathbf{U})^{3/2}\mathbf{R}^2\mathrm{d}\mathbf{R}, \\
\mathbf{S}' &= \mathbf{F}\int_{-\infty}^{\mathbf{E}} \mathbf{F}_*\mathbf{Q}'_*\mathrm{d}\mathbf{E}_* + \mathbf{F}'\left(\int_{-\infty}^{\mathbf{E}} \mathbf{F}_*\mathbf{Q}_*\mathrm{d}\mathbf{E}_* + \mathbf{Q}\int_{\mathbf{E}}^{\infty} \mathbf{F}_*\mathrm{d}\mathbf{E}_*\right) \\
0 &= \mathbf{S}'' + \mathbf{F}'\frac{\partial \mathbf{Q}}{\partial \mathbf{T}} - \mathbf{Q}'\frac{\partial \mathbf{F}}{\partial \mathbf{T}} + \left(\frac{3}{4}b - \frac{3}{2}c\right)\mathbf{Q}\mathbf{F}' - c\mathbf{F}\mathbf{Q}',
\end{aligned} \tag{3.42}$$

where the prime is used to denote a partial derivative with respect to $\mathbf{E}$ and the constants, b and c, are defined as

$$\begin{aligned}
b &= \frac{1}{\beta}\frac{\mathrm{d}\beta}{\mathrm{d}\mathbf{T}}, \\
c &= \frac{1}{\gamma}\frac{\mathrm{d}\gamma}{\mathrm{d}\mathbf{T}}.
\end{aligned} \tag{3.43}$$

3.2.2 Total mass and kinetic energy

It is important not only to think of our fundamental equations in the terms given in (3.42d), but also as the physical quantities they represent. In this section, we will follow the derivation of the equations for the total mass and kinetic energy found in Hénon (1961).

First, we examine the general case. If we consider N_E to be the number of stars whose total energy is less than E, the total mass and the total kinetic energy of this population are defined as

$$m_{\mathrm{tot},E} = \int_0^{\infty} m\mathrm{d}m \int_0^{r_{\max}} 4\pi r^2 \mathrm{d}r \int_U^E 4\pi\,(2E_* - 2U)^{1/2}\,f_*\mathrm{d}E_* \tag{3.44}$$

and

$$E_{\text{kin},E} = \int_0^\infty m\mathrm{d}m \int_0^{r_{\max}} 4\pi r^2 \mathrm{d}r \int_U^E 2\pi \left(2E_* - 2U\right)^{3/2} f_* \mathrm{d}E_*, \tag{3.45}$$

respectively. By inverting the order of operations and using (3.20) and (3.21), we find

$$\begin{aligned} m_{\text{tot},E} &= 16\pi^2 \int_0^\infty m\mathrm{d}m \int_{-\infty}^E f_* q'_* \mathrm{d}E_*, \\ E_{\text{kin},E} &= 24\pi^2 \int_0^\infty m\mathrm{d}m \int_{-\infty}^E f_* q_* \mathrm{d}E_*. \end{aligned} \tag{3.46}$$

Using (3.24), we find the total mass and kinetic energy for a single mass system

$$\begin{aligned} m_{\text{tot},E} &= 16\pi^2 m_1 \int_{-\infty}^E F_* q'_* \mathrm{d}E_*, \\ E_{\text{kin},E} &= 24\pi^2 m_1 \int_{-\infty}^E F_* q_* \mathrm{d}E_*. \end{aligned} \tag{3.47}$$

We transform $m_{\text{tot},E}$ and $E_{\text{kin},E}$ as above to arrive at

$$\begin{aligned} m_{\text{tot},E} &= \left(16\pi^2 m_1\right)^{-1/2} G^{-3/2} M, \\ E_{\text{kin},E} &= \left(16\pi^2 m_1\right)^{-1/2} G^{-3/2} L. \end{aligned} \tag{3.48}$$

Thus the simplified equations for the scaled total mass M_E and kinetic energy L_E of the system are

$$\begin{aligned} M_E &= \int_{-\infty}^E F_* Q'_* \mathrm{d}E_*, \\ L_E &= \frac{3}{2} \int_{-\infty}^E F_* Q_* \mathrm{d}E_*. \end{aligned} \tag{3.49}$$

This gives a better picture of some of the physical quantities represented in (3.26). As can be seen in (3.49a) and (3.49b), when $E \to \infty$, M_E and L_E tend toward the total mass and the total kinetic energy of the system, respectively.

We parametrize M_E and L_E to obtain

$$\begin{aligned} M_E &= \beta^{3/4} \gamma^{-1/2} \mathbf{M}, \\ L_E &= \beta^{7/4} \gamma^{-1/2} \mathbf{L}, \end{aligned} \tag{3.50}$$

to give us the final form

$$\begin{aligned} \mathbf{M_E} &= \int_{-\infty}^{\mathbf{E}} \mathbf{F}_* \mathbf{Q}'_* \mathrm{d}\mathbf{E}_*, \\ \mathbf{L_E} &= \int_{-\infty}^{\mathbf{E}} \mathbf{F}_* \mathbf{Q}_* \mathrm{d}\mathbf{E}_*. \end{aligned} \tag{3.51}$$

3.2.3 Homological evolution

As done in Hénon (1961), we find the homological solution to our system. Homological evolution, or self-similar evolution, is evolution where the structure of the system remains the same except for our time-dependent scaling factors. Although, the dimensions of the system evolve by a time-dependent scaling factor (Heggie and Stevenson (1988)). We have defined such scaling factors to be γ and β, but are now represented by the constants b and c, as shown in (3.43).

To create a self-similar system the conditions

$$\begin{aligned} \frac{\partial \mathbf{F}}{\partial \mathbf{T}} &= 0, \\ \frac{\partial \mathbf{Q}}{\partial \mathbf{T}} &= 0. \end{aligned} \tag{3.52}$$

must hold. When these conditions are considered, (3.42e) becomes

$$0 = \mathbf{S}'' + \left(\frac{3}{4}b - \frac{3}{2}c\right)\mathbf{Q}\mathbf{F}' - c\mathbf{F}\mathbf{Q}'. \tag{3.53}$$

The self-similar solution would need to satisfy this equation.

3.3 Approximations close to the edge

In our simple model discussed in Chapter 2, we assumed that the system was isolated for simplicity. In reality, globular clusters are not isolated systems; they exist in a parent galaxy and the effects of the gravitational field of the galaxy on the globular cluster are non-negligible (Binney and Tremaine, 2008). Thus, in this model we follow the work of Hénon (1961) when considering the effects of an external gravitational field from the galaxy on the internal evolution of the globular cluster. The galactic potential, U_G, can be described approximately in the following way

$$U_G = U_G(0) + \frac{1}{2}\left(\frac{\partial^2 U_G}{\partial x^2}x^2 + \frac{\partial^2 U_G}{\partial y^2}y^2 + \frac{\partial^2 U_G}{\partial z^2}z^2\right). \tag{3.54}$$

The density of the galaxy is small in comparison to the density of the cluster. Therefore, the Laplacian of the galactic potential is negligible in the cluster. In other words we can assume the condition

$$\frac{\partial^2 U_G}{\partial x^2} + \frac{\partial^2 U_G}{\partial y^2} + \frac{\partial^2 U_G}{\partial z^2} = 0, \tag{3.55}$$

for our system.

The potential of the cluster is approximately

$$U_C = -\frac{Gm_{\text{tot}}}{r}. \tag{3.56}$$

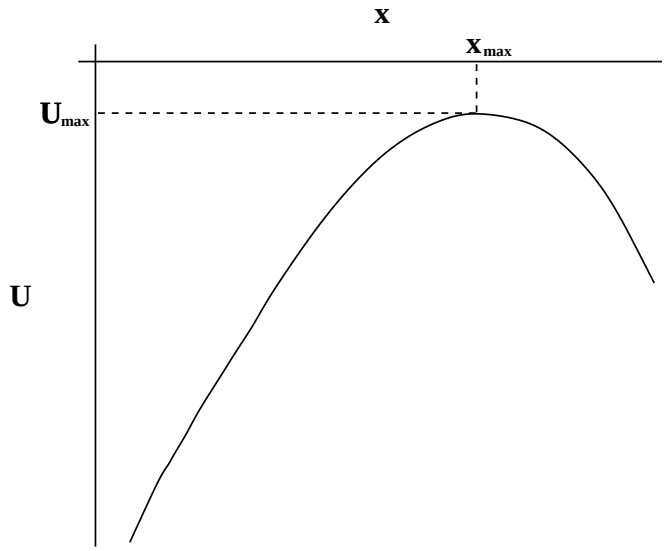

Figure 3.1: We show potential $U(x)$ (x is the distance from the center in the direction of the Lagrangian points) of a globular cluster in the gravitational field of a galaxy. Note that the origin is in the upper left. When the energy of a star is greater than $U_{\max} = U(x_{\max})$, the star escapes the potential well of the globular cluster. The corresponding $x_{\max}$ is seen in (3.59).

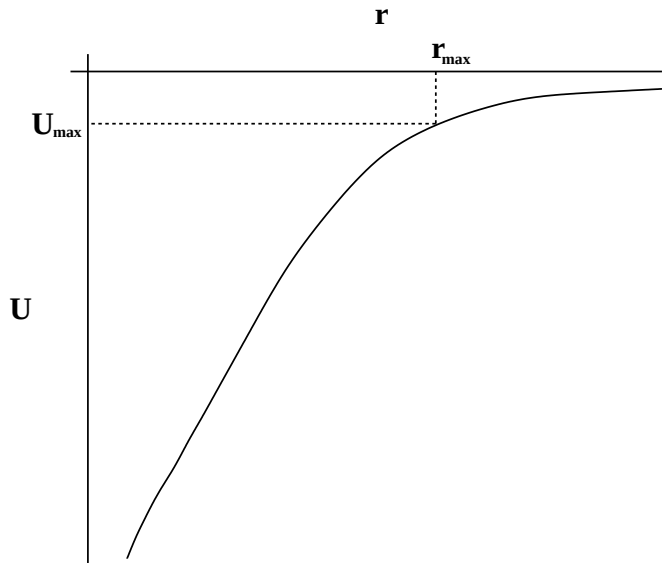

Figure 3.2: We show potential $U(r)$ of our system. The line reflects the manner in which the potential of the system would behave if it were isolated. However, we are imposing the maximum value for the potential $U_{\max}$ to correspond with $U_{\max}$ shown in Fig 3.1. Therefore, we impose $r_{\max}$ to be the maximum value of r for our system.

As shown in Fig. 3.1, when a star in an unisolated cluster reaches a certain energy, $U_{\max}$, the star escapes the cluster. We assume the the system is spherically symmetric and we will find the maximum value of U in the direction x which is the direction on which the Lagrangian points lie (the Lagrangian point x_{max} is defined such that $\partial U/\partial x\,(x_{\max}) = 0$). We begin by finding the total potential of the system

$$U = U_G + U_C. \tag{3.57}$$

Then we will find the potential energy in the x-direction

$$U = U_G(0) + \frac{1}{2}\frac{\partial^2 U_G}{\partial^2 x^2}x^2 - \frac{Gm_{\text{tot}}}{x}. \tag{3.58}$$

Therefore, the Lagrangian point is

$$x_{\max} = -(Gm_{\text{tot}})^{1/3}\left(\frac{\partial^2 U_G}{\partial x^2}\right)^{-1/3}, \tag{3.59}$$

and the corresponding maximum potential energy is

$$U_{\max} = U_G(0) + \frac{3}{2}(Gm_{\text{tot}})^{2/3}\left(\frac{\partial^2 U_G}{\partial x^2}\right)^{1/3}. \tag{3.60}$$

If any star crosses $x_{\max}$, it has enough energy to escape the cluster permanently. Therefore, a star must have an energy less than $U_{\max}$ to remain in the cluster. Thus,

$$f(E) = 0, \tag{3.61}$$

when

$$E \geq U_{\max}.$$

In our Fokker-Planck model we will approximate a globular cluster in a galactic gravitational field by neglecting U_G, but still imposing $U_{\max}$, found in (3.60), on our system. The graphical representation of this method is found in Fig. 3.2. The maximum radius $r_{\max}$, which corresponds to $U_{\max}$ such that

$$U_{\max} = U\,(r_{\max}) \tag{3.62}$$

is not the same as the $x_{\max}$ shown in Fig. 3.1 and (3.59). We calculate $r_{\max}$ with the approximation

$$r_{\max} = \frac{Gm_{\text{tot}}}{U_G(0) - U_{\max}}, \tag{3.63}$$

which is obtained by neglecting the second term on the right of (3.58). We substitute (3.60) to find

$$r_{\max} = -\frac{2}{3}(Gm_{\text{tot}})^{1/3}\left(\frac{\partial^2 U_G}{\partial x^2}\right)^{-1/3} = \frac{2}{3}x_{\max} \tag{3.64}$$

This relation connects the mass and the radius of the cluster. The evolution of the galaxy occurs over a much larger timescale than for the cluster, therefore the term $\partial^2 U_G/\partial x^2$ can be assumed to be constant and our relation can be simplified further

$$r_{\max} \propto m_{\text{tot}}^{1/3}. \tag{3.65}$$

3.3.1 Mass-radius relationship

The relation (3.65) can be rewritten as

$$r_{\max} \propto m_{\text{tot}}^{\lambda}, \tag{3.66}$$

where $\lambda = 1/3$ for the case of a globular cluster affected by a galactic potential field.

We substitute (3.36c), (3.43a), (3.43b) and (3.50a) into (3.66) to find

$$-\frac{b}{4} - \frac{c}{2} + \frac{\mathrm{d}\log \mathbf{R}_{\max}}{\mathrm{d}\mathbf{T}} = \lambda\left(\frac{3b}{4} - \frac{c}{2} + \frac{\mathrm{d}\log \mathbf{M}_{\max}}{\mathrm{d}\mathbf{T}}\right), \tag{3.67}$$

where $\mathbf{M}_{\max}$ is the scaled total mass of the system and $\mathbf{R}_{\max}$ is the scaled maximum radius found in (3.64).

Since we are interested in the homological solution $\frac{\mathrm{d}\log \mathbf{R}_{\max}}{\mathrm{d}\mathbf{T}} = \frac{\mathrm{d}\log \mathbf{M}_{\max}}{\mathrm{d}\mathbf{T}} = 0$. Thus, (3.67) simplifies to

$$(3\lambda + 1)\, b + (2 - 2\lambda)\, c = 0. \tag{3.68}$$

We define the origin of the potential field such that

$$U_{\max} = 0. \tag{3.69}$$

Therefore, the total energy of the star will be negative.

3.4 Approximations close to the center

We continue to follow the work of Hénon (1961) in deriving the approximation of $\mathbf{F}$ close to the center. Hénon originally attempted to find a solution using a finite central density. When calculating the evolution of a model with a finite central density, he found the central density kept increasing in a manner inconsistent with homological evolution. We now know this phenomenon as core collapse, which was discussed in Sect. 1.4. For the purposes of finding a homological solution, we need to assume the central density to be infinite. This is equivalent to a globular cluster in post-collapse evolution.

If we assume ρ is infinite in the center, it follows from (3.5) that the distribution function behaves similarly. In (3.53), the terms in $\mathbf{S''}$ must be of the order $\mathbf{F^2Q}$ (as can be seen in (3.42d). The terms in the latter part of the equation must be of the order $\mathbf{FQ}$ and therefore must be negligible in comparison to $\mathbf{S''}$. It follows that (3.53) is approximately

$$\mathbf{S''} = 0. \tag{3.70}$$

We will improve upon this approximation later. For now, we will only consider the approximation given in (3.70). The solution to this equation is

$$\mathbf{S} = \alpha_1 + \alpha_2 \mathbf{E}, \tag{3.71}$$

where α_1 and α_2 are constants.

We assume, momentarily, that α_1 and α_2 are null. We write the equations (3.28), (3.29) in the form

$$\begin{aligned} \mathbf{S} &= \mathbf{F}^{(-1)} \int_{-\infty}^{\mathbf{E}} \mathbf{F}_* \mathbf{Q}'_* \mathrm{d}\mathbf{E}_* - \mathbf{F} \int_{-\infty}^{\mathbf{E}} \mathbf{F}_*^{(-1)} \mathbf{Q}'_* \mathrm{d}\mathbf{E}_* = 0, \\ \mathbf{S}' &= \mathbf{F} \int_{-\infty}^{\mathbf{E}} \mathbf{F}_* \, \mathbf{Q}'_* \mathrm{d}\mathbf{E}_* - \mathbf{F}' \int_{-\infty}^{\mathbf{E}} \mathbf{F}_*^{(-1)} \mathbf{Q}'_* \mathrm{d}\mathbf{E}_* = 0. \end{aligned} \tag{3.72}$$

These equations can be written as

$$\begin{aligned} \frac{\mathbf{F}^{(-1)}}{\mathbf{F}} &= \frac{\int_{-\infty}^{\mathbf{E}} \mathbf{F}_*^{(-1)} \mathbf{Q}'_* \mathrm{d}\mathbf{E}_*}{\int_{-\infty}^{\mathbf{E}} \mathbf{F}_* \mathbf{Q}'_* \mathrm{d}\mathbf{E}_*}, \\ \frac{\mathbf{F}}{\mathbf{F}'} &= \frac{\int_{-\infty}^{\mathbf{E}} \mathbf{F}_*^{(-1)} \mathbf{Q}'_* \mathrm{d}\mathbf{E}_*}{\int_{-\infty}^{\mathbf{E}} \mathbf{F}_* \mathbf{Q}'_* \mathrm{d}\mathbf{E}_*}, \end{aligned} \tag{3.73}$$

From the above equations we can see that

$$\frac{\mathbf{F}}{\mathbf{F^{(-1)}}} = \frac{\mathbf{F}'}{\mathbf{F}}. \tag{3.74}$$

The solution

$$\mathbf{F} = C_3 e^{-C_4 \mathbf{E}}, \tag{3.75}$$

can be found by integrating (3.74). In (3.75), C_3 and C_4 are constants. Since $\mathbf{F}$ is positive and increasing as $E \to -\infty$, then $C_3, C_4 > 0$.

We can define β and γ in such a way that the constants C_3 and C_4 are normalized. Thus, the distribution function takes the form

$$\mathbf{F} = e^{-\mathbf{E}}. \tag{3.76}$$

Note that this is an isothermal solution. It is important that we have obtained an isothermal solution close to the center because when the density is very large, the relaxation time is very short and the system should be close to isothermal.

Using the equation above, we can approximate $\mathbf{D}$, $\mathbf{R}$ and $\mathbf{Q}$ with (3.42a), (3.42b) and (3.42c), respectively, to arrive at

$$\begin{aligned}\mathbf{D} &= \left(\frac{\pi}{2}\right)^{1/2} e^{-\mathbf{U}},\\ \mathbf{R} &= \left(\frac{8}{\pi}\right)^{1/4} e^{\mathbf{U/2}},\\ \mathbf{Q} &= K_D e^{\mathbf{3E/2}},\end{aligned} \tag{3.77}$$

where

$$K_D = \frac{16}{9\sqrt{3}\,(8\pi)^{1/4}}. \tag{3.78}$$

We use the solution in (3.77b) because it is the only solution to the differential equation (3.42b) that allows $\mathbf{D}$ to become infinite at the center. The solution for $\mathbf{D}$ is

$$\mathbf{D} = \frac{2}{\mathbf{R}^2}. \tag{3.79}$$

Thus, the potential close to the center is approximately

$$\mathbf{U} = \frac{1}{2}\log\frac{\pi}{8} + 2\log\mathbf{R}, \tag{3.80}$$

which tends towards $-\infty$ as $R \to 0$, thus the energy of an individual star must exist in $(-\infty, 0)$.

We use (3.76) and (3.77c) to find approximations for integrals which will be used in further calculations. These integrals are

$$\begin{aligned}\int_{-\infty}^{\mathbf{E}} \mathbf{F}_*\mathbf{Q}_*\mathrm{d}\mathbf{E}_* &= 2K_D e^{\mathbf{E}/2},\\ \int_{-\infty}^{\mathbf{E}} \mathbf{F}_*\mathbf{Q}'_*\mathrm{d}\mathbf{E}_* &= 3K_D e^{\mathbf{E}/2}.\end{aligned} \tag{3.81}$$

To find our asymptotic solution for F, we must examine the perturbed case, where α_1 and α_2 in (3.71) are non-zero to represent small perturbations. We look at the perturbed solution of (3.71),

$$\mathbf{F} = e^{-\mathbf{E}} + \alpha_1 Y_1 + \alpha_2 Y_2, \tag{3.82}$$

where Y_1 and Y_2 are functions of E.

It is important to note that Hénon does not explain how he finds the differential equations that lead to his solution for $\mathbf{F}$, so we give our derivation for finding these equations which may or may not be the method used in Hénon (1961).

We begin by solving (3.28) for $\int_{-\infty}^{E} F_*^{(-1)} Q'_* \mathrm{d}E_*$,

$$\int_{-\infty}^{E} F_*^{(-1)} Q'_* \mathrm{d}E_* = \frac{F^{(-1)}\int_{-\infty}^{E} F_* Q'_* \mathrm{d}E_* - S}{F}, \tag{3.83}$$

and substitute this into (3.29). By implementing straightforward canonical transformations found in (3.36), we arrive at the relation

$$\frac{\mathbf{F}\mathbf{S}' - \mathbf{F}'\mathbf{S}}{\int_{-\infty}^{\mathbf{E}} \mathbf{F}_* \mathbf{Q}'_* \mathrm{d}\mathbf{E}_*} = \mathbf{F}^2 - \mathbf{F}^{(-1)}\mathbf{F}'. \tag{3.84}$$

This is the same as the derivation of (3.74), with the exception that S and S' are not assumed to be zero. Nevertheless the left hand side is small compared with the right hand side, and so we can substitute our zero-order solution in the left-hand side.

Using the substitutions (3.76) and (3.77) for the left-hand side of (3.84) and (3.82) for the right-hand side of (3.84), and bearing in mind that we are only interested in a solution with first order perturbations, we arrive at the differential equations

$$\begin{aligned} Y_1^{(-1)} + 2Y_1 + Y_1' &= \frac{e^{-\mathbf{E}/2}}{3K_D}, \\ Y_2^{(-1)} + 2Y_2 + Y_2' &= \frac{(1+\mathbf{E})\, e^{-\mathbf{E}/2}}{3K_D}. \end{aligned} \tag{3.85}$$

Then it is easily found that the solutions to these equations are

$$\begin{aligned} Y_1 &= C_{11}e^{-\mathbf{E}} + C_{12}\mathbf{E}e^{-\mathbf{E}} - \frac{2}{3K_D}e^{-\mathbf{E}/2}, \\ Y_2 &= C_{21}e^{-\mathbf{E}} + C_{22}\mathbf{E}e^{-\mathbf{E}} + \frac{2}{3K_D}(5-\mathbf{E})\, e^{-\mathbf{E}/2}, \end{aligned} \tag{3.86}$$

where the C_{ij} are arbitrary constants. The terms C_{ij} can be eliminated by modifying our standardization of $\mathbf{F}(\mathbf{E})$, leaving us with the asymptotic solution of the distribution function

$$\mathbf{F} = e^{-\mathbf{E}} + \frac{2}{3K_D}(5\alpha_2 - \alpha_1 - \alpha_2\mathbf{E})\, e^{-\mathbf{E}/2}. \tag{3.87}$$

It is important to note that the first term in (3.87) becomes dominant, as $E \to -\infty$, regardless of the value of α_1 and α_2.

3.4.1 Flow of mass and energy close to the center

Continuing with the work of Hénon (1961), we will find the flow of mass and energy through the surface $E =$ constant. With this we can determine whether or not there are any constraints on the value of the constants α_1 and α_2.

We consider ρ_v, the mass density of stars with a velocity less than v, which we define as

$$\rho_v = \int_0^\infty m\mathrm{d}m \int_0^v 4\pi f_{(r,v_*)} v_*^2 \mathrm{d}v_*. \tag{3.88}$$

Similarly to (3.24), we use the transformation

$$f_{(r,v)} = \delta(m - m_1) F_{(r,v)}, \tag{3.89}$$

to find the density of stars with velocity less than v in the case where the masses are equal. Doing so, we arrive at the equation for ρ_v in a single mass system

$$\rho_v = m_1 \int_0^v 4\pi F_{(r,v_*)} v_*^2 \mathrm{d}v_*. \tag{3.90}$$

Using (3.9), it follows that

$$\left(\frac{\partial \rho_v}{\partial t}\right)_{\text{coll}} = 64\pi^3 G^2 m_1^2 \log N \left[F_{(r,v)} \int_0^v F_{(r,v_*)} v_*^2 \mathrm{d}v_* + \frac{1}{3} \frac{\partial F_{(r,v)}}{\partial v} \left(\frac{1}{v} \int_0^v F_{(r,v_*)} v_*^4 \mathrm{d}v_* + v^2 \int_v^\infty F_{(r,v_*)} \mathrm{d}v_* \right) \right]. \tag{3.91}$$

The total mass of stars with velocity less than v is defined by

$$m_{\text{tot},v} = \int_0^{r_{\max}} 4\pi \rho_v r^2 \mathrm{d}r. \tag{3.92}$$

This yields the derivative

$$\left(\frac{\partial m_{\text{tot},v}}{\partial t}\right)_{\text{coll}} = 4\pi \int_0^{r_{\max}} \left[\left(\frac{\partial \rho_v}{\partial t}\right)_{\text{coll}} + \frac{\partial \rho_v}{\partial v} \left(\frac{\partial v}{\partial t}\right)_E \right] r^2 \mathrm{d}r, \tag{3.93}$$

where $(\partial v/\partial t)_E$ is derived from (3.14) as

$$\left(\frac{\partial v}{\partial t}\right)_E = -\left(2E - 2U\right)^{-1/2} \frac{\partial U}{\partial t}. \tag{3.94}$$

Using (3.8), (3.14), (3.21), (3.22), (3.20), (3.90), (3.91), (3.94) and (3.93), $(\partial m_{\text{tot}}/\partial t)_{\text{coll}}$ can be written as

$$\left(\frac{\partial m_{\text{tot},E}}{\partial t}\right)_{\text{coll}} = 256\pi^4 G^2 m_1^2 \log N \left[F \int_{-\infty}^E F_* q_*' \mathrm{d}E_* + F' \left(\int_{-\infty}^E F_* q_* \mathrm{d}E_* + q \int_E^\infty F_* \mathrm{d}E_* \right) \right] + 16\pi^2 F \frac{\partial q}{\partial t}. \tag{3.95}$$

Utilizing (3.25c), (3.25d), (3.30) and (3.49a), the rate of change for the mass can be simplified to

$$\frac{\partial M_E}{\partial T} = S' + F \frac{\partial Q}{\partial T}. \tag{3.96}$$

We calculate the energy derivative through a surface E = constant, in the same manner. We define h_v to be the energy density for stars with a speed less than v. This can be written as

$$h_v = m_1 \int_0^v 4\pi F_{(r,v_*)} E_* v_*^2 \mathrm{d}v. \tag{3.97}$$

This equation leads to the rate of change in the energy density,

$$\left(\frac{\partial h_v}{\partial t}\right)_{\text{coll}} = m_1 \int_0^v 4\pi \left[\left(\frac{\partial F_{(r,v_*)}}{\partial t}\right)_{\text{coll}} E_* + F_{(r,v_*)} \frac{\partial U}{\partial t} \right] v_*^2 \mathrm{d}v_*. \tag{3.98}$$

The total energy of stars with velocity less than v is given by

$$h_{\text{tot},v} = \int_0^{r_{\max}} 4\pi h_v r^2 \mathrm{d}r. \tag{3.99}$$

The transformation for h_{tot} can be found by utilizing the other transformations found in (3.24), (3.25c) and (3.25d) to find

$$h_{\text{tot},v} = (16\pi^2 m_1)^{-1/2} G^{-3/2} H. \tag{3.100}$$

Using the equations (3.20), (3.21), (3.22), (3.25), (3.97), (3.98) and (3.99) we find an expression for the flow of energy

$$\frac{\partial H_E}{\partial T} = \int_{-\infty}^{E} \left(E_* S_*' - S_*\right)' dE_* + EF\frac{\partial Q}{\partial T} - \int_{-\infty}^{E} F_* \frac{\partial Q_*}{\partial T} \mathrm{d}E_*. \tag{3.101}$$

We reduce this equation to

$$\frac{\partial H_E}{\partial T} = ES' - S + EF\frac{\partial Q}{\partial T} - \int_{-\infty}^{E} F_* \frac{\partial Q_*}{\partial T} \mathrm{d}E_*. \tag{3.102}$$

In (3.96) the S' is on the order of F^2Q and the last term is on the order of FQ. Therefore, close to the center, $\partial M_E/\partial T$ can be approximated by

$$\frac{\partial M_E}{\partial T} = S'. \tag{3.103}$$

Similarly, $\partial H_E/\partial T$ is approximately

$$\frac{\partial H_E}{\partial T} = ES' - S, \tag{3.104}$$

close to the center.

Using (3.36f) and (3.71) we can find $\partial M_E/\partial T$ and $\partial H_E/\partial T$ in terms of our parameters α_1 and α_2

$$\begin{aligned} \frac{\partial M_E}{\partial T} &= \beta^{3/4}\gamma^{1/2}\alpha_2, \\ \frac{\partial H_E}{\partial T} &= -\beta^{7/4}\gamma^{1/2}\alpha_1. \end{aligned} \tag{3.105}$$

Using (3.36e), (3.50a) and (3.50b), this is reduced to

$$\begin{aligned} \frac{\partial \mathbf{M_E}}{\partial \mathbf{T}} &= \alpha_2, \\ \frac{\partial \mathbf{H_E}}{\partial \mathbf{T}} &= -\alpha_1. \end{aligned} \tag{3.106}$$

It does not make sense, physically, for there to be flow of mass as $R \to 0$. Therefore,

$$\alpha_2 = 0. \tag{3.107}$$

Unlike mass, binary heating (see Sect 1.5 for a detailed description) allows it to be possible to have a non-zero flow of energy in the center of the cluster. Therefore, α_1 is a free parameter.

3.4.2 Further approximations close to the center

We will extend our approximations close to the center, so that we can use a more accurate approximation for the computations. For simplification, we will define the parameter K

$$K = -\frac{2\alpha_1}{3K_D}. \tag{3.108}$$

We substitute (3.107) and (3.108) into (3.87) to obtain

$$\mathbf{F} = e^{-\mathbf{E}} + Ke^{-\mathbf{E}/2} \tag{3.109}$$

with (3.109), we can approximate $\mathbf{D}$, $\mathbf{R}$ and $\mathbf{Q}$ as we did in deriving (3.77a), (3.77b) and (3.77c). Doing this we arrive at

$$\begin{aligned}
\mathbf{D} &= \left(\frac{\pi}{2}\right)^{1/2}\left(e^{-\mathbf{U}} + 2\sqrt{2}Ke^{-\mathbf{U}/2}\right), \\
\mathbf{R} &= \left(\frac{8}{\pi}\right)^{1/4}\left(e^{\mathbf{U}/2} - \frac{K}{\sqrt{2}}e^{\mathbf{U}}\right), \\
\mathbf{Q} &= K_D\left(e^{3\mathbf{E}/2} - \frac{9\sqrt{3}}{8\sqrt{2}}Ke^{2\mathbf{E}}\right).
\end{aligned} \tag{3.110}$$

We find a higher order term for $\mathbf{F}^{(-1)}$ and $\mathbf{F}$ by using (3.84) in a similar manner to that described in deriving the lower order approximation. This gives us

$$\begin{aligned}
\mathbf{F}^{(-1)} &= -e^{-\mathbf{E}} - 2Ke^{-\mathbf{E}/2} + \frac{3}{2}b - \frac{3\sqrt{3}}{8\sqrt{2}}K^2, \\
\mathbf{F} &= e^{-\mathbf{E}} + Ke^{-\mathbf{E}/2} + 0.
\end{aligned} \tag{3.111}$$

It follows that the two integrals in our fundamental equation (3.53) can be approximated to

$$\begin{aligned}
\int_{-\infty}^{\mathbf{E}} \mathbf{F}_*\mathbf{Q}_*\mathrm{d}\mathbf{E}_* &= K_D\left[2e^{\mathbf{E}/2} + \left(1 - \frac{9\sqrt{3}}{8\sqrt{2}}\right)Ke^{\mathbf{E}} - \frac{3\sqrt{3}}{4\sqrt{2}}K^2e^{3\mathbf{E}/2}\right], \\
\int_{-\infty}^{\mathbf{E}} \mathbf{F}_*\mathbf{Q}'_*\mathrm{d}\mathbf{E}_* &= \frac{3}{2}K_D\left[2e^{\mathbf{E}/2} + \left(1 - \frac{3\sqrt{3}}{2\sqrt{2}}\right)Ke^{\mathbf{E}} - \frac{\sqrt{3}}{\sqrt{2}}K^2e^{3\mathbf{E}/2}\right].
\end{aligned} \tag{3.112}$$

We will not continue to evaluate the higher order approximations here. The calculations would become much more complicated and would provide very little additional insight.

3.5 The Fokker-Planck model

We have derived the equations for the Fokker-Planck model and all the necessary information needed to find a homological solution. Following in the work of Hénon

(1961), we use numerical methods to compute an approximate solution. The numerical method will be discussed in further detail in Sect. 3.5.1. In this section, we will arrange our system in a manner more suitable for the numerical calculations. We will also discuss the conditions and asymptotic solutions necessary for the computation.

We will define $\mathbf{E}$ and $\mathbf{U}$ to be our independent variables and will calculate $\mathbf{D}$, $\mathbf{R}$ and $\mathbf{Q}$, from (3.42a), (3.42b) and (3.42c). To compute a solution of our system of equations, we consider the following changes. Since $\mathbf{R}$ varies quickly as $\mathbf{E} \to 0$, we substitute a variable $\mathbf{Z}$, where

$$\mathbf{R} = \frac{1}{\mathbf{Z}}. \tag{3.113}$$

By integrating (3.53), we have

$$C = \mathbf{S}' + \left(\frac{3}{4}b - \frac{3}{2}c\right)\int_{-\infty}^{\mathbf{E}} \mathbf{Q}_*\mathbf{F}'_*\mathrm{d}\mathbf{E}_* - c\int_{-\infty}^{\mathbf{E}} \mathbf{F}\mathbf{Q}'\mathrm{d}\mathbf{E}_*, \tag{3.114}$$

where C is a constant.

For similar reasons in those discussed in the beginning of Sect. 3.4, the dominant term in (3.114) when $\mathbf{E} \to -\infty$ is $\mathbf{S}$. We've determined the asymptotic solution for $\mathbf{S}'$ is equal to α_2 in (3.71) and we determined in (3.107) that α_2 is zero. This implies that $C \to 0$ when $\mathbf{E} \to -\infty$. Since C is a constant, it follows that C must be zero $\forall$ $\mathbf{E}$.

We substitute (3.30) for $\mathbf{S}'$ and use integration by parts to arrive at the final form of our fundamental equation

$$0 = \mathbf{F}\int_{-\infty}^{\mathbf{E}} \mathbf{F}_*\mathbf{Q}'_*\mathrm{d}\mathbf{E}_* + \mathbf{F}'\left(\int_{-\infty}^{\mathbf{E}} \mathbf{F}_*\mathbf{Q}_*\mathrm{d}\mathbf{E}_* - \mathbf{Q}\mathbf{F}^{(-1)}\right) + \left(\frac{3}{4}b - \frac{3}{2}c\right)\mathbf{F}\mathbf{Q} + \left(\frac{1}{2}c - \frac{3}{4}b\right)\int_{-\infty}^{\mathbf{E}} \mathbf{F}_*\mathbf{Q}'_*\mathrm{d}\mathbf{E}_*. \tag{3.115}$$

Thus, the system of equations can be written as

$$\begin{aligned}
\mathbf{D} &= \int_{\mathbf{U}}^{\infty} (2\mathbf{E} - 2\mathbf{U})^{1/2}\,\mathbf{F}\mathrm{d}\mathbf{E}, \\
\frac{\mathrm{d}^2\mathbf{Z}}{\mathrm{d}\mathbf{U}^2} &= -\mathbf{D}\left(\frac{\mathrm{d}\mathbf{Z}}{\mathrm{d}\mathbf{U}}\right)^3 \mathbf{Z}^{-4}, \\
\mathbf{R} &= \frac{1}{\mathbf{Z}}, \\
\mathbf{Q} &= \frac{1}{3}\int_{-\infty}^{\mathbf{E}} (2\mathbf{E} - 2\mathbf{U})^{1/2}\mathbf{R}^3\mathrm{d}\mathbf{U}, \\
\mathbf{F}' &= -\frac{\mathbf{F}\int_{-\infty}^{\mathbf{E}} \mathbf{F}_*\mathbf{Q}'_*\mathrm{d}\mathbf{E}_* + \left(\frac{3}{4}b - \frac{3}{2}c\right)\mathbf{F}\mathbf{Q} + \left(\frac{1}{2}c - \frac{3}{4}b\right)\int_{-\infty}^{\mathbf{E}} \mathbf{F}_*\mathbf{Q}'_*\mathrm{d}\mathbf{E}_*}{\int_{-\infty}^{\mathbf{E}} \mathbf{F}_*\mathbf{Q}_*\mathrm{d}\mathbf{E}_* - \mathbf{Q}\mathbf{F}^{(-1)}}, \\
0 &= (3\lambda + 1)\,b + (2 - 2\lambda)\,c.
\end{aligned} \tag{3.116}$$

The equations described in (3.116a), (3.116b), (3.116c), (3.116d) and (3.116e), will be used to iteratively solve for our the homological solution. We will also require the

following asymptotic solutions for $\mathbf{E} \to -\infty$

$$\begin{aligned}
\mathbf{F} &= e^{-\mathbf{E}} + Ke^{-\mathbf{E}/2}, \\
\mathbf{F}^{(-1)} &= -e^{-\mathbf{E}} - 2Ke^{-\mathbf{E}/2} + \frac{3}{2}b - \frac{3\sqrt{3}}{8\sqrt{2}}K^2 \\
\mathbf{R} &= \left(\frac{8}{\pi}\right)^{1/4}\left(e^{\mathbf{U}/2} - \frac{K}{\sqrt{2}}e^{\mathbf{U}}\right), \\
\int_{-\infty}^{\mathbf{E}} \mathbf{F}_*\mathbf{Q}_*\mathrm{d}\mathbf{E}_* &= K_D\left[2e^{\mathbf{E}/2} + \left(1 - \frac{9\sqrt{3}}{8\sqrt{2}}\right)Ke^{\mathbf{E}} - \frac{3\sqrt{3}}{4\sqrt{2}}K^2e^{3\mathbf{E}/2}\right], \\
\int_{-\infty}^{\mathbf{E}} \mathbf{F}_*\mathbf{Q}'_*\mathrm{d}\mathbf{E}_* &= \frac{3}{2}K_D\left[2e^{\mathbf{E}/2} + \left(1 - \frac{3\sqrt{3}}{2\sqrt{2}}\right)Ke^{\mathbf{E}} - \frac{\sqrt{3}}{\sqrt{2}}K^2e^{3\mathbf{E}/2}\right], \qquad (3.117)
\end{aligned}$$

for various reasons in our computation. These reasons will be explained further in Sect. 3.5.1

As shown in (3.61), the edge of the cluster is $E = 0$. Thus, any star that has energy $E_s \geq 0$ will have escaped the system. Therefore, when calculating our numerical solution we must ensure that the conditions

$$\begin{aligned}
\mathbf{F}(0) &= 0, \\
\mathbf{F}^{(-1)}(0) &= -\int_0^{\infty} \mathbf{F}_*\mathrm{d}\mathbf{E}_* = 0, \qquad (3.118)
\end{aligned}$$

hold.

3.5.1 Numerical method

To compute a numerical solution for our model, we follow the method described in Hénon (1961). The code for this model can be seen in Appendix B. We use the asymptotic solutions described in (3.117a) and (3.117b) to obtain an initial guess for $\mathbf{F}$ and $\mathbf{F}^{(-1)}$. We initially define c and K in such a way that the conditions (3.118a) and (3.118b) hold. With the initial distribution function we can then calculate $\mathbf{D}$, $\mathbf{R}$ and $\mathbf{Q}$ using (3.116a), (3.116b) and (3.116d), respectively. The calculation of $\mathbf{R}$ uses the asymptotic solution found in (3.117c) for $\mathbf{R}(\mathbf{U}_{\min})$, where $\mathbf{U}_{\min}$ is the minimum value of the potential energy used in our calculation.

Once we obtain our initial values, we find that (3.116e) is equivalent to a system with variables

$$\begin{aligned}
y_1 &= \int_{-\infty}^{\mathbf{E}} \mathbf{F}_*\mathbf{Q}_*\mathrm{d}\mathbf{E}_*, \\
y_2 &= \int_{-\infty}^{\mathbf{E}} \mathbf{F}_*\mathbf{Q}'_*\mathrm{d}\mathbf{E}_*, \\
y_3 &= \mathbf{F}^{(-1)}, \\
y_4 &= \mathbf{F}, \qquad (3.119)
\end{aligned}$$

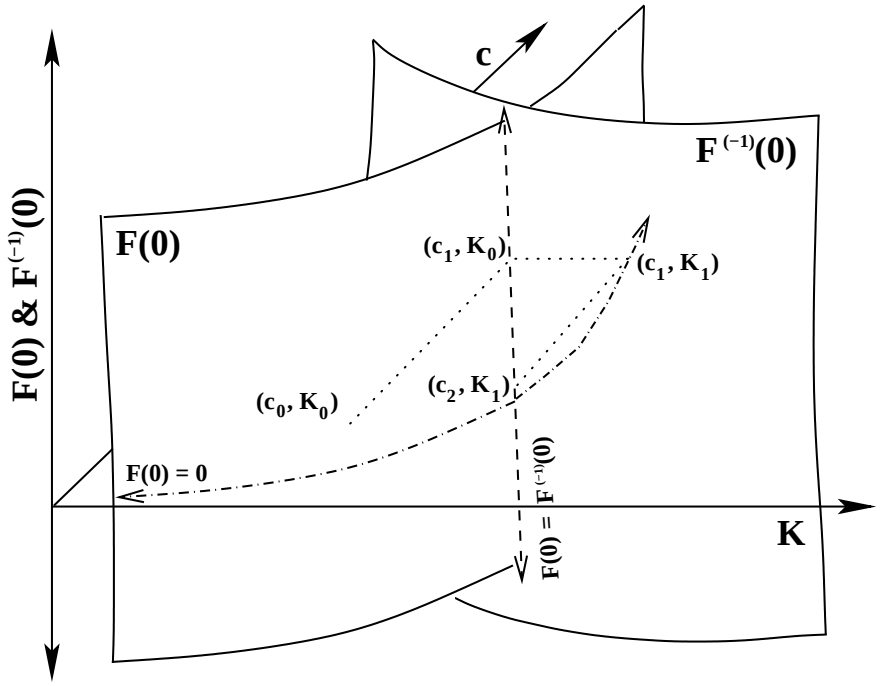

Figure 3.3: Method for iterating c and K such that $\mathbf{F} = \mathbf{F}^{(-1)} = 0$.

which can be written as

$$\begin{aligned} y_1' &= y_4\mathbf{Q}, \\ y_2' &= y_4\mathbf{Q}', \\ y_3' &= y_4, \\ y_4' &= -\frac{y_4 y_2 + \left(\frac{3}{4}b - \frac{3}{2}c\right) y_4\mathbf{Q} + \left(\frac{1}{2}c - \frac{3}{4}b\right) y_2}{y_1 - \mathbf{Q}y_3}. \end{aligned} \tag{3.120}$$

We integrate this system using the Euler Method and vary c and K such that the criteria (3.118a) and (3.118b) hold. This process of varying c and K is done at each iteration. Hénon did not go into much detail on the numerical method used to solve vary c and K. The method that we used can be shown pictorially in Fig. 3.3. We varied c to obtain $\mathbf{F}(0) = \mathbf{F}^{(-1)}(0)$, then varied K to obtain $\mathbf{F}(0) = 0$. We repeated this process until we found $\mathbf{F}(0) = \mathbf{F}^{(-1)}(0) = 0$.

Once this is done, we repeat using the new c, K, and $\mathbf{F}$. When c and K converge to a constant, then the calculation is finished and the final values for c, K, $\mathbf{D}$, $\mathbf{R}$, $\mathbf{Q}$ and $\mathbf{F}$ describe our self-similar solution.

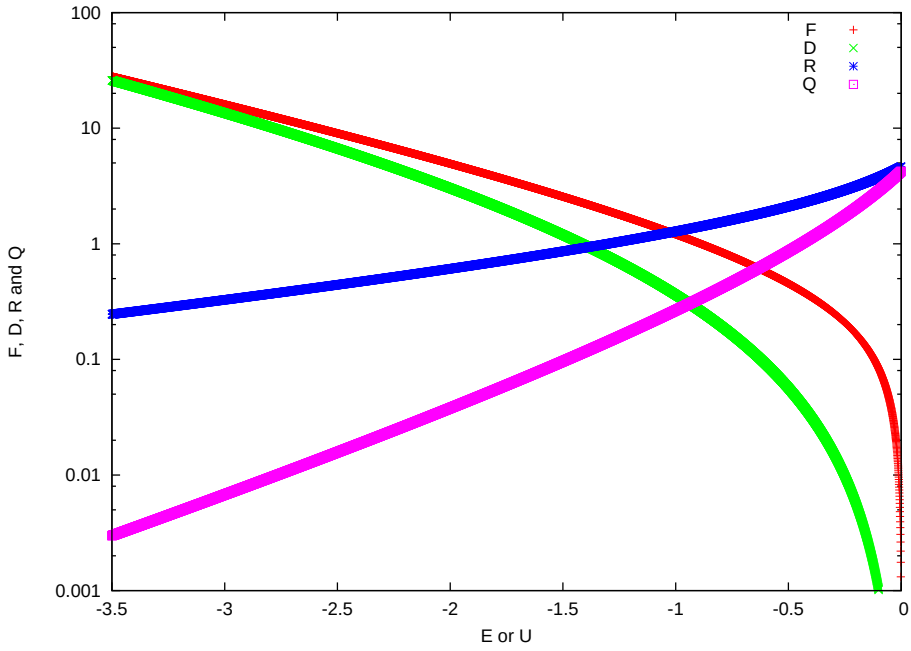

Figure 3.4: $\mathbf{F}(\mathbf{E})$, $\mathbf{D}(\mathbf{U})$, $\mathbf{R}(\mathbf{U})$ and $\mathbf{Q}(\mathbf{E})$, which we can compare with Fig.4 in Hénon (1961) (see Fig. 3.5).

3.5.2 Results

In this section we will show our numerical results for the Fokker-Planck model. We will compare them with the results shown in Hénon (1961). We will also show the effect of varying the step size, $d\mathbf{E}$, and the minimum value for $\mathbf{E}$, $\mathbf{E}_{\rm min}$.

Since this model is intended to model a globular cluster, there are certain features that our model should obtain. The center of the cluster should be the most dense region of the cluster and the density should decrease as the radius increases and the distribution function should behave similarly to the density. The potential energy should decrease towards $-\infty$ as the radius tends towards zero. In other words, the radius should increase as the potential energy increases. From (3.20) we can see that $\mathbf{Q}$ should be small towards the center of the cluster and increase as the radius increases. It is important that our model behaves in this manner. Otherwise, it will not be accurately modeling globular clusters.

In Fig. 3.4, we plot $\mathbf{D}(\mathbf{U})$, $\mathbf{R}(\mathbf{U})$, $\mathbf{Q}(\mathbf{E})$ and $\mathbf{F}(\mathbf{E})$. In this example, our step size is 5×10^{-4} and our minimum value for $\mathbf{E}$ and $\mathbf{U}$, $\mathbf{E}_{\rm min} = \mathbf{U}_{\rm min} = -5$. The range of the dependent axis is $[-3.5 : 0]$ for direct comparison with Fig. 4 in Hénon (1961). The small values of $\mathbf{E}$ and $\mathbf{U}$ correspond to the center of the cluster, whereas the large values of $\mathbf{E}$ and $\mathbf{U}$ correspond to the edge of the system. We find that $\mathbf{D}$ and $\mathbf{F}$ have their maxima towards the center of the cluster and tend towards zero at the edge. $\mathbf{R}$

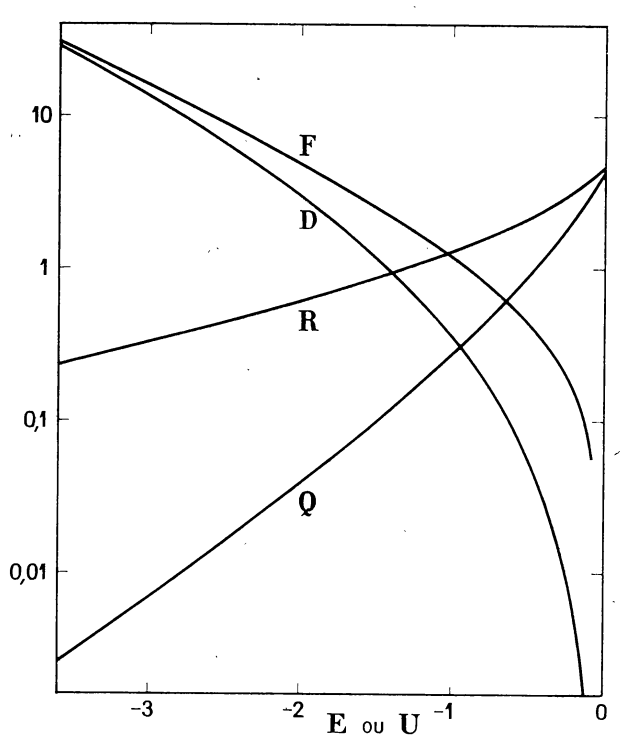

Figure 3.5: **F**(**E**), **D**(**U**), **R**(**U**) and **Q**(**E**), which was Fig. 4 in Hénon (1961)

and **Q** are smallest close to the center and increase towards the edge of the cluster. These are consistent with the expected behavior of **D**, **R**, **Q** and **F** in a globular cluster.

Since our results reflect the general behavior of a globular cluster, we will compare them qualitatively and quantitatively with Hénon (1961). Now we compare our results with the results given in Hénon (1961). In Fig 3.5, we show Fig. 4 from Hénon (1961) which gives **D**(**U**), **R**(**U**), **Q**(**E**) and **F**(**E**) as found by Hénon. The results shown in Fig. 3.5 are qualitatively very similar to Fig. 3.4. To look at this quantitatively, we will look at the error between our computed functions of **D**, **R**, **Q** and **F** and the functions shown in Table 1 in Hénon (1961).

In Fig. 3.6 we show the error between our computed **D**(**E**), **R**(**E**), **Q**(**E**) and **F**(**E**) and that shown in Table 1 of Hénon (1961). In all these examples the error begins small and increases as **E** increases, with a maximum error of 3%, with the exception of **D** which has a large increase in error when **E** approaches zero. Even in the case of **D**, the maximum error is only slightly above 3%.

The final values of c and K, found in Hénon (1961) were $c = 0.4078$ and $K = -0.94$. In Fig. 3.7 we have the value of c and K after each iteration, for the same example used in Fig. 3.4. This figure shows the values of c and K converge to $c = 0.4191$ and

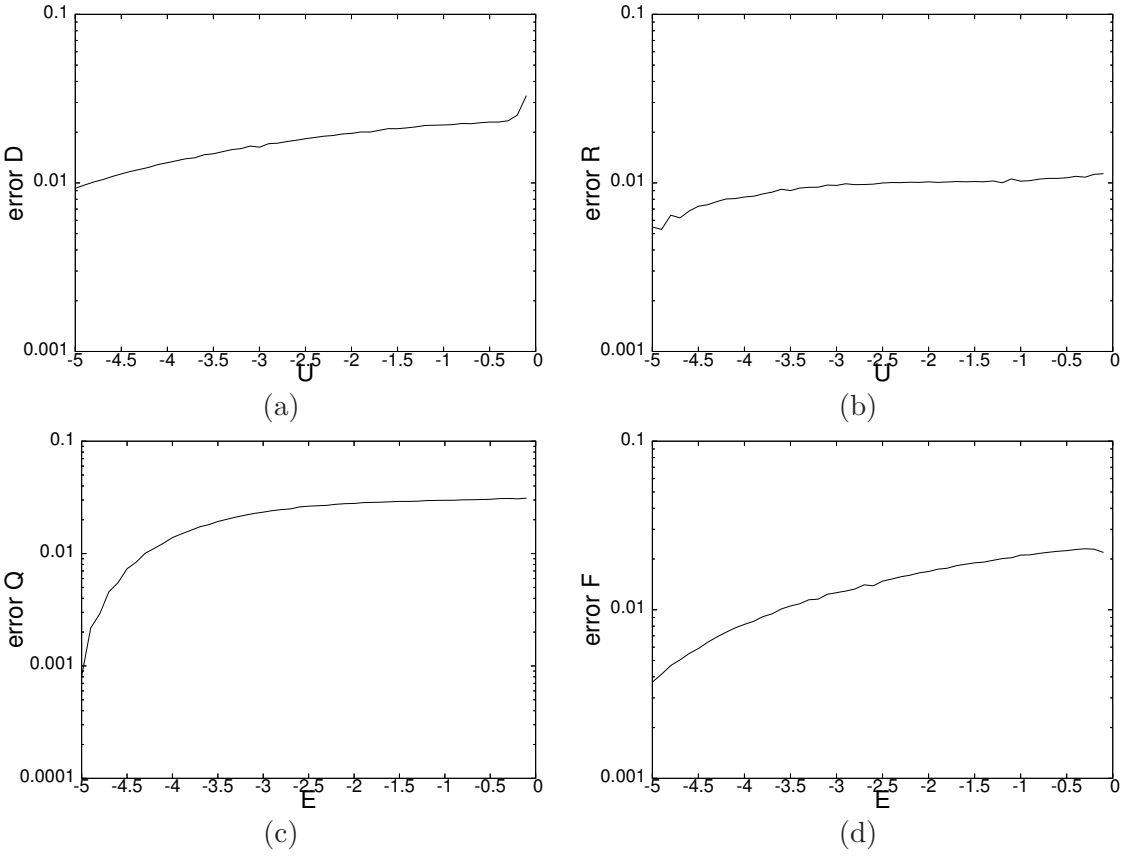

Figure 3.6: The error between our results for the case where where $d\mathbf{E} = 5 \times 10^{-4}$ and $\mathbf{E}_{\min} = -5$ and the results shown in Table 1 of Hénon (1961).

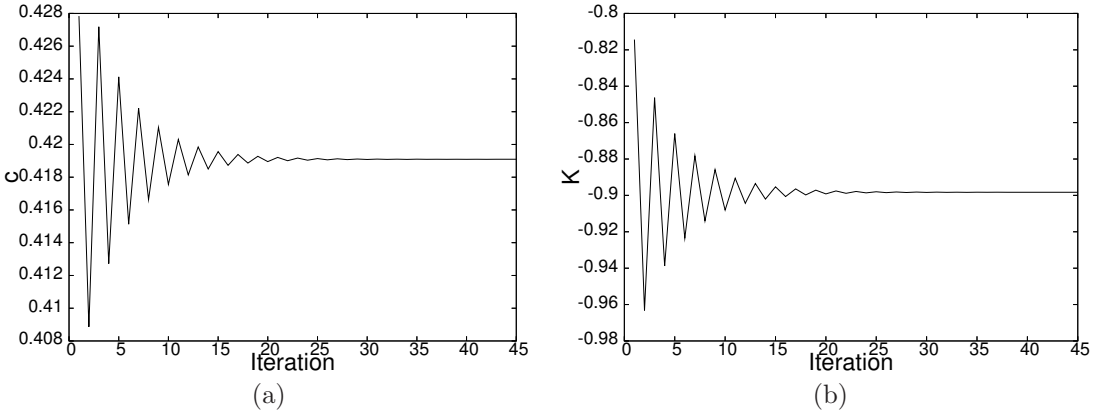

Figure 3.7: The value of c and K after each iteration in the case where $d\mathbf{E} = 5 \times 10^{-4}$ and $\mathbf{E}_{\min} = -5$.

$d\mathbf{E}$	$\mathbf{E}_{\min} = -4$	$\mathbf{E}_{\min} = -5$	$\mathbf{E}_{\min} = -6$
1×10^{-3}	$c = 0.42607$	$c = 0.4182$	- -
	$K = -0.8939$	$K = -0.8982$	- -
5×10^{-4}	$c = 0.4266$	$c = 0.4191$	$c = 0.4155$
	$K = -0.8943$	$K = -0.8983$	$K = -0.9045$
2.5×10^{-4}	- -	$c = 0.4195$	- -
	- -	$K = -0.8983$	- -

Table 3.1: The final values of c and K with varying parameters $d\mathbf{E}$ and $\mathbf{E}_{\min}$.

$K = -0.8983$. This amounts to an error of 2.7% for c and 4.6% for K. Although the error for c is consistent with the higher error found in Fig 3.6, the error for K is notably more. To investigate this further we will examine the final values of c and K while varying some parameters.

We vary the parameters $\mathbf{E}_{\min}$ and the step size, $d\mathbf{E}$, to find how this affects the final values of c and K. The results are shown in Table 3.1. We find that $d\mathbf{E}$ does not make a significant difference to the final values of c and almost no difference on K. The value of $\mathbf{E}_{\min}$ has a much more noticeable impact on the final values of c and K. Moreover, as $\mathbf{E}_{\min}$ gets smaller, c and K get closer to the values found by Hénon (1961). We had assumed that Table 1 in Hénon (1961), which showed $\mathbf{E}_{\min} = -5$, were the complete results of Hénon's homological solution. However, it is possible that this is only a section of the results and that $\mathbf{E}_{\min}$ was actually lower than the table suggests. If this is so, then our results for c and K would be reasonably consistent with the results found in Hénon (1961).

We have reproduced the work presented in Hénon (1961). We have analyzed the the derivation of the equations of the Fokker-Planck model in great detail. We have found the homological solution for our system, numerically, and found it to be in satisfactory agreement with the numerical results found in Hénon (1961). Now we can derive equations for a 2-component model and and attempt to find its solution in a similar manner to the work presented in this chapter.

4

Two-Component Fokker-Planck Model

In Chapter 6 of Hénon (1961), equations for a two-component system are derived in the case where the number of heavy stars are assumed to be negligible in comparison to the number of light stars. This also implied that the interactions between heavy stars can be neglected which led to a simplified model for this case.

In this chapter, we will derive the equations for a two-component system with no restriction on the heavy star population. We will do so by extending upon the work shown in Chapter 3.

4.1 Deriving the equations for a two-component system

In this section we will utilize the general equations derived in Sect 3.1.1 to create a two-component Fokker-Planck model. First we will look at the density of a two component system. Our density was shown generally in (3.5) to be

$$\rho = 4\pi \int_0^\infty m \int_U^\infty (2E - 2U)^{1/2} f \mathrm{d}E \mathrm{d}m. \tag{4.1}$$

In Sect. 3.2, we used the δ-function shown in (3.24) to adjust our general Fokker-Planck model for the single mass case. Similarly in the two-component case, f is defined as

$$f = \delta(m - m_1)F_1 + \delta(m - m_2)F_2, \tag{4.2}$$

where m_1 is the individual mass of the light stars, F_1 is the distribution of the light stellar population, $m_2 > m_1$ is the individual mass of the heavy stars and F_2 is the distribution of the heavy stellar population. We will use the definition of the distribution function found in (4.2) to adjust our general Fokker-Planck model for the two-component case. With this expression of f our density function becomes

$$\rho = 4\pi \int_U^\infty (2E - 2U)^{1/2} \left(m_1 F_1 + m_2 F_2\right) \mathrm{d}E\mathrm{d}m. \tag{4.3}$$

We define μ to be the ratio of the individual masses of each population

$$\mu = m_2/m_1. \tag{4.4}$$

Note that μ is the same as $\tilde{m}$ used in Chapter 2, but we use μ to follow the notation used by Hénon. Using μ, we can simplify ρ to

$$\rho = 4\pi m_1 \int_U^\infty (2E - 2U)^{1/2} \left(F_1 + \mu F_2\right) \mathrm{d}E\mathrm{d}m. \tag{4.5}$$

The general fundamental equation

$$16\pi^2 G^2 \log N \int_0^\infty m_* \frac{\partial}{\partial E}\left[mf \int_{-\infty}^E f_* q_*' \mathrm{d}E_* + m_* f' \left(\int_{-\infty}^E f_* q_* \mathrm{d}E_* + q\int_E^\infty f_* \mathrm{d}E_*\right)\right]\mathrm{d}m_* + f'\frac{\partial q}{\partial t} - q'\frac{\partial f}{\partial t} = 0, \tag{4.6}$$

was found in (3.23). We can think of this as describing the evolution of a population of test stars (with distribution f and mass m) being acted upon by a population of field stars in the cluster (with distribution f_* and mass m_*)

First we consider the effects of the stellar population on the light stars. We can think of the light stars as the test stars and the total stellar population in the cluster as the field stars. We use (4.2), F_1 and m_1 for f_*, f and m, respectively. With this in

mind we find

$$16\pi^2 G^2 \log N \frac{\partial}{\partial E}\Bigg[m_1 F_1 \int_{-\infty}^{E}\Bigg\{\Bigg(\int_0^\infty m_*\delta(m_*-m_1)\mathrm{d}m\Bigg)F_{1*}+ \Bigg(\int_0^\infty m_*\delta(m_*-m_2)\mathrm{d}m\Bigg)F_{2*}\Bigg\}q'_*\mathrm{d}E_* + F_1'\Bigg(\int_{-\infty}^{E}\Bigg\{\Bigg(\int_0^\infty m_*^2\delta(m_*-m_1)\mathrm{d}m\Bigg)F_{1*}+ \Bigg(\int_0^\infty m_*^2\delta(m_*-m_2)\mathrm{d}m\Bigg)F_{2*}\Bigg\}q_*\mathrm{d}E_* + q\int_E^\infty\Bigg\{\Bigg(\int_0^\infty m_*^2\delta(m_*-m_1)\mathrm{d}m\Bigg)F_{1*}+ \Bigg(\int_0^\infty m_*^2\delta(m_*-m_2)\mathrm{d}m\Bigg)F_{2*}\Bigg\}\mathrm{d}E_*\Bigg)\Bigg] + F_1'\frac{\partial q}{\partial t} - q'\frac{\partial F_1}{\partial t} = 0, \quad (4.7)$$

where q, q' and $\mathrm{d}q/\mathrm{d}t$ are the same as defined in (3.20), (3.21) and (3.22), respectively.

When integrating over the mass, this becomes

$$16\pi^2 G^2 \log N \frac{\partial}{\partial E}\Bigg[m_1 F_1 \int_{-\infty}^{E}\left(m_1 F_{1*} + m_2 F_{2*}\right) q'_*\mathrm{d}E_* + F_1'\Bigg(\int_{-\infty}^{E}\left(m_1^2 F_{1*} + m_2^2 F_{2*}\right) q_*\mathrm{d}E_* + q\int_E^\infty\left(m_1^2 F_{1*} + m_2^2 F_{2*}\right)\mathrm{d}E_*\Bigg)\Bigg] + F_1'\frac{\partial q}{\partial t} - q'\frac{\partial F_1}{\partial t} = 0. \quad (4.8)$$

Using (4.4) this can be simplified to

$$16\pi^2 m_1^2 G^2 \log N \frac{\partial}{\partial E}\Bigg[F_1 \int_{-\infty}^{E}\left(F_{1*} + \mu F_{2*}\right) q'_*\mathrm{d}E_* + F_1'\Bigg(\int_{-\infty}^{E}\left(F_{1*} + \mu^2 F_{2*}\right) q_*\mathrm{d}E_* + q\int_E^\infty\left(F_{1*} + \mu^2 F_{2*}\right)\mathrm{d}E_*\Bigg)\Bigg] + F_1'\frac{\partial q}{\partial t} - q'\frac{\partial F_1}{\partial t} = 0. \quad (4.9)$$

Similarly, the fundamental equation for the heavy stars is found to be

$$16\pi^2 m_1^2 G^2 \log N \frac{\partial}{\partial E}\Bigg[\mu F_2 \int_{-\infty}^{E}\left(F_{1*} + \mu F_{2*}\right) q'_*\mathrm{d}E_* + F_2'\Bigg(\int_{-\infty}^{E}\left(F_{1*} + \mu^2 F_{2*}\right) q_*\mathrm{d}E_* + q\int_E^\infty\left(m_1^2 F_{1*} + \mu^2 F_{2*}\right)\mathrm{d}E_*\Bigg)\Bigg] + F_1'\frac{\partial q}{\partial t} - q'\frac{\partial F_1}{\partial t} = 0, \quad (4.10)$$

We use the transformations

$$\begin{aligned} \rho &= 4\pi m_1 D, \\ r &= \left(16\pi^2 G m_1\right)^{-1/2} R, \\ q &= \left(16\pi^2 G m_1\right)^{-3/2} Q, \\ dt &= \left(16\pi^2 G^2 m_1^2 \log N\right)^{-1} dT. \end{aligned} \quad (4.11)$$

to simplify our equations by the removal of constants. After the appropriate transformation the equations become

$$\begin{aligned}
D &= \int_U^\infty (2E-2U)^{1/2}\,(F_1+\mu F_2)\,\mathrm{d}E,\\
\frac{\partial^2 U}{\partial R^2} &+ \frac{2}{R}\frac{\partial U}{\partial R} = D,\\
Q &= \frac{1}{3}\int_0^{R_m} (2E-2U)^{3/2} R^2 \mathrm{d}R,\\
0 &= \frac{\partial}{\partial E}\Bigg[\mu^{(i-1)} F_i \int_{-\infty}^{E} (F_{1*}+\mu F_{2*})\,Q'_* \mathrm{d}E_* + F_i'\Bigg(\int_{-\infty}^{E}\left(F_{1*}+\mu^2 F_{2*}\right) Q_* \mathrm{d}E_* +\\
&\qquad Q\int_E^\infty \left(F_{1*}+\mu^2 F_{2*}\right)\mathrm{d}E_*\Bigg)\Bigg] + F_i'\frac{\partial Q}{\partial T} - Q'\frac{\partial F_i}{\partial T}, \qquad (4.12)
\end{aligned}$$

where $i = 1, 2$.

As in Sect. 3.2.1, we create a self-similar system and we define our canonical transformation to be

$$\begin{aligned}
E &= \beta \mathbf{E},\\
F_1 &= \gamma \mathbf{F}_1,\\
F_2 &= \gamma \mathbf{F}_2. \qquad (4.13)
\end{aligned}$$

In Hénon (1961) a third parameter γ_2 is used to use to scale F_2. This is acceptable in the case where the number of heavy stars N_2 is negligible. Since we are not making this assumption about the heavy population, we need to use the same scaling parameter for F_1 and F_2 to ensure that the evolution is self-similar.

The transformations shown in (4.13) lead to the following transformations

$$\begin{aligned}
U &= \beta \mathbf{U},\\
D &= \beta^{3/2}\gamma \mathbf{D},\\
R &= \beta^{-1/4}\gamma^{-1/2}\mathbf{R},\\
Q &= \beta^{3/4}\gamma^{-3/2}\mathbf{Q},\\
dT &= \gamma^{-1}\mathbf{dT},\\
S &= \beta^{7/4}\gamma^{1/2}\mathbf{S}. \qquad (4.14)
\end{aligned}$$

Transforming our system of equations is straightforward with the exception of the last two terms in (4.12d). In a similar manner as in the derivation of (3.42d), we write the last two terms of (4.12d) as the determinate of the Jacobian matrix

$$\frac{\partial\left(F_i, Q\right)}{\partial\left(E, T\right)} = \begin{vmatrix} \frac{\partial F_i}{\partial E} & \frac{\partial F_i}{\partial T} \\ \frac{\partial Q}{\partial E} & \frac{\partial Q}{\partial T} \end{vmatrix} = \frac{\partial F_i}{\partial E}\frac{\partial Q}{\partial T} - \frac{\partial Q}{\partial E}\frac{\partial F_i}{\partial T}. \qquad (4.15)$$

We use

$$\frac{\partial\left(F_i,Q\right)}{\partial\left(E,T\right)}=\frac{\partial\left(F_i,Q\right)}{\partial\left(\mathbf{E},\mathbf{T}\right)}\frac{\partial\left(\mathbf{E},\mathbf{T}\right)}{\partial\left(E,T\right)}. \tag{4.16}$$

to transform the determinate of the Jacobian given in (4.15). Similarly to the notation used in Chapter 3, the bold indicates the scaled variables. From (4.15) and (4.16) it follows that

$$\frac{\partial F_i}{\partial E}\frac{\partial Q}{\partial T}-\frac{\partial Q}{\partial E}\frac{\partial F_i}{\partial T}=\frac{\gamma}{\beta}\left[\frac{\partial F_i}{\partial \mathbf{E}}\frac{\partial Q}{\partial \mathbf{T}}-\frac{\partial Q}{\partial \mathbf{E}}\frac{\partial F_i}{\partial \mathbf{T}}\right]. \tag{4.17}$$

Then we use straightforward transformations found in (4.14) to arrive at

$$\begin{aligned}\frac{\partial F_i}{\partial E}\frac{\partial Q}{\partial T}-\frac{\partial Q}{\partial E}\frac{\partial F_i}{\partial T}=\beta^{-1/4}\gamma^{1/2}\Bigg[&\frac{\partial \mathbf{F}_i}{\partial \mathbf{E}}\frac{\partial \mathbf{Q}}{\partial \mathbf{T}}-\frac{\partial \mathbf{Q}}{\partial \mathbf{E}}\frac{\partial \mathbf{F}_i}{\partial \mathbf{T}}+\mathbf{Q}\frac{\partial \mathbf{F}_i}{\partial \mathbf{E}}\left(\frac{3}{4\beta}\frac{\partial \beta}{\partial \mathbf{T}}-\frac{3}{2\gamma}\frac{\partial \gamma}{\partial \mathbf{T}}\right)\\&-\mathbf{F}_i\frac{\partial \mathbf{Q}}{\partial \mathbf{E}}\frac{1}{\gamma}\frac{\partial \gamma}{\partial \mathbf{T}}\Bigg].\end{aligned} \tag{4.18}$$

The canonical equations of our system are

$$\begin{aligned}\mathbf{D} &= \int_{\mathbf{U}}^{\infty}\left(2\mathbf{E}-2\mathbf{U}\right)^{1/2}\left(\mathbf{F}_1+\mu\mathbf{F}_2\right)\mathrm{d}\mathbf{E},\\ \frac{\partial^2\mathbf{U}}{\partial\mathbf{R}^2} &+ \frac{2}{\mathbf{R}}\frac{\partial\mathbf{U}}{\partial\mathbf{R}}=\mathbf{D},\\ \mathbf{Q} &= \frac{1}{3}\int_0^{\mathbf{R}_m}\left(2\mathbf{E}-2\mathbf{U}\right)^{3/2}\mathbf{R}^2\mathrm{d}\mathbf{R},\\ 0 &= \frac{\partial}{\partial\mathbf{E}}\Bigg[\mu^{(i-1)}\mathbf{F}_i\int_{-\infty}^{\mathbf{E}}\left(\mathbf{F}_{1*}+\mu\mathbf{F}_{2*}\right)\mathbf{Q}'_*\mathrm{d}\mathbf{E}_*+\mathbf{F}'_i\Bigg(\int_{-\infty}^{\mathbf{E}}\left(\mathbf{F}_{1*}+\mu^2\mathbf{F}_{2*}\right)\\ &\quad\mathbf{Q}_*\mathrm{d}\mathbf{E}_*+\mathbf{Q}\int_{\mathbf{E}}^{\infty}\left(\mathbf{F}_{1*}+\mu^2\mathbf{F}_{2*}\right)\mathrm{d}\mathbf{E}_*\Bigg)\Bigg]+\frac{\partial\mathbf{F}_i}{\partial\mathbf{E}}\frac{\partial\mathbf{Q}}{\partial\mathbf{T}}-\frac{\partial\mathbf{Q}}{\partial\mathbf{E}}\frac{\partial\mathbf{F}_i}{\partial\mathbf{T}}\\ &\quad+\mu^2\left(\frac{3}{4}b-\frac{3}{2}c\right)\mathbf{Q}\mathrm{F}'_i-\mu^2c\mathbf{F}_i\mathbf{Q}',\end{aligned} \tag{4.19}$$

where the prime represents a partial derivative with respect to $\mathbf{E}$ and

$$\begin{aligned}b &= \frac{1}{\mu^2\beta}\frac{\mathrm{d}\beta}{\mathrm{d}\mathbf{T}},\\ c &= \frac{1}{\mu^2\gamma}\frac{\mathrm{d}\gamma}{\mathrm{d}\mathbf{T}}.\end{aligned} \tag{4.20}$$

Note that we include a factor of $1/\mu^2$ in (4.20) which was not used in (3.43). This is to ensure that in the case where $\mathbf{F}_1=0,\ \forall\ \mathbf{E}$ (i.e. the case in which there are no light stars) the equation for the heavy stars (4.19d, for $i=2$) reduces to the single-mass case shown in (3.42d).

It is also important to notice that the relation between b and c found in (3.68), with $\lambda=1/3$, still holds in our two-component system. The argument which leads

to this relation does not depend on the number of stellar populations in the system. Therefore it does not matter if the system is a single mass system or a two-component system.

As in (3.2.3), we are interested in homological evolution. We can create a system which is self similar with the conditions

$$\begin{aligned} \frac{\partial \mathbf{F}_1}{\partial \mathbf{T}} &= 0, \\ \frac{\partial \mathbf{F}_2}{\partial \mathbf{T}} &= 0, \\ \frac{\partial \mathbf{Q}}{\partial \mathbf{T}} &= 0. \end{aligned} \tag{4.21}$$

With these conditions, (4.19d) can be written as

$$\begin{aligned} 0 = \frac{\partial}{\partial \mathbf{E}} \Bigg[\mu^{(i-1)} \mathbf{F}_i \int_{-\infty}^{\mathbf{E}} \left(\mathbf{F}_{1*} + \mu \mathbf{F}_{2*}\right) \mathbf{Q}'_* \mathrm{d}\mathbf{E}_* + \mathbf{F}'_i \Bigg(\int_{-\infty}^{\mathbf{E}} \left(\mathbf{F}_{1*} + \mu^2 \mathbf{F}_{2*}\right) \\ \mathbf{Q}_* \mathrm{d}\mathbf{E}_* + \mathbf{Q} \int_{\mathbf{E}}^{\infty} \left(\mathbf{F}_{1*} + \mu^2 \mathbf{F}_{2*}\right) \mathrm{d}\mathbf{E}_* \Bigg) \Bigg] + \mu^2 \left(\frac{3}{4} b - \frac{3}{2} c \right) \mathbf{Q} \mathrm{F}'_i - \mu^2 c \mathbf{F}_i \mathbf{Q}, \end{aligned} \tag{4.22}$$

Our two-component system would then consist of (4.19a-c) and (4.22).

4.2 Approximations close to the center

We assume that the central density is infinite for reasons expressed in Sect. 3.4. This, amongst other assumptions, will lead to approximations close to the center for $\mathbf{D}$, $\mathbf{R}$, $\mathbf{Q}$, $\mathbf{F}_1$ and $\mathbf{F}_2$.

4.2.1 Distribution function for the population of heavy stars

We will consider the approximations close to the center for $\mathbf{F}_2$. Since the heavy stars dominate the center of the cluster, we anticipate that our approximations will be similar to that of the single mass case found in Sect. 3.4.

We begin by examining our equation for the heavy stars

$$\begin{aligned} 0 = \frac{\partial}{\partial \mathbf{E}} \Bigg[\mu \mathbf{F}_2 \int_{-\infty}^{\mathbf{E}} \left(\mathbf{F}_{1*} + \mu \mathbf{F}_{2*}\right) \mathbf{Q}'_* \mathrm{d}\mathbf{E}_* + \mathbf{F}'_2 \Bigg(\int_{-\infty}^{\mathbf{E}} \left(\mathbf{F}_{1*} + \mu^2 \mathbf{F}_{2*}\right) \mathbf{Q}_* \mathrm{d}\mathbf{E}_* + \\ \mathbf{Q} \int_{\mathbf{E}}^{\infty} \left(\mathbf{F}_{1*} + \mu^2 \mathbf{F}_{2*}\right) \mathrm{d}\mathbf{E}_* \Bigg) \Bigg] + \mu^2 \left(\frac{3}{4} b - \frac{3}{2} c \right) \mathbf{Q} \mathbf{F}'_2 - \mu^2 c \mathbf{F}_2 \mathbf{Q}'. \end{aligned} \tag{4.23}$$

To simplify the above equation, we use the following expressions

$$\begin{aligned}
\mathbf{S}'_{22} &= \mathbf{F}_2 \int_{-\infty}^{\mathbf{E}} \mathbf{F}_{2*}\mathbf{Q}'_* \mathrm{d}\mathbf{E}_* + \mathbf{F}'_2 \left(\int_{-\infty}^{\mathbf{E}} \mathbf{F}_{2*}\mathbf{Q}_* \mathrm{d}\mathbf{E}_* + \mathbf{Q} \int_{\mathbf{E}}^{\infty} \mathbf{F}_{2*} \mathrm{d}\mathbf{E}_* \right), \\
\mathbf{S}'_{21} &= \mu \mathbf{F}_2 \int_{-\infty}^{\mathbf{E}} \mathbf{F}_{1*}\mathbf{Q}'_* \mathrm{d}\mathbf{E}_* + \mathbf{F}'_2 \left(\int_{-\infty}^{\mathbf{E}} \mathbf{F}_{1*}\mathbf{Q}_* \mathrm{d}\mathbf{E}_* + \mathbf{Q} \int_{\mathbf{E}}^{\infty} \mathbf{F}_{1*} \mathrm{d}\mathbf{E}_* \right), \\
\mathbf{B}_2 &= \left(\frac{3}{4} b - \frac{3}{2} c \right) \mathbf{Q}\mathbf{F}'_2 - c\mathbf{F}_2\mathbf{Q}',
\end{aligned} \tag{4.24}$$

where

$$\mathbf{S}_{22} = \mathbf{F}_2^{(-1)} \int_{-\infty}^{\mathbf{E}} \mathbf{F}_{2*}\mathbf{Q}'_* \mathrm{d}\mathbf{E}_* - \mathbf{F}_2 \int_{-\infty}^{\mathbf{E}} \mathbf{F}_{2*}^{(-1)} \mathbf{Q}'_* \mathrm{d}E_*. \tag{4.25}$$

It is important to note that we have been able to find no analytical expression $\mathbf{S}_{21}$ whose derivative is $\mathbf{S}'_{21}$. However, we use the notation $\mathbf{S}'_{21}$ in (4.24b) for consistency with the other $\mathbf{S}_{ij}$ notation.

Using (4.24a), (4.24b) and (4.24c), we reduce the equation for the heavy stars to

$$0 = \mu^2 \mathbf{S}''_{22} + \mathbf{S}''_{21} + \mu^2 \mathbf{B}_2. \tag{4.26}$$

Since the heavy stars are dominant in the center we will assume that

$$\mathbf{F}_2(\mathbf{E}) \gg \mathbf{F}_1(\mathbf{E}), \tag{4.27}$$

when $\mathbf{E}$ is very large and negative. From (4.24a) and (4.24b) we can see that the terms of $\mathbf{S}''_{22}$ are of the order $\mathbf{F}_2^2\mathbf{Q}$ and the terms of $\mathbf{S}''_{21}$ are of the order $\mathbf{F}_1\mathbf{F}_2\mathbf{Q}$, thus

$$\mathbf{S}''_{22} \gg \mathbf{S}''_{21}. \tag{4.28}$$

when $\mathbf{E}$ is very large and negative.

Also from (4.24a) and (4.24c) we can see that terms in $\mathbf{S}''_{22}$ are of order $\mathbf{F}_2^2\,\mathbf{Q}$, whereas the terms in $\mathbf{B}_2$ must be of order $\mathbf{F}_2\,\mathbf{Q}$. Since we have assumed that the density is infinite in the center, $\mathbf{F}_2$ must also be infinite at the center. This implies that

$$\mathbf{S}''_{22} \gg \mathbf{B}_2, \tag{4.29}$$

when $\mathbf{E}$ is very large and negative. Therefore for the purpose of finding an asymptotic solution of the distribution of heavy stars, (4.26) simplifies to

$$\mathbf{S}''_{22} = 0. \tag{4.30}$$

The solution for $\mathbf{S}_{22}$ is

$$\mathbf{S}_{22} = \alpha_1 + \alpha_2 \mathbf{E}. \tag{4.31}$$

For the moment, we will assume that α_1 and α_2 are zero. It follows that

$$\begin{aligned}
\mathbf{S}_{22} &= \mathbf{F}_2^{(-1)} \int_{-\infty}^{\mathbf{E}} \mathbf{F}_{2*}\mathbf{Q}'_*\mathrm{d}\mathbf{E}_* - \mathbf{F}_2 \int_{-\infty}^{\mathbf{E}} \mathbf{F}_{2*}^{(-1)}\mathbf{Q}'_*\mathrm{d}E_* = 0, \\
\mathbf{S}'_{22} &= \mathbf{F}_2 \int_{-\infty}^{\mathbf{E}} \mathbf{F}_{2*}\ \mathbf{Q}'_*\mathrm{d}\mathbf{E}_* - \mathbf{F}'_2 \int_{-\infty}^{\mathbf{E}} \mathbf{F}_{2*}^{(-1)}\mathbf{Q}'_*\mathrm{d}\mathbf{E}_* = 0.
\end{aligned} \tag{4.32}$$

These equations can be manipulated to the form

$$\begin{aligned}
\frac{\mathbf{F}_2^{(-1)}}{\mathbf{F}_2} &= \frac{\int_{-\infty}^{\mathbf{E}} \mathbf{F}_{2*}^{(-1)}\mathbf{Q}'_*\mathrm{d}E_*}{\int_{-\infty}^{\mathbf{E}} \mathbf{F}_{2*}\mathbf{Q}'_*\mathrm{d}\mathbf{E}_*}, \\
\frac{\mathbf{F}_2}{\mathbf{F}'_2} &= \frac{\int_{-\infty}^{\mathbf{E}} \mathbf{F}_{2*}^{(-1)}\mathbf{Q}'_*\mathrm{d}E_*}{\int_{-\infty}^{\mathbf{E}} \mathbf{F}_{2*}\mathbf{Q}'_*\mathrm{d}\mathbf{E}_*},
\end{aligned} \tag{4.33}$$

from which we can find the relation

$$\frac{\mathbf{F}_2^{(-1)}}{\mathbf{F}_2} = \frac{\mathbf{F}_2}{\mathbf{F}'_2}. \tag{4.34}$$

By integration this yields the general solution

$$\mathbf{F}_2 = C_3 e^{-C_4\mathbf{E}}. \tag{4.35}$$

where C_3 and C_4 are constants. These constants need to be positive in order for (4.35) to be positive and increase when E decreases.

We can make a similar argument to that stated in Sect. 3.4; there is freedom in the choice of β and γ which allows us to choose C_3 and C_4 freely. Thus, the equation for F_2 can be written as

$$\mathbf{F}_2 = e^{-\mathbf{E}}. \tag{4.36}$$

We approximate the values of $\mathbf{D}$, $\mathbf{R}$ and $\mathbf{Q}$ with (4.19). While doing this, we use (4.27) and the first order asymptotic solution for F_2 (4.36) to reach the following approximations

$$\begin{aligned}
\mathbf{D} &= \mu \left(\frac{\pi}{2}\right)^{1/2} e^{-\mathbf{U}} \\
\mathbf{R} &= \mu^{-1/2} \left(\frac{8}{\pi}\right)^{1/4} e^{\mathbf{U/2}}, \\
\mathbf{Q} &= \frac{K_D}{\mu} e^{\mathbf{3E/2}},
\end{aligned} \tag{4.37}$$

where K_D is defined in (3.77). It can be seen in (4.37a-c) that the asymptotic solutions for $\mathbf{D}$, $\mathbf{R}$ and $\mathbf{Q}$ in the two-component model are the same as in the single mass model (3.77a-c) with the addition of some factor of μ.

Using (4.36) and (4.37c), we find approximations for the integrals that are important for the current derivations

$$\begin{aligned}\int_{-\infty}^{\mathbf{E}} \mathbf{F}_{2*}\mathbf{Q}_*\mathrm{d}\mathbf{E}_* &= \frac{2K_D}{\mu}e^{\mathbf{E}/2},\\ \int_{-\infty}^{\mathbf{E}} \mathbf{F}_{2*}\mathbf{Q}'_*\mathrm{d}\mathbf{E}_* &= \frac{3K_D}{\mu}e^{\mathbf{E}/2}.\end{aligned} \tag{4.38}$$

We consider the perturbed case (i.e. the case where α_1 and α_2 are not zero). The perturbed solution of (4.31) is

$$\mathbf{F}_2 = e^{-\mathbf{E}} + \alpha_1 Y_1 + \alpha_2 Y_2, \tag{4.39}$$

where Y_1 and Y_2 are functions of $\mathbf{E}$.

We find the relation

$$\frac{\mathbf{F}_2\mathbf{S}' - \mathbf{F}'_2\mathbf{S}}{\int_{-\infty}^{\mathbf{E}} \mathbf{F}_{2*}\mathbf{Q}'_*\mathrm{d}\mathbf{E}_*} = \mathbf{F}_2^2 - \mathbf{F}_2^{(-1)}\mathbf{F}'_2, \tag{4.40}$$

in the same way as shown in deriving (3.84). We substitute (4.37c) and (4.36) on the left-hand side of (4.40) and (4.39) on the right-hand side. This can be reduced to two ordinary differential equations

$$\begin{aligned}Y_1^{(-1)} + 2Y_1 + Y_1' &= \frac{\mu e^{-\mathbf{E}/2}}{3K_D},\\ Y_2^{(-1)} + 2Y_2 + Y_2' &= \frac{\mu\left(1+\mathbf{E}\right)e^{-\mathbf{E}/2}}{3K_D}.\end{aligned} \tag{4.41}$$

The solutions to these equations are

$$\begin{aligned}Y_1 &= C_{11}e^{-\mathbf{E}} + C_{12}\mathbf{E}e^{-\mathbf{E}} - \frac{2\mu}{3K_D}e^{-\mathbf{E}/2},\\ Y_2 &= C_{21}e^{-\mathbf{E}} + C_{22}\mathbf{E}e^{-\mathbf{E}} + \frac{2\mu}{3K_D}\left(5-\mathbf{E}\right)e^{-\mathbf{E}/2},\end{aligned} \tag{4.42}$$

where the C_{ij} are constant. We can scale $\mathbf{F}_2$ to eliminate the C_{ij}, leaving our approximation for the distribution of heavy stars

$$\mathbf{F}_2 = e^{-\mathbf{E}} + \frac{2\mu}{3K_D}\left(5\alpha_2 - \alpha_1 - \alpha_2\mathbf{E}\right)e^{-\mathbf{E}/2}. \tag{4.43}$$

As we expected, the asymptotic solution for $\mathbf{F}_2$ is very similar to the single mass case (3.87). The only difference is the additional factor of μ in the second term. It is also important to note that when $\mu = 1$, (4.43) is exactly the same as the single mass case.

4.2.2 Distribution function for the population of light stars

We will derive an approximation for $\mathbf{F}_1$ close to the center. We will begin in a similar manner as shown for the heavy stars. Our equation for the light stars is

$$0 = \frac{\partial}{\partial \mathbf{E}}\Bigg[\mathbf{F}_1 \int_{-\infty}^{\mathbf{E}} \left(\mathbf{F}_{1*} + \mu \mathbf{F}_{2*}\right) \mathbf{Q}'_* \mathrm{d}\mathbf{E}_* + \mathbf{F}'_1 \Bigg(\int_{-\infty}^{\mathbf{E}} \left(\mathbf{F}_{1*} + \mu^2 \mathbf{F}_{2*}\right) \mathbf{Q}_* \mathrm{d}\mathbf{E}_* + \mathbf{Q} \int_{\mathbf{E}}^{\infty} \left(\mathbf{F}_{1*} + \mu^2 \mathbf{F}_{2*}\right) \mathrm{d}\mathbf{E}_* \Bigg)\Bigg] + \mu^2 \left(\frac{3}{4} b - \frac{3}{2} c\right) \mathbf{Q}\mathbf{F}'_1 - \mu^2 c \mathbf{F}_1 \mathbf{Q}'. \quad (4.44)$$

We simplify this equation with the substitutions

$$\begin{aligned}
\mathbf{S}'_{12} &= \frac{1}{\mu}\mathbf{F}_1 \int_{-\infty}^{\mathbf{E}} \mathbf{F}_{2*} \mathbf{Q}'_* \mathrm{d}\mathbf{E}_* + \mathbf{F}'_1 \left(\int_{-\infty}^{\mathbf{E}} \mathbf{F}_{2*} \mathbf{Q}_* \mathrm{d}\mathbf{E}_* + \mathbf{Q} \int_{\mathbf{E}}^{\infty} \mathbf{F}_{2*} \mathrm{d}\mathbf{E}_* \right), \\
\mathbf{S}'_{11} &= \mathbf{F}_1 \int_{-\infty}^{\mathbf{E}} \mathbf{F}_{1*} \mathbf{Q}'_* \mathrm{d}\mathbf{E}_* + \mathbf{F}'_1 \left(\int_{-\infty}^{\mathbf{E}} \mathbf{F}_{1*} \mathbf{Q}_* \mathrm{d}\mathbf{E}_* + \mathbf{Q} \int_{\mathbf{E}}^{\infty} \mathbf{F}_{1*} \mathrm{d}\mathbf{E}_* \right), \\
\mathbf{B}_1 &= \left(\frac{3}{4} b - \frac{3}{2} c\right) \mathbf{Q}\mathrm{F}'_1 - c \mathbf{F}_1 \mathbf{Q}', \qquad (4.45)
\end{aligned}$$

where

$$\mathbf{S}_{11} = \mathbf{F}_1^{(-1)} \int_{-\infty}^{\mathbf{E}} \mathbf{F}_{1*} \mathbf{Q}'_* \mathrm{d}\mathbf{E}_* - \mathbf{F}_1 \int_{-\infty}^{\mathbf{E}} \mathbf{F}_{1*}^{(-1)} \mathbf{Q}'_* \mathrm{d}E_*. \quad (4.46)$$

However, it is important to note that we have been able to find no analytical expression $\mathbf{S}_{12}$ whose derivative is $\mathbf{S}'_{12}$, but we use the notation $\mathbf{S}'_{12}$ in (4.45) for consistency with the other $\mathbf{S}_{ij}$ notation.

The equation for the light stars can be written as

$$0 = \mu^2 \mathbf{S}''_{12} + \mathbf{S}''_{11} + \mu^2 \mathbf{B}_1. \quad (4.47)$$

From (4.45a) and (4.45b) we can see that the terms of $\mathbf{S}''_{12}$ are of the order $\mathbf{F}_1\mathbf{F}_2\mathbf{Q}$ and the terms of $\mathbf{S}''_{11}$ are of the order $\mathbf{F}_1^2\mathbf{Q}$. When we consider (4.27), it is obvious that

$$\mathbf{S}''_{12} \gg \mathbf{S}''_{11}, \quad (4.48)$$

when $\mathbf{E}$ is large and negative. Also, $\mathbf{S}''_{12}$ is of the order $\mathbf{F}_1\mathbf{F}_2\mathbf{Q}$ and $\mathbf{B}_1$ is of the order $\mathbf{F}_1\mathbf{Q}$. Considering (4.27) we find

$$\mathbf{S}''_{12} \gg \mathbf{B}_1, \quad (4.49)$$

when $\mathbf{E}$ is large and negative.

Therefore (4.47) can be written approximately as

$$\mathbf{S}''_{12} = 0. \quad (4.50)$$

As we stated previously, there is no known expression whose derivative is $\mathbf{S}'_{12}$. Therefore, we can only analytically solve for $\mathbf{S}'_{12}$. The solution for $\mathbf{S}'_{12}$ is

$$\mathbf{S}'_{12} = \alpha_3, \tag{4.51}$$

where α_3 is a constant.

We use (4.36) and (4.37c) in (4.45a) to reduce (4.51) to

$$\left(\frac{3}{\mu}\mathbf{F}_1 + 3\mathbf{F}'_1\right) K_D e^{\mathbf{E}/2} = \alpha_3. \tag{4.52}$$

The homogeneous solution to (4.52) is

$$\mathbf{F}_1 = \alpha_4 e^{-\mathbf{E}/\mu}, \tag{4.53}$$

where α_4 is a constant. The solution for $\mathbf{F}_1$ should be of the form

$$\mathbf{F}_1 = \alpha_4 e^{-\mathbf{E}/\mu} + \alpha_3 Y_3. \tag{4.54}$$

We use (4.54), (4.43), (4.37c) and (4.24a) to substitute $\mathbf{F}_1$, $\mathbf{F}_2$, $\mathbf{Q}$ and $\mathbf{S}'_{12}$, respectively, into (4.51). Then we use the functions

$$\begin{aligned} I_1 &= \int_{-\infty}^{\mathbf{E}} \left(e^{-\mathbf{E}_*} + \frac{2\mu}{3K_D}\left(3\alpha_2 - \alpha_1 - \alpha_2\mathbf{E}_*\right) e^{-\mathbf{E}_*/2}\right) e^{3\mathbf{E}_*/2} \mathrm{d}\mathbf{E}_*, \\ I_2 &= \int_{\mathbf{E}}^{\infty} \left(e^{-\mathbf{E}_*} + \frac{2\mu}{3K_D}\left(3\alpha_2 - \alpha_1 - \alpha_2\mathbf{E}_*\right) e^{-\mathbf{E}_*/2}\right) \mathrm{d}\mathbf{E}_* \end{aligned} \tag{4.55}$$

to simplify our equations. Once we make our substitution, we can see with much less difficulty that our equation becomes

$$\left(\frac{\alpha_4}{\mu}e^{-\mathbf{E}/\mu} + \frac{\alpha_3}{\mu}Y_3\right)\frac{3K_D}{2\mu}I_1 + \left(-\frac{\alpha_4}{\mu}e^{-\mathbf{E}/\mu} + \frac{\alpha_3}{\mu}Y'_3\right)\left(I_1 + e^{3\mathbf{E}/2}I_2\right)\frac{K_D}{\mu} = \alpha_3. \tag{4.56}$$

We can rearrange (4.56) to obtain a first order differential equation for Y_3

$$Y'_3 + \frac{3}{2\mu}\cdot\frac{I_1}{I_1 + e^{3\mathbf{E}/2}I_2}Y_3 = \frac{\mu}{K_D}\cdot\frac{1}{I_1 + e^{3\mathbf{E}/2}I_2} - \frac{3\alpha_4}{2\mu\alpha_3}\cdot\frac{I_1}{I_1 + e^{3\mathbf{E}/2}I_2}e^{-\mathbf{E}/\mu} + \frac{\alpha_4}{\mu\alpha_3}e^{-\mathbf{E}/\mu}. \tag{4.57}$$

When we substitute (4.55a) and (4.55b) for I_1 and I_2 in 4.57 we can simplify this expression to arrive at

$$Y_3' + \frac{3}{2\mu}\left(\frac{2e^{\mathbf{E}/2} + \frac{2\mu}{3K_D}(4\alpha_2 - \alpha_1 - \alpha_2\mathbf{E})\,e^{\mathbf{E}}}{3e^{\mathbf{E}/2} + \frac{2\mu}{K_D}(3\alpha_2 - \alpha_1 - \alpha_2\mathbf{E})\,e^{\mathbf{E}}}\right) Y_3 =$$

$$\frac{\mu}{3K_D}\left(\frac{1}{3e^{\mathbf{E}/2} + \frac{2\mu}{K_D}(3\alpha_2 - \alpha_1 - \alpha_2\mathbf{E})\,e^{\mathbf{E}}}\right) - \tag{4.58}$$

$$\frac{3\alpha_4}{2\mu\alpha_3}\left(\frac{2e^{\left(\frac{1}{2}-\frac{1}{\mu}\right)\mathbf{E}} + \frac{2\mu}{3K_D}(4\alpha_2 - \alpha_1 - \alpha_2\mathbf{E})\,e^{\left(1-\frac{1}{\mu}\right)\mathbf{E}}}{3e^{\mathbf{E}/2} + \frac{2\mu}{K_D}(3\alpha_2 - \alpha_1 - \alpha_2\mathbf{E})\,e^{\mathbf{E}}}\right) + \tag{4.59}$$

$$\frac{\alpha_4}{\mu\alpha_3}e^{-\mathbf{E}/mu} \tag{4.60}$$

For **E** large and negative, this can be simplified to

$$Y_3' + \frac{1}{\mu}Y_3 = \frac{\mu}{9K_D}e^{-\mathbf{E}/2} - \frac{\alpha_4}{3K_D\alpha_3}(4\alpha_2 - \alpha_1 - \alpha_2\mathbf{E})\,e^{\left(\frac{1}{2}-\frac{1}{\mu}\right)\mathbf{E}} \tag{4.61}$$

Note that the latter term would be negligible if $\mu > 2$. Therefore, to solve for F_1, we need to consider the cases $\mu > 2$ and $\mu < 2$. The intermediate case $\mu = 2$ will be mentioned in Sect 4.2.2.3.

4.2.2.1 Case 1: $\mu > 2$

It can be shown through some simple rearrangements and the assumption $\mu > 2$ that, when **E** is large and negative (4.57) simplifies to

$$Y_3' + \frac{1}{\mu}Y_3 = \frac{\mu}{9K_D}e^{-\mathbf{E}/2} \tag{4.62}$$

This gives the solution for Y_3

$$Y_3 = \frac{2\mu^2}{9K_d\,(2-\mu)}e^{-\mathbf{E}/2}. \tag{4.63}$$

Therefore the approximation for F_1 close to the center is

$$\mathbf{F}_1 = \alpha_4 e^{-\mathbf{E}/\mu} + \frac{2\mu^2\alpha_3}{9K_D\,(2-\mu)}e^{-\mathbf{E}/2}. \tag{4.64}$$

4.2.2.2 Case 2: $1 < \mu < 2$

Similarly, with some algebraic manipulation and the assumption $\mu < 2$, (4.57) simplifies to

$$Y_3' + \frac{1}{\mu}Y_3 = \frac{\mu}{9K_D}e^{-\mathbf{E}/2} - \frac{\alpha_4}{3K_D\alpha_3}(4\alpha_2 - \alpha_1 - \alpha_2 E)\,e^{((\mu-2)\mathbf{E})/(2\mu)}. \tag{4.65}$$

The solution for Y_3 in this case is

$$Y_3 = \frac{2\mu^2}{9K_d\,(2-\mu)}e^{-\mathbf{E}/2} - \frac{2\alpha_4}{9K_D\alpha_3}(4\alpha_2 - \alpha_1 - \alpha_2\mathbf{E})\,e^{((\mu-2)\mathbf{E})/(2\mu)}. \tag{4.66}$$

Therefore the approximation for F_1 close to the center for this case is

$$\mathbf{F}_1 = \alpha_4 e^{-\mathbf{E}/\mu} + \frac{2\mu^2\alpha_3}{9K_D\,(2-\mu)} e^{-\mathbf{E}/2} - \frac{2\alpha_4}{9K_D}\left(4\alpha_2 - \alpha_1 - \alpha_2\mathbf{E}\right) e^{((\mu-2)\mathbf{E})/(2\mu)}. \quad (4.67)$$

4.2.2.3 Case 2: $\mu = 2$

If we considered the case where $\mu = 2$, the terms of order $e^{-\mathbf{E}/2}$ and $e^{-\mathbf{E}/\mu}$ would both be significant. From the second term of (4.64) and (4.67) we can see that $\mu \neq 2$.

4.2.3 Flow of energy and mass near the center

We will calculate the flow of energy and mass close to the center of the cluster for each component. The method used is the same as in the single mass case shown in Sect. 3.4.1. First we need to derive an expression for the density of stars with a velocity less than v for the light stars and heavy stars are ρ_{1v} and ρ_{2v}, respectively. The general equation for density of component i with a velocity less than v can be written as

$$\rho_{iv} = \int_0^v 4\pi m_i F_{i(r,v_*)} v_*^2 \mathrm{d}v_*. \quad (4.68)$$

To find the rate of change of ρ_i, we must first find $(\partial F_i(r,v)/\partial t)_{\text{coll}}$. We do so by adapting (3.9) with the same method we used to adapt (4.12d) from the general equation, (3.23). We find

$$\left(\frac{\partial F_i(r,v)}{\partial t}\right)_{\text{coll}} = 16\pi^2 G^2 \log N \int_0^\infty m_* \frac{1}{v^2}\frac{\partial}{\partial v}\left[m_i F_{i(r,v)} \int_0^v f_{(r,v_*)} v_*^2 \mathrm{d}v_* + \frac{m_*}{3}\frac{\partial F_{i(r,v)}}{\partial v}\left(\frac{1}{v}\int_0^v f_{(r,v_*)} v_*^4 \mathrm{d}v_* + v^2 \int_v^\infty f_{(r,v_*)} v_* \mathrm{d}v_*\right)\right] \mathrm{d}m_*, \quad (4.69)$$

where F_i is the distribution function of the test stars, which we assume to either be the light stars or the heavy stars. The distribution function of the field stars is $f_{(r,v_*)}$ and is assumed to be the total stellar population. Similar to (4.2), $f_{(r,v)}$ can be written as

$$f_{(r,v)} = \delta(m - m_1) F_{1(r,v)} + \delta(m - m_2) F_{2(r,v)}. \quad (4.70)$$

We substitute (4.70) into (4.69) and obtain

$$\left(\frac{\partial F_i(r,v)}{\partial t}\right)_{\text{coll}} = 16\pi^2 G^2 \log N \frac{1}{v^2}\frac{\partial}{\partial v}\left[m_i F_{i(r,v)} \int_0^v \left(m_1 F_{1(r,v_*)} + m_2 F_{2(r,v_*)}\right) v_*^2 \mathrm{d}v_* + \frac{1}{3}\frac{\partial F_{i(r,v)}}{\partial v}\left(\frac{1}{v}\int_0^v \left(m_1^2 F_{1(r,v_*)} + m_2^2 F_{2(r,v_*)}\right) v_*^4 \mathrm{d}v_* + v^2 \int_v^\infty \left(m_1^2 F_{1(r,v_*)} + m_2^2 F_{2(r,v_*)}\right) v_* \mathrm{d}v_*\right)\right]. \quad (4.71)$$

The rate of change of the density of component i due to collisions can be written as

$$\left(\frac{\partial \rho_{iv}}{\partial t}\right)_{\text{coll}} = \int_0^v 4\pi m_i \left(\frac{\partial F_{i(r,v_*)}}{\partial t}\right)_{coll} v_*^2 \mathrm{d}v_*. \tag{4.72}$$

With the substitutions (4.69) and (4.70) this becomes

$$\begin{aligned}\left(\frac{\partial \rho_{iv}}{\partial t}\right)_{\text{coll}} = \int_0^v 64\pi^3 G^2 \log N \frac{1}{v_*^2}\frac{\partial}{\partial v_*}\Bigg[\\ m_i F_{i(r,v_*)} \int_0^{v_*} \left(m_1 F_{1(r,v_{**})} + m_2 F_{2(r,v_{**})}\right) v_{**}^2 \mathrm{d}v_{**} \\ + \frac{1}{3}\frac{\partial F_{i(r,v_*)}}{\partial v_*}\Bigg(\frac{1}{v_*}\int_0^{v_*} \left(m_1^2 F_{1(r,v_{**})} + m_2 F_{2(r,v_{**})}\right) v_{**}^4 \mathrm{d}v_{**} \\ + v_*^2 \int_{v_*}^{\infty} \left(m_1^2 F_{1(r,v_{**})} + m_2^2 F_{2(r,v_{**})}\right) v_{**} \mathrm{d}v_{**}\Bigg)\Bigg] v_*^2 \mathrm{d}v_*, \end{aligned} \tag{4.73}$$

where v_{**} is a variable for integration. We integrate this to obtain

$$\begin{aligned}\left(\frac{\partial \rho_{iv}}{\partial t}\right)_{\text{coll}} = 64\pi^3 G^2 \log N \Bigg[m_i F_{i(r,v)} \int_0^v \left(m_1 F_{1(r,v_*)} + m_2 F_{2(r,v_*)}\right) v_*^2 \mathrm{d}v_* + \\ \frac{1}{3}\frac{\partial F_{i(r,v)}}{\partial v}\Bigg(\frac{1}{v}\int_0^v \left(m_1^2 F_{1(r,v_*)} + m_2 F_{2(r,v_*)}\right) v_*^4 \mathrm{d}v_* \\ + v^2 \int_v^{\infty} \Big(m_1^2 F_{1(r,v)} + m_2^2) F_{2(r,v)}\Big) v_* \mathrm{d}v_*\Bigg)\Bigg]. \end{aligned} \tag{4.74}$$

Now that we have density and the rate of change of the density for population i we move on to find the total mass of population i

$$m_{iv,\text{tot}} = \int_0^{r_{\max}} 4\pi \rho_{iv} r^2 \mathrm{d}r. \tag{4.75}$$

Similar to (3.93), the rate of change for population i is

$$\left(\frac{\partial m_{iv,\text{tot}}}{\partial t}\right)_{\text{coll}} = 4\pi \int_0^{r_{\max}} \left[\left(\frac{\partial \rho_{iv}}{\partial t}\right)_{\text{coll}} + \frac{\partial \rho_{iv}}{\partial v}\left(\frac{\partial v}{\partial t}\right)_E\right] r^2 \mathrm{d}r, \tag{4.76}$$

where

$$\left(\frac{\partial v}{\partial t}\right)_E = -\left(2E - 2U\right)^{-1/2} \frac{\partial U}{\partial t}. \tag{4.77}$$

Using (3.20), (3.21), (3.22) and (4.74), we arrive at an expression for the rate of change of mass of population.

$$\begin{aligned}\left(\frac{\partial m_{iE,\text{tot}}}{\partial t}\right)_{\text{coll}} = 256\pi^4 G^2 \log N \Bigg[m_i F_i \int_{-\infty}^{E} \left(m_1 F_{1*} + m_2 F_{2*}\right) q_*' \mathrm{d}E_* + \\ F_i'\Bigg(\int_{-\infty}^{E} \left(m_1^2 F_{1*} + m_2^2 F_{2*}\right) q_* \mathrm{d}E_* + q \int_E^{\infty} \left(m_1^2 F_{1*} + m_2^2 F_{2*}\right) \mathrm{d}E_*\Bigg)\Bigg] + 16\pi^2 F_i \frac{\partial q}{\partial t}. \end{aligned} \tag{4.78}$$

This can be transformed using (4.11) to find the rate of change of mass for the light stars $\partial M_{1E}/\partial T$ and the rate of change of mass for the heavy stars $\partial M_{2E}/\partial T$,

$$\begin{aligned} \frac{\partial M_{1E}}{\partial T} &= S'_{11} + S'_{12} + F_1 \frac{\partial Q}{\partial T} \\ \frac{\partial M_{2E}}{\partial T} &= S'_{21} + S'_{22} + F_2 \frac{\partial Q}{\partial T} \end{aligned} \tag{4.79}$$

We now examine the flow of energy through a surface $E =$ constant. We define the energy density for the stars of population i with a speed less than v

$$h_{iv} = \int_0^v 4\pi m_i F_{i(r,v_*)} E_* v_*^2 \mathrm{d}v. \tag{4.80}$$

The rate of change due to collisions is

$$\left(\frac{\partial h_{iv}}{\partial t}\right)_{\text{coll}} = m_i \int_0^v 4\pi \left[\left(\frac{\partial F_{(ir,v_*)}}{\partial t}\right)_{\text{coll}} E_* + F_{i(r,v_*)} \frac{\partial U}{\partial t}\right] v_*^2 \mathrm{d}v_*. \tag{4.81}$$

Therefore the total energy of population i is

$$h_{iv,\text{tot}} = \int_0^{r_{\max}} 4\pi h_{iv} r^2 \mathrm{d}r. \tag{4.82}$$

Using (4.11), the transformation for the total energy of population i can be written as

$$h_{iv,\text{tot}} = (16\pi^2 m_1)^{-1/2} G^{-3/2} H_i. \tag{4.83}$$

We use (4.80), (4.81), (4.82) and (4.83) to find the rate of change of the total energy of population i

$$\begin{aligned} \frac{\partial H_{1E}}{\partial T} &= \int_{-\infty}^{E} E_* \left(S''_{12*} + S''_{11*}\right) \mathrm{d}E_* + E F_1 \frac{\partial Q}{\partial T} - \int_{-\infty}^{E} F_{1*} \frac{\partial Q_*}{\partial T} \mathrm{d}E_* \\ \frac{\partial H_{2E}}{\partial T} &= E\left(S'_{21} + S'_{22}\right) - S_{21} - S_{22} + E F_2 \frac{\partial Q}{\partial T} - \int_{-\infty}^{E} F_{2*} \frac{\partial Q_*}{\partial T} \mathrm{d}E_*. \end{aligned} \tag{4.84}$$

As stated previously, S_{12} is undefined, but we use this notation for consistency with the other S_{ij} notation. As we will see, we do not need an analytical expression for S_{12} to find a solution for $\partial H_{1E}/\partial T$.

4.2.4 Restrictions on parameters

We will now look at the flow of mass and energy for each population found in the previous section in order to examine the implications this has for our parameters α_1, α_2, α_3, α_4. To do this, we first need to simplify the rate of change of mass and energy for each population to their leading terms.

The assumptions made to find (4.28) and (4.48) can be used to show that

$$\begin{aligned} S'_{22} &\gg S'_{21}, \\ S_{22} &\gg S_{21}, \\ S'_{12} &\gg S'_{11}, \\ S_{12} &\gg S_{11}, \end{aligned} \tag{4.85}$$

when E is large and negative. This simplifies the rate of change of mass for each population to

$$\begin{aligned} \frac{\partial M_{1E}}{\partial T} &= S'_{12} + F_1 \frac{\partial Q}{\partial T}, \\ \frac{\partial M_{2E}}{\partial T} &= S'_{22} + F_2 \frac{\partial Q}{\partial T}, \end{aligned} \tag{4.86}$$

We simplify this further by noting that the first term of (4.86a) and (4.86b) are of the order F_1F_2Q and F_2^2Q, respectively. Close to the center, these are much larger than the later terms in (4.86a) and (4.86b) which are of the order F_1Q and F_2Q respectively. Thus the flow of mass for each population can be approximated by its leading term

$$\begin{aligned} \frac{\partial M_{1E}}{\partial T} &= S'_{12}, \\ \frac{\partial M_{2E}}{\partial T} &= S'_{22}. \end{aligned} \tag{4.87}$$

As for the rate of change of energy, we can use (4.85) to simplify (4.84a) and (4.84b) to the following expressions

$$\begin{aligned} \frac{\partial H_{1E}}{\partial T} &= \int_{-\infty}^{E} E_* S''_{12*} \mathrm{d}E_* + EF_1 \frac{\partial Q}{\partial T} - \int_{-\infty}^{E} F_{1*} \frac{\partial Q_*}{\partial T} \mathrm{d}E_*, \\ \frac{\partial H_{2E}}{\partial T} &= ES'_{22} - S_{22} + EF_2 \frac{\partial Q}{\partial T} - \int_{-\infty}^{E} F_{2*} \frac{\partial Q_*}{\partial T} \mathrm{d}E_*. \end{aligned} \tag{4.88}$$

When E is large and negative, the first term of (4.88a) and the first two terms of (4.88b) are of the order F_1F_2QE and F_2^2QE respectively. The latter two terms of (4.88a) and (4.88b) are of the order F_1QE and F_2QE respectively. Therefore, the flow of energy for each population can be simplified to

$$\begin{aligned} \frac{\partial H_{1E}}{\partial T} &= \int_{-\infty}^{E} E_* S''_{12*} \mathrm{d}E_*, \\ \frac{\partial H_{2E}}{\partial T} &= ES'_{22} - S_{22}. \end{aligned} \tag{4.89}$$

Using (4.14), (4.31) and (4.51) we find (4.87a) and (4.87b) are approximately

$$\begin{aligned} \frac{\partial \mathbf{M_{1E}}}{\partial \mathbf{T}} &= \alpha_3, \\ \frac{\partial \mathbf{M_{2E}}}{\partial \mathbf{T}} &= \alpha_2. \end{aligned} \tag{4.90}$$

There cannot physically be a flow of mass in the center of a globular cluster, unless possibly if there is a central black hole. However, we will not consider black holes in this system. Therefore we assume that $\partial \mathbf{M}_{i\mathbf{E}}/\partial \mathbf{T} = 0$ for the either component or for the population of the globular cluster as a whole. Therefore, the conditions

$$\begin{aligned} \alpha_2 &= 0, \\ \alpha_3 &= 0, \end{aligned} \tag{4.91}$$

must hold.

Again, considering (4.14), (4.31) and (4.51) we find (4.89a) and (4.89b) are approximately

$$\begin{aligned} \frac{\partial \mathbf{H}_{1\mathbf{E}}}{\partial \mathbf{T}} &= 0, \\ \frac{\partial \mathbf{H}_{2\mathbf{E}}}{\partial \mathbf{T}} &= -\alpha_1. \end{aligned} \tag{4.92}$$

Binary heating could be the cause of a flow of energy close to the center. Thus, (4.92a) and (4.92b) implies that interactions with binary stars close to the center directly affects the heavy stars and not the light stars. Since the region where $\mathbf{R} \to 0$ is dominated by heavy stars, it makes physical sense that the flow of energy close to the center affects only the heavy stellar population. Obviously, binary heating would also affect the light stars both indirectly, through two-body interactions with heavy stars which had gained energy through previous three-body interactions, and directly, through three-body interactions between a single light star and a binary system that is slightly further away from the center. However a binary star at the center of the cluster will likely only have three-body interactions with other heavy stars, so for this reason when we are considering the rate of change of energy at the center $\frac{\partial \mathbf{H}_{1\mathbf{E}}}{\partial \mathbf{T}} = 0$ and $\frac{\partial \mathbf{H}_{2\mathbf{E}}}{\partial \mathbf{T}}$ is not necessarily zero. We conclude that α_1 is a free parameter.

4.3 Implications of our parameters

The next step would be to solve for F_1 and F_2 numerically with a similar method used in Sect 3.5.1. We would need to satisfy the following conditions

$$\begin{aligned} \mathbf{F}_2(0) &= 0, \\ \mathbf{F}_2^{(-1)}(0) &= 0, \\ \mathbf{F}_1(0) &= 0. \end{aligned} \tag{4.93}$$

At first glance, this seems plausible. We have three parameters c, α_1 and α_4 to vary to ensure the three conditions (4.93) hold. However, the constant α_4 is proportional

μ	c_2
0.0	-0.6240
0.2	-0.3998
0.4	-0.1838
0.6	0.0233
0.8	0.2208
1.0	0.4078
1.2	0.5829
1.4	0.7430

Table 4.1: These are the values of c_2 found in the two-component model presented in (Hénon, 1961) with varying values of $\mu = m_2/m_1$.

to the total mass ratio

$$\alpha_4 \propto M_1/M_2. \tag{4.94}$$

This can be seen in the asymptotic solutions of the distribution functions (4.43), (4.64) and (4.67). Since α_4 is proportional to the total mass ratio, it should be possible to assign its value arbitrarily. Therefore, we cannot find a self-similar solution to a two-component system with a given value of M_1/M_2 using this approach.

4.4 Discussion

As explained in the previous section, a two-component self-similar model cannot be produced using the approach presented in this chapter, except possibly for isolated values of α_4. Finding these isolated cases would require varying α_4 in the same manner as we vary the other variables c and α_1. Since $\alpha_4 \propto M_1/M_2$, it should not be necessary to vary α_4 to find a solution and such solutions would have no more than academic interest.

In our model, we assume that the ratio of total mass for each component is constant. We can see from the two-component Fokker-Planck model with a small number of heavy stars shown in Hénon (1961) that this assumption is not valid in a system that is not isolated (i.e. a system that is subject to the gravitational field of a galaxy as discussed in Sect. 3.3). The model shown in Hénon's paper has the total mass of the heavy and light stars vary according to two scaling factors, γ and γ_2, and that these two factors have different time dependence. Since the heavy stars are negligible, the light stars behave similarly as in the single mass case discussed in Chapter 3. The light stars are scaled by a time-dependent scaling factor γ. As done with c in (4.20b), we define a

constant c_2

$$c_2 = \frac{1}{\gamma_2}\frac{d\gamma_2}{d\mathbf{T}}. \tag{4.95}$$

For the total mass ratio to remain constant, this would mean that the time dependent scaling factors would have to behave in such a way that $c = c_2$. In Table 4.1, we show the values of c_2 found in Hénon (1961) for each given μ. The value for c is unchanged from the value in the single mass model ($c = 0.4078$). Thus, from Table 4.1 we can see that c and c_2 are only equal in the single mass case ($\mu = 1$). Since the total mass of the heavy stars and the light stars are not evolving proportionally when $\mu \neq 1$, then we should not be able to assume that M_1/M_2 is constant in an unisolated two-component system.

To consider physical reasons for the change in total mass ratio, we must consider the timescales of evaporation and ejection in Sect. 1.2. The evaporation time is much smaller than the ejection time. This implies that many more stars will be lost through evaporation than through ejection. In a two-component system the mass loss for the light stars will be greater than the mass loss for the heavy stars because the light stars dominate the region near the boundary $E = 0$. With this in mind, one cannot expect the total mass ratio of an unisolated two-component system to be constant; the ratio M_1/M_2 would likely decrease with time.

It may be possible to find a homologous two-component Fokker-Planck model for an isolated system. A Fokker-Planck model of an isolated system does not have stars lost through evaporation (Hénon, 1960), so it would be a reasonable approximation to assume that M_1/M_2 is constant. A single mass Fokker-Planck model where the total mass is constant was shown in Hénon (1965). Extending upon this model to find a self-similar two-component system would be a worthwhile area of research. It is important to consider that the Hénon worked on this project for four years from the results shown in (Hénon, 1961) to compose the model shown in (Hénon, 1965). Extending upon Hénon (1965) would not be a trivial project. The work presented in this chapter would provide significant ground work for a promising avenue of research. With the exception of the outer boundary conditions, the work shown here would be applicable to finding a self-similar solution to a two-component Fokker-Planck equation.

5

Conclusions and Outlook

In this thesis we have considered homologous post-collapse evolution of globular clusters using various models. In Chapter 2 we developed a simple two-component model without a core and a single mass model with a core. We merged these two models to obtain a two-component model with a core and a binary heating term (model IIIb). When deriving the equations for these models we considered only the processes of two-body relaxation and binary heating. We have shown that this model has self-similar post-collapse evolution, therefore the processes considered in creating this model must be enough to create this type of evolution. Finally, we compared model IIIb with N-body simulations. From this comparison we found model IIIb to be within reasonable qualitative agreement with the N-body models most cases.

In Chapter 3 we reviewed the single mass Fokker-Planck model developed in Hénon (1961) and approximated the solution numerically. We found that our numerical results were in satisfactory agreement with Hénon (1961).

In Chapter 4 we extend upon the work presented in Chapter 3 and Hénon (1961) for a two-component Fokker-Planck model with no restrictions on the number of heavy stars. From deriving the equations for the Fokker-Planck model, we found that a homologous solution cannot be found in this manner for the reasons expressed in

Sect. 4.4.

5.1 Outlook

The work used in the simple model could be used for the groundwork of more complicated simple models. For example, we may be able to add a binary heating term that considers primordial binary stars in addition to binary stars formed by three-body interactions. If one were to compute a binary heating term which includes primordial binary stars in the same manner as we have calculated our binary heating term, then this could be added to the model with little additional work. Any further changes to this model would likely require completely reworking the model, but the work done here could be useful guide for such future research.

In Chapter 4, we have already given discussion of future research using an isolated Fokker-Planck model based upon Hénon (1965). This seems promising to give future results because the isolated model would not have the same issue with the change in the total mass ratio due to evaporation. This work could utilize much of the work for the two-component Fokker-Planck model presented in Chapter 4, but would need additional work in the boundary conditions.

A

Deriving condition

In Sect. 2.1.2 we have stated that

$$\zeta - r_2/r_1 < 0. \tag{A.1}$$

We would like to show that this is true. We use the definition of ζ shown in (2.22b) and rewrite the equation such that the left side of (A.1) becomes

$$\frac{M_1 M_2 r_2^4 - M_1^2 r_1^2 r_2^2 - M_1 M_2 r_1^2 r_2^2 - M_2^2 r_1^3 r_2}{M_2 r_1 (M_2 r_1^3 + 2 M_1 r_2^3)}. \tag{A.2}$$

We can simplify this further so that the nominator is in terms of the total mass ratio $\tilde{M} = M_2/M_1$ and the ratio of the half-mass radius of each component $\tilde{r} = r_2/r_1$

$$\frac{\tilde{r}\left(\tilde{M}\tilde{r}^3 - \tilde{r} - \tilde{M}\tilde{r} - \tilde{M}^2\right)}{M_1^2 M_2 r_1^5 (M_2 r_1^3 + 2 M_1 r_2^3)}. \tag{A.3}$$

Taking into account our assumption $0 \leq \tilde{r} \leq 1$ and $\tilde{M} \geq 0$ we have

$$\tilde{M}\tilde{r}^3 \leq \tilde{M}\tilde{r}. \tag{A.4}$$

Therefore, we can say that

$$\zeta - r_2/r_1 = \frac{\tilde{r}\left(\tilde{M}\tilde{r}^3 - \tilde{r} - \tilde{M}\tilde{r} - \tilde{M}^2\right)}{M_1^2 M_2 r_1^5 (M_2 r_1^3 + 2 M_1 r_2^3)} \leq -\frac{\tilde{r}\left(\tilde{r} + \tilde{M}^2\right)}{M_1^2 M_2 r_1^5 (M_2 r_1^3 + 2 M_1 r_2^3)}. \tag{A.5}$$

Since $M_1, M_2, r_2, r_1 > 0$, we have shown that

$$\zeta - r_2/r_1 < 0. \tag{A.6}$$

B

Code for single mass Fokker-Planck model

We show the code for finding the numerical solution for the single mass Fokker-Planck model. The description of the method can be found in Sect 3.5.1.

```
      program fpm
c=======================================================================
      implicit none
c-----------------------------------------------------------------------
      integer*4 i, j, l, tally, NX
      integer*4 tick1, tick2, tick3, tick4, tick5
      parameter( NX = 10001 )

      real*8 Emin, Umin, dE, dU, K, c, lambda, b, denom(NX)
      real*8 E(NX), U(NX), D(NX), Q(NX), dQ(NX)
      real*8 F(NX), intF(NX), Flimit, intFlimit
      real*8 oldD, newD, integrandQ, integrandD, Simpson, Rlimit, Z(NX)
      real*8 newQ,  tc, tK, dc, dK, diff, old_diff, oldF0
      real*8 lastc, lastK, error
```

```
      character*2 tindex

c-----------------------------------------------------------------------

      Emin  = -5.d0
      Umin  = Emin
      dE    = (0.d0-Emin)/(NX-1)
      dU    = (0.d0-Umin)/(NX-1)
      tally = 0


c      K is defined s.t. F(0) in (5.3c) is 0
      K = -1.d0
c      c is defined s.t. F^(-1)(0) in (4.36a) is 0
      c = -((3.d0*dsqrt(3.d0))/(8.d0*dsqrt(2.d0))) + 1.d0
c      lambda is 1/3 as stated just below (5.3)
      lambda = 1.d0/3.d0
c      b is found from equation (5.2f)
      b= ((2.d0*lambda - 2.d0)/(3.d0*lambda + 1.d0))*c


c      initializing E, U, D & Q
      do i=1, NX
         E(i) = Emin + (i - 1)*dE
         U(i) = Umin + (i -1)*dU
      enddo
c      initializing F and F^(-1) to (5.3c) and (4.36a), respectively
      open(unit = 4, file = 'init_dist', form= 'formatted')

      do i = 1, NX
         F(i) = Flimit(E(i), K)
         intF(i) = intFlimit(E(i), K, b)

         write(4, *)  E(i), F(i), intF(i)
      enddo

      close(4)
```

```
c      checking that conditions (5.3a,b) are satisfied
       if (abs(F(NX)) .gt. 1d-10 .or.abs(intF(NX)).gt.1d-10) then
          write(*, *) 'Stopped: Initial conditions are not satisfied'
          write(*, *) '  F(0) = ', F(NX),' F^(-1)(0) = ',intF(NX)
          stop
       endif
c-----------------------------------------------------------------------
!!!!!!!Calculating D!!!!!!!!!!!!!!!!!!!!!!!!!!!!!!!!!!!!!!!!!!!!!!!!!!
       open(unit = 14, file = 'constants', form = 'formatted')
 10    tally = tally + 1
       tick3 = 0

       do i = 1, NX
          D(i)  = 0.d0
          Z(i)  = 0.d0
          Q(i)  = 0.d0
          dQ(i) = 0.d0
       enddo

       write(tindex, '(i2.2)') tally
       open(unit = 7, file = 'density'//tindex, form= 'formatted')

c      We calculate D with eqn 5.2a using Simpson's Rule and the
c      assumption that E(i) = U(i)

       do i=1, NX-1
          j = 0
 20       oldD = D(i)

          newD = Simpson(dE, integrandD(U(i+j), U(i), F(i + j)),
     &         integrandD((U(i+j) + U(i+j+1))/2.d0, U(i),
     &         (F(i+j+1) + F(i+j))/2.d0),
     &         integrandD(U(i) + (j+1)*dE, U(i), F(i+j+1)))

          j = j + 1
          D(i) = D(i) + newD

          if(j + i + 1 .le. NX) then
```

```
            if(j .lt. 2) goto 20
            if(abs((D(i) - oldD)/oldD) .ge. 1d-10) goto 20
         endif

         write(7,*) U(i), D(i)
      enddo

      D(NX) = 0.d0
      write(7,*) U(NX), D(NX)

      close(7)

c-----------------------------------------------------------------------
!!!!!!!Calculating Z!!!!!!!!!!!!!!!!!!!!!!!!!!!!!!!!!!!!!!!!!!!!!!!!!!

      open(unit = 8, file = 'radius'//tindex, form = 'formatted')

c      using (5.3d) and (5.2c) to calculate first 2 values of Z
      do i = 1, 2
         Z(i) = 1.d0/Rlimit(U(i), K)
         write(8,*)  U(i), 1.d0/Z(i)
      enddo
c      using linear interpolation of (5.2b) to calculate Z
      do i = 1, NX-2
          Z(i+2) = (-D(i+1)/dU)*((Z(i+1)-Z(i))**(3.d0))*
     &         (Z(i+1)**(-4.d0)) + 2.d0*Z(i+1) - Z(i)
         write(8,*)  U(i+2), 1.d0/Z(i+2)
      enddo

      close(8)


c-----------------------------------------------------------------------
!!!!!!!Calculating Q!!!!!!!!!!!!!!!!!!!!!!!!!!!!!!!!!!!!!!!!!!!!!!!!!!

      newQ = 0.d0
      open(unit = 9, file = 'Q'//tindex, form = 'formatted')
c        calculating Q with equation with Simpsons Rule for (5.2d)
```

```
c        using Z calculated above with (5.2b)
      do i = 2, NX
         do j = 1, i-1
            newQ = Simpson(dU, integrandQ(E(i), U(i-j+1), Z(i-j+1)),
     &           integrandQ(E(i), (U(i-j+1) + U(i-j))/2.d0,
     &           (Z(i-j+1) + Z(i-j))/2.d0),
     &           integrandQ(E(i), U(i-j), Z(i-j)))

            Q(i) = Q(i) + newQ
         enddo
      enddo

c         using Z= 1/R, with limit R given as U -> -inf, given in (5.3d)
c          so that I can calculate Q using U < Umin
      do i = 1, NX
         l = 0
         newQ = 1d10

         do while (newQ .gt. 1d-20)
            newQ = Simpson(dU, integrandQ(E(i), E(1) - l*dE,
     &           (1.d0/Rlimit(E(1) - l*dE, K)) ),
     &           integrandQ(E(i), E(1)  - (l + 0.5d0)*dE,
     &           (1.d0/Rlimit(E(1) - (l + 0.5d0)*dE, K))),
     &           integrandQ(E(i), E(1) -(l+1)*dE,
     &           (1.d0/Rlimit(E(1) - (l+1)*dE, K)) ))

            Q(i) = Q(i) + newQ
            l = l+1
         enddo
         Q(i) = Q(i)/3.d0
         l = 0
      enddo

c- - - - - - - - - - - - - - - - - - - - - - - - - - - - - - - - - - - -
c      calculating Q'(1)
      dQ(1) = (Q(2) - Q(1))/dE
```

```
      write(9, *) E(1), Q(1), dQ(1)

c      calculating Q'(i) for i = 2, NX-1
      do i = 2, NX-1
         dQ(i) = (Q(i+1) - Q(i-1))/(2.d0*dE)
         write(9, *) E(i), Q(i), dQ(i)
      enddo
c      calculating Q(NX)
      dQ(NX) = (Q(NX) - Q(NX-1))/dE

      write(9, *) E(NX), Q(NX), dQ(NX)


      close(9)

c--------------------------------------------------------------------------
!!!!!!!Calculating F and intF!!!!!!!!!!!!!!!!!!!!!!!!!!!!!!!!!!!!!!!!!!!

      tc = c
      tK = K

 30   dc = 0.001d0
      dK = 0.001d0
      tick1 = 0
      tick2 = 0
      open(unit = 11, file = 'diff'//tindex, form = 'formatted')


c      Find F(0) - intF(0) with initial values of c and K
      call mysystem(F, intF, dE, Q, dQ, denom, tc, tK, Emin,
     &     NX)

c      Vary c and find value of F(0) - intF(0)
      tc = c + dc

      call mysystem(F, intF, dE, Q, dQ, denom, tc, tK, Emin,
     &     NX)
```

```
      diff = F(NX) - intF(NX)
      write(11, *) diff, F(NX), intF(NX), tc, tK, dc, dK


      tick4 = 0
      tick5 = 0

c      Vary c so that F(0) - intF(0) = 0.
      do while (abs(diff) .gt. 1d-8)

         tc = tc + dc

         call mysystem(F, intF, dE, Q, dQ, denom, tc, tK, Emin,
     &        NX)

         old_diff = diff
         diff = F(NX) - intF(NX)

         write(11, *) diff, F(NX), intF(NX), tc, tK, dc, dK

c      If we haven't gone past the value of c where diff = 0 then...
         if (diff*old_diff .gt. 0.d0) then
            if(tick4 .gt. 5 .and. tick5 .gt. 5) then
               dc = 0.5*dc
               tick4 = 0
               tick5 = 0
            else if (abs(diff) .lt. abs(old_diff)) then
c      If the difference is getting smaller, keep going in the same direction
               dc = dc
               tick4 = tick4 + 1
            else
c      If the difference is getting bigger, change direction
               dc = -dc
               tick5 = tick5 + 1
            endif
c       If we have gone past the value of c where diff = 0 then...
          else if(diff*old_diff .lt. 0.d0) then
c       Change direction and reduce the stepsize
```

```
            dc = -0.5d0*dc
         endif

         tick1 = tick1 + 1
      enddo

      close(11)


      open(unit = 12, file = 'zero'//tindex, form = 'formatted')
c      Varying K so intF(0) = 0



      tick4 = 0
      tick5 = 0

      do while (abs(F(NX)) .gt. 1d-6)
         oldF0 = F(NX)

         tK = tK + dK

          call mysystem(F, intF, dE, Q, dQ, denom, tc, tK, Emin,
     &         NX)

          if (F(NX)*oldF0 .gt. 0.d0) then
             if (tick4 .gt. 5 .and. tick5 .gt. 5) then
                dK = 0.5*dK
                tick4 = 0
                tick5 = 0
             else if (abs(F(NX)) .lt. abs(oldF0)) then
c      If F0 is getting smaller, keep going in the same direction
                dK = dK
                tick4 = tick4+1
             else
c      If F0 is getting bigger, change direction
                dK = -dK
                tick5 = tick5 +1
```

```
            endif
c       If we have gone past the value of K where intF0 = 0 then...
          else if(F(NX)*oldF0 .lt. 0.d0) then
c       Change direction and reduce the stepsize
            dK = -0.5d0*dK
          endif

          diff = F(NX) - intF(NX)
         write(12, *) diff, F(NX), intF(NX), tc, tK, dc, dK

         tick2 = tick2 + 1
      enddo

      close(12)

      tick3 = tick3 + 1

      write(*, *) tally, tick1, tick2, tick3

      if (abs(intF(NX)) .gt. 1d-6) go to 30

      lastc = c
      lastK = K

      c = tc
      K = tK

      error = 0.d0

      if (tally .gt. 2) then
            error = abs((lastc - c)/c) + abs((lastK - K)/K)
      endif

      open(unit = 13, file = 'dist'//tindex, form= 'formatted')

      do i = 1, NX

      write(13, *)  E(i), F(i), intF(i)
```

```
      enddo

      close(13)

      write(14, *)  tally, c, K, error

      if(tally .lt. 3 .or. error .gt. 1d-6 ) then
         c = 0.5d0*(lastc + c)
         K = 0.5d0*(lastK + K)
         go to 10
      endif

      close(14)

      end


c=======================================================================
      function Flimit(Ei, K)
c=======================================================================
      implicit none
c=======================================================================
      real*8 Ei, Flimit, K

      Flimit = exp(-Ei) + K*exp(-Ei/2.d0)

      return
      end

c=======================================================================
      function intFlimit(Ei, K, b)
c=======================================================================
      implicit none
c-----------------------------------------------------------------------
      real*8 intFlimit, K, Ei, b
c-----------------------------------------------------------------------

      intFlimit = (-exp(-Ei) -2.d0*K*exp(-0.5d0*Ei) + 1.5d0*b -
```

```
     &     ((3.d0*dsqrt(3.d0))/(8.d0*dsqrt(2.d0)))*K**2)

      return

      end
c=======================================================================
      function integrandD(Ei, Ui, F)
c=======================================================================
      implicit none

      real*8 Ei, Ui, F, integrandD

      integrandD = dsqrt(2.d0*Ei - 2.d0*Ui)*F

      return
      end

c=======================================================================
      function Simpson(delta, funct1, funct2, funct3)
c=======================================================================
      implicit none

      real*8 delta, funct1, funct2, funct3, Simpson

      Simpson = (delta/6.d0)*(funct1 + 4.d0*funct2 + funct3)

      return

      end
c=======================================================================
      function integrandQ(Ei, Ui, zee)
c=======================================================================
      implicit none
c-----------------------------------------------------------------------
      real*8 Ei, Ui, zee, integrandQ

      integrandQ = dsqrt(2.d0*Ei - 2.d0*Ui)/(zee*zee*zee)
```

```
      return

      end
c=======================================================================
      function Rlimit(Ui, K)
c=======================================================================
      implicit none
c-----------------------------------------------------------------------
      real*8 Ui, pi, K, Rlimit

      pi = 2.d0*acos(0.d0)

      Rlimit = (8.d0/pi)**(0.25d0)*
     &     (exp(Ui/2.d0) - K/dsqrt(2.d0)*exp(Ui))

      return

      end

c=======================================================================
      function intFQlimit(Ei, K, Kd)
c=======================================================================
      implicit none
c-----------------------------------------------------------------------
      real*8 intFQlimit, K, Ei, Kd
c-----------------------------------------------------------------------

      intFQlimit = Kd*(2.d0*exp(0.5d0*Ei)+ (1.d0 -
     &     ((9.d0*dsqrt(3.d0))/(8.d0*dsqrt(2.d0))))*K*exp(Ei) -
     &     ((3.d0*dsqrt(3.d0))/(4.d0*dsqrt(2.d0)))*(K**2)*
     &     exp(1.5d0*Ei))

      return

      end

c=======================================================================
      function intFdQlimit(Ei, K, Kd)
```

```
c=======================================================================
      implicit none
c-----------------------------------------------------------------------
      real*8 intFdQlimit, K, Ei, Kd
c-----------------------------------------------------------------------

      intFdQlimit =1.5d0*Kd*(2.d0*exp(0.5d0*Ei)+(1.d0-
     &     ((3.d0*dsqrt(3.d0))/(2.d0*dsqrt(2.d0))))*K*exp(Ei) -
     &     (dsqrt(3.d0)/dsqrt(2.d0))*(K**2)*exp(1.5d0*Ei))

      return

      end

c=======================================================================
      subroutine mysystem(F, intF, dE, Q, dQ, denom, tc, tK, Emin, NX)
c=======================================================================
      implicit none
c-----------------------------------------------------------------------
      integer*4 i, NX

      real*8 F(NX), intF(NX), intFQ(NX), intFdQ(NX), Q(NX), dQ(NX)
      real*8 dE, tc, tK, tb, Kd, lambda, x1, x2, x3, x4, pi, denom(NX)
      real*8 Flimit, intFlimit, intFQlimit, intFdQlimit, Emin
c-----------------------------------------------------------------------

      pi = 2.d0*acos(0.d0)

c      Kd from (4.7e)
      Kd = 16.d0/(9.d0*dsqrt(3.d0)*(8.d0*pi)**(0.25d0))
c      lambda is 1/3 as stated just below (5.3)
      lambda = 1.d0/3.d0

      tb= ((2.d0*lambda - 2.d0)/(3.d0*lambda + 1.d0))*tc
c      For intFQ(1) and intFdQ(1), we use (4.37a) and (4.37b),
c      respectively
           intFQ(1)  = intFQlimit(Emin, tK, Kd)
           intFdQ(1) = intFdQlimit(Emin, tK, Kd)
```

```
c      For F(1) and intF(1) we use (5.3c) and (4.36), respectively
           F(1)      = Flimit(Emin, tK)
           intF(1)   = intFlimit(Emin, tK, tb)
c              write(*, *) j, l, F(1), intF(1)
c      let our similar system be:
c      y1 = intFdQ, y2 = F, y3 = intFQ, y4 = F^(-1)
c      then,
c      y1' = y2Q', y3' = y2Q, y4' = y2 (from the equations above)
c      y2' = -(y2y1+(3/4b-3/2c)y2Q+(1/2c-3/4b)y1)/(y3 - Qy4) (from 5.2e)

c     solving this similar system with Euler Method

           do i = 1, NX-1

              intFdQ(i+1) = dE*F(i)*dQ(i)
              intFdQ(i+1) = intFdQ(i+1) + intFdQ(i)

              intFQ(i+1) = dE*F(i)*Q(i)
              intFQ(i+1) = intFQ(i+1) + intFQ(i)

              intF(i+1)  = dE*F(i)
              intF(i+1)  = intF(i+1) + intF(i)

              x1 = F(i)*intFdQ(i)
              x2 = (0.75d0*tb - 1.5d0*tc)*F(i)*Q(i)
              x3 = (0.5d0*tc - 0.75d0*tb)*intFdQ(i)
              x4 = Q(i)*intF(i)
              x4 = intFQ(i) - x4

              denom(i) = x4

              F(i+1) = x1 + x2 + x3
              F(i+1) = -dE*(F(i+1)/x4)
              F(i+1) = F(i+1) + F(i)

           enddo
```

```
end
```

Nomenclature

α	Constant used in Lynden-Bell and Eggleton (1980) for self-similar evolution.
α_1	Constant used to find the asymptotic solution of the Fokker-Planck models.
α_2	Constant used to find the asymptotic solution of the Fokker-Planck models.
α_3	Constant used to find the asymptotic solution of the light stars in the two-component Fokker-Planck model.
α_4	Constant used to find the asymptotic solution of the light stars in the two-component Fokker-Planck model.
α_ρ	Scaling factor for homologous evolution of density.
α_M	Scaling factor for homologous evolution of mass.
$\alpha_{\langle v^2 \rangle}$	Scaling factor for homologous evolution of mean square velocity.
$\beta(t)$	Time-dependent scaling factors for E in the self-similar Fokker-Planck models.
β_{Spitzer}	Constant in criterion for equipartition found by Spitzer (1969).
β_{sh}	Function related to the local mean kinetic energy and is used to determine whether binary systems are soft or hard.
$\gamma(t)$	Time-dependent scaling factors for the distribution functions in the self-similar Fokker-Planck models.
ϵ	Rate of increase for kinetic energy per unit mass due to binary heating.
η	Function defined in (2.22a) for the purpose of simplifying the equations for the analytical two-component models.

ζ	Function defined in (2.22b) for the purpose of simplifying the equations for the analytical two-component models.
θ	Function defined in (2.20) for the purpose of simplifying the equations for the analytical two-component models.
λ	Constant found in relationship between the maximum radius and the total mass in the Fokker-Planck models of a globular cluster.
λ_1	Eigenvalue of the Jacobian matrix.
λ_2	Eigenvalue of the Jacobian matrix.
μ	Individual mass ratio equivalent to $\tilde{m}$.
μ_T	Scaled Temperature variable.
ξ	Scaled radial variable.
ρ	Mass density.
ρ_0	Central density.
ρ_c	Density of the core.
ρ_{01}	Central density of light stars.
σ^2	One-dimensional velocity dispersion.
ϕ	Angular momentum vector.
Ψ	Function defined such that $\Psi(v, \Delta v)d\Delta v$ is the probability that during a unit time interval a star with velocity v will change by Δv within the range $d\Delta v$.
A	Arbitrary constant.
a	Semi-major axis.
$\overrightarrow{a}$	Acceleration vector.
$\mathbf{B}_1$	Function used for simplification during the derivation of the asymptotic solution of the light stars in the two-component Fokker-Planck model.
$\mathbf{B}_2$	Function used for simplification during the derivation of the asymptotic solution of the light stars in the two-component Fokker-Planck model.

B	Arbitrary constant.
b	Function related to the time-dependent scaling factor β.
c	Function related to the time-dependent scaling factor γ.
C_1	Arbitrary constant.
C_2	Arbitrary constant.
c_2	Function related to the time-dependent scaling factor γ_2.
C_3	An arbitrary positive constant.
C_4	An arbitrary positive constant.
$\mathbf{D}$	The density for the canonical form shown in (3.36b).
D	Density with the transformation shown in (3.25a).
$D[v_i v_j]$	Diffusion coefficient.
$D[v_i]$	Diffusion coefficient.
$\mathrm{d}T$	The time increment with the transformation shown in (3.25d).
$\mathrm{d}\mathbf{T}$	The time increment after being transformed to the canonical form using (3.36e).
$\mathbf{E}$	The canonical form of the total energy per unit mass.
$\mathbf{E}_{\mathrm{min}}$	Minimum value of energy used for approximating the solution to the single mass Fokker-Planck model.
E	Total energy per unit mass.
E_{int}	Internal Energy.
E_{bind}	Binding Energy.
$E_{\mathrm{kin},E}$	Kinetic Energy of stars with energy less than E.
$\mathbf{F}$	The canonical form of the distribution function.
F	The distribution function as defined in (3.24).
f	Distribution function.
G	Gravitational constant.

g	Function defined such that $g(E, m, t)\mathrm{d}E\mathrm{d}m$ is the total number of stars with an energy within the range $[E, E + \mathrm{d}E]$ and a mass within the range $[m, m + dm]$.
$h_{\mathrm{tot},v}$	Total energy of stars with velocity less than v.
I_1	Function used for simplification.
I_2	Function used for simplification.
$\breve{J}$	Jacobian matrix.
J	Angular momentum.
K	Constant related to K_D.
K_D	Constant used in Fokker-Planck models.
L_E	Kinetic Energy of stars with energy less than E with the transformation shown in (3.25).
M	Total stellar mass.
M_E	Total Mass of stars with energy less than E with the transformation shown in (3.25) .
$\tilde{M}$	Ratio of the total mass of the light stars and heavy stars in Model Ia.
$\tilde{M}_{\max}$	Maximum value of $\tilde{M}$ for which equipartition is possible in Model Ia.
m	Individual stellar mass.
$m_{\mathrm{tot},E}$	Total Mass of stars with energy less than E.
$\tilde{m}$	Ratio of the individual mass of the light stars and heavy stars in Model Ia.
N	Number of stars.
P_0	Pressure at the center.
$\mathbf{Q}$	The function Q after being transformed to the canonical form using (3.36d).
Q	The function q with the transformation shown in (3.25c).
q	Function related to E, U and r shown in (3.21a).

$\mathbf{R}$	The radius for the canonical form shown in (3.36c).
R	Radius with the transformation shown in (3.25b).
r	Radius.
$\overrightarrow{r}$	Position vector.
$r_{\rm c}$	Core radius.
$r_{\rm h}$	Half-mass radius.
$r_{\rm max}$	Maximum value of r for a star to remain in the cluster.
$\tilde{r}$	Ratio of characteristic radii of the light stars and heavy stars in Model Ia.
$\tilde{r}_{\tilde{M}_{\rm max}}$	Value of $\tilde{r}$ that corresponds to $\tilde{M}_{\rm max}$.
$\mathbf{S}$	The function S after being transformed to the canonical form using (3.36f).
S	Function used for simplification in Fokker-Planck models.
$\dot{T}_{\rm enc}$	Instantaneous rate of change in kinetic energy caused by encounters.
T	Kinetic Energy.
t	Time.
$t_{\rm eq}$	Equipartition time.
$t_{\rm cc}$	Core collapse time.
$t_{\rm rc}$	Core relaxation time.
$t_{\rm cross}$	Crossing time.
$t_{\rm eject}$	Ejection time.
$t_{\rm evap}$	Evaporation time.
$t_{\rm rh}$	Half-mass relaxation time.
$t_{\rm r}$	Relaxation time.
$\mathbf{U}$	The gravitational potential for the canonical form shown in (3.36a).
U	Gravitational potential.

U_C	Gravitational potential due to the cluster.
U_G	Gravitational potential due to the galaxy.
$U_{\max}$	Maximum value of the gravitational potential.
V	Potential Energy.
v	Typical velocity.
$\overrightarrow{v}$	Velocity vector.
$\langle v^2 \rangle$	Mean square velocity.
$\langle v_c^2 \rangle$	Mean square velocity of the core.
v_r	Radial velocity.
v_t	Tangential Velocity.
W	Total energy.
$x_{\max}$	Maximum value of x for a star to remain in the cluster.
Y_1	Function of energy used to find the asymptotic solution of the Fokker-Planck model.
y_1	Function of energy used for simplifying single mass Fokker-Planck model for finding a numerical solution.
Y_2	Function of energy used to find the asymptotic solution of the Fokker-Planck model.
y_2	Function of energy used for simplifying single mass Fokker-Planck model for finding a numerical solution.
Y_3	Function of energy used to find the asymptotic solution of the light stars in the two-component Fokker-Planck model.
y_3	Function of energy used for simplifying single mass Fokker-Planck model for finding a numerical solution.
y_4	Function of energy used for simplifying single mass Fokker-Planck model for finding a numerical solution.

Bibliography

Aarseth, S. J.: 2000, in V. G. Gurzadyan and R. Ruffini (eds.), *The Chaotic Universe, Proceedings of the Second ICRA Network Workshop, Advanced Series in Astrophysics and Cosmology, vol.10, Edited by V. G. Gurzadyan and R. Ruffini, World Scientific, 2000, p.286*

Aarseth, S. J.: 2003, *Gravitational N-Body Simulations*, Cambridge University Press, Cambridge

Aarseth, S. J., Henon, M., and Wielen, R.: 1974, *Astron. Astrophys.* **37**, 183

Antonov, V. A.: 1962, *Solution of the problem of stability of stellar system Emden's density law and the spherical distribution of velocities*, Vestnik Leningradskogo Universiteta, Leningrad: University, 1962

Barnes, J. and Hut, P.: 1986, *Nature* **324**, 446

Baumgardt, H., Heggie, D. C., Hut, P., and Makino, J.: 2003, *Mon. Not. R. Astron. Soc.* **341**, 247

Baumgardt, H., Hut, P., and Heggie, D. C.: 2002, *Mon. Not. R. Astron. Soc.* **336**, 1069

Benacquista, M. J.: 2006, *Living Reviews in Relativity* 9(2)

Binney, J. and Tremaine, S.: 2008, *Galactic Dynamics: Second Edition*, Princeton University Press

Carretta, E., Gratton, R. G., Clementini, G., and Fusi Pecci, F.: 2000, *Astrophys. J.* **533**, 215

Chandrasekhar, S.: 1942, *Principles of stellar dynamics*, University of Chicago Press, Chicago

Chandrasekhar, S.: 1943a, *Astrophys. J.* **97**, 255

Chandrasekhar, S.: 1943b, *Astrophys. J.* **97**, 263

Chang, J. S. and Cooper, G.: 1970, *J. Comput. Phys* **6**, 1

Chernoff, D. F. and Djorgovski, S.: 1989, *Astrophys. J.* **339**, 904

Chernoff, D. F. and Weinberg, M. D.: 1990, *Astrophys. J.* **351**, 121

Cohn, H.: 1979, *Astrophys. J.* **234**, 1036

Cohn, H.: 1980, *Astrophys. J.* **242**, 765

Djorgovski, S. and King, I. R.: 1986, *Astrophys. J., Lett.* **305**, L61

Einsel, C. and Spurzem, R.: 1999, *Mon. Not. R. Astron. Soc.* **302**, 81

Fregeau, J. M., Gürkan, M. A., Joshi, K. J., and Rasio, F. A.: 2003, *Astrophys. J.* **593**, 772

Giersz, M.: 1998, *Mon. Not. R. Astron. Soc.* **298**, 1239

Giersz, M. and Heggie, D. C.: 1996, *Mon. Not. R. Astron. Soc.* **279**, 1037

Hachisu, I. and Sugimoto, D.: 1978, *Progress of Theoretical Physics* **60**, 123

Heggie, D. C.: 1975a, *Mon. Not. R. Astron. Soc.* **173**, 729

Heggie, D. C.: 1975b, in A. Hayli (ed.), *Dynamics of the Solar Systems*, Vol. 69 of *IAU Symposium*, p. 73

Heggie, D. C. and Hut, P.: 2003, *The gravitational million-body problem*, Cambridge University Press, Cambridge

Heggie, D. C. and Stevenson, D.: 1988, *Mon. Not. R. Astron. Soc.* **230**, 223

Hénon, M.: 1960, *Annales d'Astrophysique* **23**, 668

Hénon, M.: 1961, *Annales d'Astrophysique* **24**, 369

Hénon, M.: 1965, *Annales d'Astrophysique* **28**, 62

Hénon, M.: 1971a, *Astrophys. Space. Sci.* **13**, 284

Hénon, M.: 1975, in A. V. Oppenheim and R. W. Schafer (eds.), *Dynamics of the Solar Systems*, Vol. 69 of *IAU Symposium*, p. 133

Hénon, M. H.: 1971b, *Astrophys. Space. Sci.* **14**, 151

Hills, J. G.: 1975, *Astron. J.* **80**, 809

Hut, P.: 1983, *Astrophys. J., Lett.* **272**, L29

Hut, P. and Bahcall, J. N.: 1983, *Astrophys. J.* **268**, 319

Hut, P., McMillan, S., Goodman, J., Mateo, M., Phinney, E. S., Pryor, C., Richer, H. B., Verbunt, F., and Weinberg, M.: 1992, *Publ. Astron. Soc. Pac.* **104**, 981

Inagaki, S. and Lynden-Bell, D.: 1983, *Mon. Not. R. Astron. Soc.* **205**, 913

Inagaki, S. and Wiyanto, P.: 1984, *Publ. Astron. Soc. Jpn.* **36**, 391

Khalisi, E., Amaro-Seoane, P., and Spurzem, R.: 2007, *Mon. Not. R. Astron. Soc.* **374**, 703

King, I.: 1962, *Astron. J.* **67**, 471

King, I. R.: 1966, *Astrophys. J.* **71**, 64

Kuzmin, G. G.: 1957, *Tartu Astr. Obs. Publ.* **33**, 75

Larson, R. B.: 1970, *Mon. Not. R. Astron. Soc.* **147**, 323

Lightman, A. P. and Fall, S. M.: 1978, *Astrophys. J.* **221**, 567

Louis, P. D.: 1990, *Mon. Not. R. Astron. Soc.* **244**, 478

Lynden-Bell, D.: 1975, in A. Hayli (ed.), *Dynamics of the Solar Systems*, Vol. 69 of *IAU Symposium*, p. 27

Lynden-Bell, D. and Eggleton, P. P.: 1980, *Mon. Not. R. Astron. Soc.* **191**, 483

Lynden-Bell, D. and Wood, R.: 1968, *Mon. Not. R. Astron. Soc.* **138**, 495

Makino, J.: 1996, *Astrophys. J.* **471**, 796

Meylan, G. and Heggie, D. C.: 1997, *Astron. Astrophys. Rev.* **8**, 1

Mikkola, S.: 1983a, *Mon. Not. R. Astron. Soc.* **203**, 1107

Mikkola, S.: 1983b, *Mon. Not. R. Astron. Soc.* **205**, 733

Ostlie, D. A. and Carroll, B. W.: 1996, *An Introduction to Modern Stellar Astrophysics*, Addison-Wesley Publishing Co.

Padmanabhan, P.: 2000, *Theoretical astrophysics. Vol.1: Astrophysical processes*, Cambridge, MA: Cambridge University Press, Cambridge

Padmanabhan, T.: 2001, *Theoretical Astrophysics - Volume 2, Stars and Stellar Systems*, Cambridge University Press, Cambridge

Plummer, H. C.: 1911, *Mon. Not. R. Astron. Soc.* **71**, 460

Quinlan, G. D.: 1996, *New Astronomy* **1**, 255

Rosenbluth, M. MacDonald, W. and Judd, D.: 1957, *American Physical Society* **107**, 1

Schive, H.-Y., Chien, C.-H., Wong, S.-K., Tsai, Y.-C., and Chiueh, T.: 2008, *New Astronomy* **13**, 418

Spitzer, L. J.: 1940, *Mon. Not. R. Astron. Soc.* **100**, 396

Spitzer, L. J.: 1969, *Astrophys. J.* **158**, L139+

Spitzer, L. J.: 1987, *Dynamical Evolution of Globular Clusters*, Princeton University Press, Princeton

Spitzer, L. J. and Hart, M. H.: 1971a, *Astrophys. J.* **164**, 399

Spitzer, L. J. and Hart, M. H.: 1971b, *Astrophys. J.* **166**, 483

Spitzer, L. J. and Thuan, T. X.: 1972a, *Astrophys. J.* **175**, 31

Spitzer, L. J. and Thuan, T. X.: 1972b, *Astrophys. J.* **175**, 31

Takahashi, K.: 1993a, *Publ. Astron. Soc. Jpn.* **45**, 233

Takahashi, K.: 1993b, *Publ. Astron. Soc. Jpn.* **45**, 789

Takahashi, K.: 1995, *Publ. Astron. Soc. Jpn.* **47**, 561

Takahashi, K.: 1996, *Publ. Astron. Soc. Jpn.* **48**, 691

Trager, S. C., King, I. R., and Djorgovski, S.: 1995, *Astron. J.* **109**, 218

von Hoerner, S.: 1960, *Zeitschrift fur Astrophysik* **50**, 184